Dissertation zur Erlangung des Doktorgrades
der Fakultät für Chemie und Pharmazie
der Ludwig-Maximilians-Universität München

Surface-functionalized sodium iodide symporter (NIS) lipopolyplexes: a targeting strategy for the *NIS* gene therapy of glioblastoma

Rebekka Theresa Spellerberg

aus

Steinheim, Deutschland

2022

Erklärung

Diese Dissertation wurde im Sinne von § 7 der Promotionsordnung vom 28. November 2011 von Frau Professor Dr. Christine Spitzweg betreut und von Herrn Professor Dr. Ernst Wagner von der Fakultät für Chemie und Pharmazie vertreten.

Eidesstattliche Versicherung

Diese Dissertation wurde eigenständig und ohne unerlaubte Hilfe erarbeitet.

München, den 12.05.2022

Rebekka Spellerberg

Dissertation eingereicht am	19.05.2022
1. Gutachter:	Prof. Dr. Ernst Wagner
2. Gutachterin:	Prof. Dr. Christine Spitzweg
Mündliche Prüfung am	09.06.2022

To my parents

Table of contents

1. Introduction

1.1. Cancer

1.1.1. Biology of cancer

Tumorigenesis is a multistep process by which normal human cells transform into malignant cells.[1] Research over the past two decades has shown that tumors are comprised of a complex patchwork quilt of normal and malignant cell types. The tumor microenvironment represents a network of regulatory signaling that controls individual and collective cellular functions resulting in tumor growth and progression.[2]

The foundation of a solid tumor is first established by cancer cells.[2] While normal cells regulate their proliferation, differentiation and apoptosis via their molecular machinery, cancer cells have lost control of their replication, invasive growth and found ways of circumventing cell death. These developments are reflected by specific and dynamic changes in their genome.[1] These so-called mutations can be classified into two types of cancer genes: first, oncogenes leading to a rise of function, and second, suppressor genes with a loss of function.[1] Mutagenesis drives the expression of oncogenes and this leads to the ability of cancer cells to generate their own progrowth, antiapoptotic and angiogenesis-initiating signals. The expression of membrane receptors for cell-cell and cell-extracellular matrix protein interactions, termed integrins, help to foster the progrowth and proangiogenic signals. The resultant signals help to activate telomerase activity to avoid chromosomal degradation.[1] At the same time, the activation of suppressor genes disrupts pathways that limit proliferation and the counterregulatory signals for homeostasis. Additionally, suppressor genes can turn off expression of integrins that mediate antigrowth signal transfer leading to reduced contact inhibition and preventing the cells from entering the postmitotic state and terminal differentiation.[1]

Cancer stem cells (CSCs) are thought to represent a minority population of neoplastic cells in tumors. CSCs have the capability to sustain and renew themselves. In addition to maintaining a cancer stem cell pool, they contribute to tumor maintenance by differentiating into heterogeneous cancer cell types.[3] They may arise from normal stem cells that undergo various mutations, or they may derive from differentiated cells that acquire the ability to self-renew through epigenetic alterations. CSCs are also thought to represent tumor initiating cells and they have been proposed to act as the progenitors or ‘seeds’ of tumor invasion and metastasis.[4]

Endothelial cells, blood vessel associated smooth muscle cells and pericytes are important players in the establishment of the tumor microenvironment. Their dynamic coaction forms the basis for the productive angiogenesis that allows tumors to grow.[5] Tumors need to develop a vascular network to satisfy their need for oxygen and nutrients.[6] The angiogenesis-promoting signals, released by hypoxic cancer cells and tumor-associated stroma cells, lead to conversion of normal endothelial cells, sprouting from pre-existing blood vessels to tumor-associated endothelial cells for neovascularization.[5] Pericytes and smooth muscle cells, recruited by signals produced by endothelial cells, cover the endothelial tubing with their finger-like projections to stabilize the vessel membrane.[2,5]

Cancer-associated fibroblasts (CAFs) represent a predominant cell population in the tumor stroma of many cancer types. These cells are derived from normal fibroblasts by genetic alteration, from epithelial or endothelial cells through epithelial- or endothelial-mesenchymal transition or by the recruitment of bone marrow derived mesenchymal stem cell progenitors that can differentiate into CAFs.[7] CAFs can show a high level of heterogeneity. Their main tasks in the tumor microenvironment include the initiation of the synthesis and remodeling of extracellular matrix, driving cell-cell interactions, promoting invasive growth and fostering tumor metastasis.[7,8]

Solid tumors have been described as something akin to a chronic wound, constantly driving the recruitment of immune cells and other cells to ‘help’ to heal the damaged tissue. This recruitment is to be driven through the actions of various cytokines and chemokines.[9] Macrophages and neutrophils, components of the innate immune system, modulate the inflammation that drives the further recruitment of immune cells. High levels of tumor-associated macrophages and neutrophils correlate with an adverse outcome for tumor patients.[10] Furthermore, inflammatory cells can produce reactive oxygen species (ROS) as part of their effector function. ROS are also highly mutagenic and can accelerate cancer cell mutation leading to tumorigenesis.[2] The presence of natural killer cells, dendritic cells and T cells often correlate with a more favorable prognosis.[10] The innate natural killer cells eliminate transformed cells by releasing cytotoxic proteins, such as perforin and proteases (e.g. granzymes), and by triggering pathways of apoptosis.[9] The dendritic cells are the interface between the innate and adaptive immune system. They present tumor antigens to T cells and prime these for an adaptive immune response.[9] After their activation by antigen presenting cells such as dendritic cells in the secondary lymphatics, T cells migrate to the tumor microenvironment where they can attack the tumor. Cytotoxic T cells (CTLs) can promote anti-tumoral destruction through exocytosis of perforin- and granzyme-containing granules.[9] During tumor progression, cancer cells develop different strategies to circumvent this effective immune response:[2] In addition to the secretion of immunosuppressive cytokines by some inflammatory cells, cancer cells can become largely invisible to natural killer cells by

downregulating cell surface proteins such as MHC class I that are used for detection. Moreover, tumors express inhibitory checkpoint molecules that allow them to escape detection by CTLs. Consequently, less immunogenic cancer cells can evade the action of CTLs leading to a cell population with an immune-resistant phenotype.[9] This tumor escape of immune destruction represents a further hallmark of cancer growth.[2]

Taken together, the instability of the genome in cancer cells, the high variation of oncogenes and tumor suppressor genes and the heterogeneity of cells in the tumor microenvironment result in a remarkably complex biology. A multidisciplinary approach of cell biology, genetics, histopathology, biochemistry, immunology and pharmacology offers the best chance of effective and successful therapy strategies on the cancer battlefield.

1.1.2. Glioblastoma

Glioblastoma (GBM) is a grade IV malignant glioma and is a tumor of the glial cells that maintain the brain and nourish nerve cells. Atypia, mitosis, endothelial proliferation and necrosis form the basis for the GBM grading system established by the World Health Organization (WHO). Grade I and II tumors are considered benign; grade III are malignant, and grade IV (GBM) represent the most aggressive form that is associated with a very poor patient prognosis.[11] Currently no curative treatment options exist with the median survival of about 14 months following diagnosis and with a 5-year survival of GBM-diagnosed patients lower than 6%.[12]

Clinical symptoms vary and depend on size and location of the tumor. Commonly reported symptoms include headache, nausea, confusion, change in personality, seizures and neurological or visual disorders. GBM may cause perilesional edema, which usually increases intracranial pressure.[11]

The risk factors associated with glial tumorigenesis include exposure to toxins, ionizing and electromagnetic radiation, viral infection by simian virus 40, Li-Fraumeni syndrome, Turcot's syndrome, tuberous sclerosis, and alterations in chromosomes 17,7,4 and 9.[11]

GBM is characterized by a high proliferation index, invasive growth behavior, intratumoral heterogeneity, and tumor recurrence.[12] The complex heterogeneous nature of GBM cells influences progression, invasion, metabolic reprogramming and therapy resistance. Infiltrating immune cells, mostly tumor-associated macrophages (TAM), can represent up to 50% of the GBM mass and high TAM density has been correlated with glioma grade and poor prognosis.[12] TAMs form a predominantly immunosuppressive and tumor supportive phenotype that promote tissue remodeling and angiogenesis, thereby driving GBM progression.[13] Furthermore, the GBM microenvironment is thought to contain glioma stem cells that play an important role in therapeutic resistance, tumor migration and invasive tumor growth. Glioma

stem cells possess properties of self-renewal, pluripotency and the ability to differentiate into various cell types. They are thought to have the ability to escape the immune response and are capable of whole tumor regeneration once treatment has been concluded.[13]

1.1.3. Therapy of glioblastoma

Currently, GBM is generally diagnosed by computed tomography or magnetic resonance imaging (MRI) with subsequent tissue biopsy.[11]

The first-line therapy of GBM is surgical resection followed by local radiation and temozolomide chemotherapy.[12]

Due to the infiltrative growth of glioblastoma, surgery is a balancing act between aggressive removal of tumor tissue and maintaining brain function. Neuronavigation and intraoperative MRI can be utilized to maximize the extent of resection. Resective surgery decompresses tumor bulk and relieves pressure and may thus result in regression of symptoms. Reduction of neoplasm volume also enhances the prospect of adjuvant postoperative management, and through specific tumor profiling, a more personalized therapy regimen can be applied.[11]

Surgical excision is generally followed by fractioned radiotherapy. The combination has shown improved results for GBM control. The results of large, randomized trials suggest an early radiation treatment helps to prolong the time to tumor progression as compared to radiotherapy applied at the time of tumor growth.[14] Drawbacks of radiotherapy include damage to vicinal healthy tissues and the presence of hypoxic tumor centers where a lack of oxygen reduces the effectiveness of radiation therapy.[11]

The adjuvant and concomitant application of temozolomide, an alkylating agent, with radiotherapy has clinically significant effects on the survival of patients with newly diagnosed glioblastoma.[11]

The Food and Drug Administration (FDA) of the United States has approved Optune® as a treatment with temozolomide for newly diagnosed GBM in 2015. Optune® is a device that creates low-intensity and alternating tumor-treating fields, which are electrical fields interfering with the dividing GBM cancer cells to slow down cancer cell division.[12]

Despite these multidisciplinary therapies, tumor recurrence within 1 to 2 years after diagnosis occurs in most patients and represents the most critical parameter responsible for the unfavorable prognosis of GBM. Recurrent tumors are challenging due to newly formed lesions, infiltrative nature, and tumor heterogeneity.[11] Patients may then undergo repeated resection, different chemotherapies, additional radiotherapy or bevacizumab therapy, a humanized monoclonal antibody neutralizing the overexpression of vascular endothelial growth factor resulting in antiangiogenic effects and approved by the FDA for treatment of recurrent GBM after prior therapy.[12] Radiotherapy is palliative because of acquired radioresistance and

insensitivity of glioma cells to chemotherapeutic agents occurs partly due to overexpression of P-glycoprotein, which causes enhanced drug efflux from tumor cells.[15] Increasing the dose of chemotherapeutic agents to achieve sufficient intratumoral therapeutic drug levels will inevitably lead to significant toxicity such as lymphopenia, thrombocytopenia and neutropenia associated with temozolomide, and hypertension, leukopenia, non-central nervous system hemorrhage and thromboembolic events associated with bevacizumab.[12] Combining drugs with non-overlapping side effects and reducing the dose of each single drug may lower risk of unfavorable events and the development of chemoresistance. Multiple clinical trials of drug combinations for GBM treatment have recently been performed.[12]

The complexity of interactions between GBM cells with the tumor microenvironment adds to the complexity of finding successful treatment avenues. Efforts have been made to find treatment strategies targeting the tumor microenvironment. New approaches, such as chimeric antigen receptor T-cells, immune checkpoint modulators and vaccine-based immunotherapy are currently in clinical phase studies for GBM but have not yet been approved by the FDA or European Medicines Agency.[16]

1.1.3.1. Blood brain barrier

The blood brain barrier (BBB) is a highly selective boarder located at the blood vessels that vascularize the central nervous system and prevents a non-selective crossing of nutrients and other molecules between the systemic circulation and the brain interstitial fluid. The BBB provides an important environment for optimal neuronal function.[15]

The BBB **(Figure 1)** is mainly formed by cerebral endothelial cells (CEC) along with astrocytes and pericytes and is further supported by neurons, microglial cells, and smooth muscle cells. Tight junctions composed of transmembrane proteins, i.e. occludin and claudin, interconnect the CECs, close paracellular fenestrations and block paracellular transport.[15]

The CECs show low rates of endocytosis and transcytosis to limit the passage of diverse molecules. Host intra- and extracellular enzymes for metabolic activity help to degrade and deactivate numerous drugs and neurotoxins.[15] The membrane bound efflux transport proteins expressed by CECs can also actively pump-out various compounds such as chemotherapy agents. This is mediated by various proteins including the para-glycoprotein (P-gp), which is a member of the large family of efflux transporters called ATP-binding cassette (ABC) transporters. The presence of microglia, perivascular macrophages and mast cells in the BBB also act as a defense against immunologic damage.[15]

As a result, only small lipophilic and gaseous molecules can cross the BBB by energy-independent transport mechanisms. Water-soluble small molecule nutrients and vitamins are transferred by carrier-mediated transcytosis, e.g. glucose and certain other hexoses via the

GLUT1 transporter and neutral amino acids via the *LAT1* transporter.[17] Macromolecule peptides and proteins traverse the BBB via endogenous peptide-specific receptors abundant on the CECs lining brain vasculatures, such as transferrin receptor, insulin receptor and low density lipoprotein receptors.[17]

The BBB represents a major challenge to the development of effective systemic therapeutics for GBM. This structure ensures a blockade of all large molecules and 98% of small molecules into the brain at sufficient therapeutic levels. From the perspective of drug permeability, various strategies have been investigated to potentially facilitate drug delivery across the BBB. These include tight junction opening and efflux transporter inhibition, intracerebral implantation or intracerebroventricular injection of pharmaceutical compounds, chemical modification to achieve more lipophilic prodrugs and suitability for carrier- or receptor-mediated transcytosis.[15] Two prominent examples of agents that were developed using these criteria are Levodopa that is applied in the treatment of Parkinson's disease, and gabapentin, an anticonvulsant drug. Both drugs are substrates of the neutral amino acid transporter LAT-1.[17]

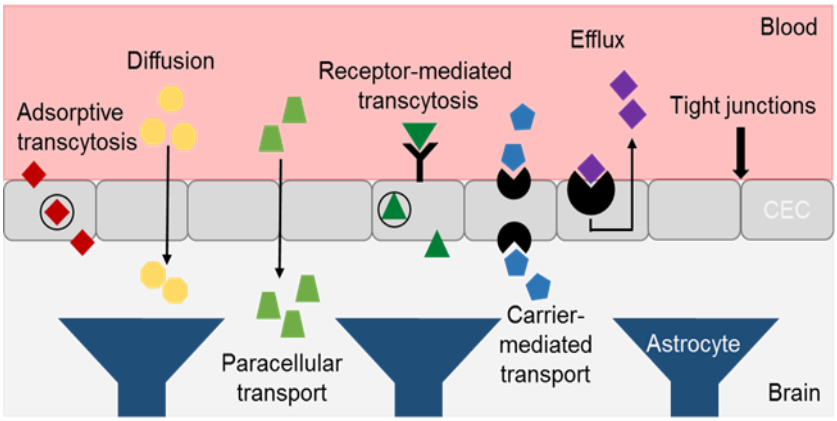

Figure 1: **The blood brain barrier (BBB).** The BBB is mainly formed by cerebral endothelial cells (CEC) and regulates the transport of compounds from blood to brain. It hinders entry of large molecules via tight junctions and efflux pumps. There are several mechanisms for transporting molecules across the BBB, including adsorptive transcytosis, diffusion, paracellular transport, receptor-mediated transcytosis and carrier-mediated transport (adapted from Caffery et al. 2019).

1.2. Sodium iodide symporter (NIS)

1.2.1. Characteristics

The sodium iodide symporter (NIS) is a plasma membrane glycoprotein with 13 transmembrane segments expressed on the basolateral membrane of thyroid follicular cells **(Figure 2A)**. NIS mediates the active transport of iodide into the thyrocytes as a crucial step in the biosynthesis of thyroid hormones. The driving force of iodide transport is provided by the Na^+ gradient generated by the NA^+/K^+ ATPase and the symport takes place in a stoichiometric ratio of two Na^+ and one I^-.[18] Functional thyroidal NIS expression is mainly regulated by the thyroid stimulating hormone (TSH). Through NIS, the thyroid gland concentrates iodide by a factor up to 40 times as compared to the plasma concentration under physiological

conditions.[19] In the thyroid gland, iodide is translocated across the apical membrane by pendrin and incorporated into tyrosyl residues along the thyroglobulin backbone through a process, which is catalyzed by thyroid peroxidase and termed as iodide organification **(Figure 2B)**.[20] In addition, NIS is constitutively expressed by the salivary glands, stomach, gastric mucosa, choroid plexus and lactating mammary glands. In these extrathyroidal tissues the expression of NIS is independent of TSH stimulation and there is a lack of an efficient iodide organification mechanism.[19,21]

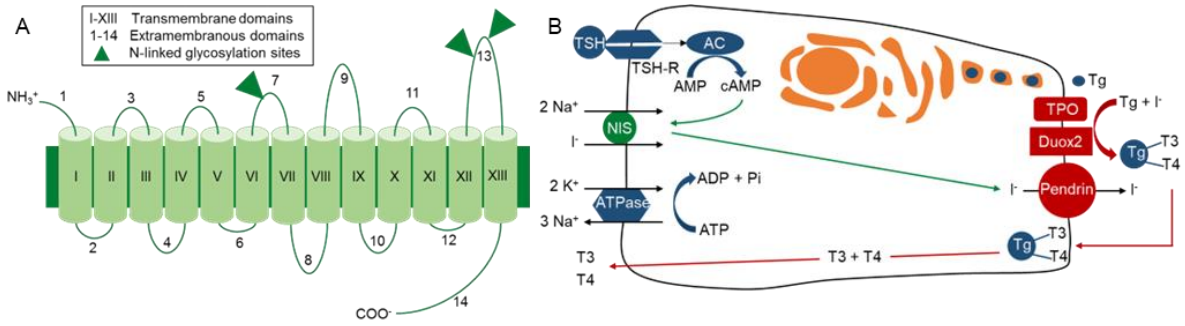

Figure 2: **Sodium iodide symporter.** The structure of NIS transmembrane protein is presented (A) (adapted from Spitzweg et al. 2001a). A schematic illustration of a thyroid follicular cell shows the physiological role of NIS in the process of thyroid hormone synthesis (B) (adapted from Spitzweg et al. 2002).

1.2.2. NIS as a theranostic tool

More than 80 years ago, the unique capability of thyroidal cells to accumulate iodide was used therapeutically for the first time when radioiodide was administered for the treatment of hyperthyroidism.[22] Since then, radioiodide-induced thyroid ablation has become an important tool in the treatment of thyroid cancer.[21,23] Based on its ability to accumulate iodide, *NIS* has emerged to a powerful dual function tool that is used as a molecular reporter as well as therapy gene **(Figure 3)** with advantageous characteristics: NIS is a 'self-protein' that is unlikely to be toxic or to elicit a significant immune response. The body distribution of its expression is well-defined. Imaging of NIS expressing cells correlates well with cell viability and offers high detection sensitivity, due to the active transport and efficient accumulation of the substrates.[24] NIS translocates various substrates, such as iodide, perrhenate, pertechnetate, astatide, tetrafluoroborate (TFB) and therefore, allows various non-invasive imaging modalities. Gamma scintigraphy and single-photon emission computed tomography can be performed by using ^{123}I, ^{125}I, ^{131}I, ^{99m}Tc, and ^{188}Re, while ^{124}I and ^{18}F-labelled TFB are tracers for positron emission tomography (PET).[24] Non-invasive detection of NIS-mediated radionuclide accumulation allows the temporal and spatial assessment of biodistribution, replication and elimination of various vector systems. It provides a detailed characterization of the level and duration of

transgene expression thus facilitating the precise planning and monitoring of clinical gene therapies. Based on the results of NIS imaging, dosimetric calculations allow an estimation of the radiation dose essential for radioablation of the individual tumor.[25] The application of potential therapeutically effective radionuclides include the β-emitters ^{131}I and ^{188}Re[25-27] or the α-emitter ^{210}At.[28] In addition to the death of NIS positive cells, the surrounding cells suffer cytotoxic destruction induced by a crossfire effect of the radionuclides.[20] This bystander effect is able to compensate heterogenous tumoral NIS expression due to the range of the beta particles (0.8 mm for ^{131}I and 3.5 mm for ^{188}Re) and makes the approach highly effective.[24] As will be detailed below, the application of NIS is under development for non-thyroid malignancies. In this regard, potential off-target effects after ^{131}I therapy mainly concern the thyroid due to iodide organification limited to the thyroid gland. Patients may be pre-treated with L-thyroxine to down-regulate the TSH-dependent NIS expression and thus the thyroidal iodide uptake. In case hypothyroidism nonetheless arises post-therapy, thyroid hormones can be substituted.[18] Perchlorate is a NIS-specific competitive inhibitor that is actively transported as a substrate and can effectively block the NIS-mediated radionuclide accumulation.[29]

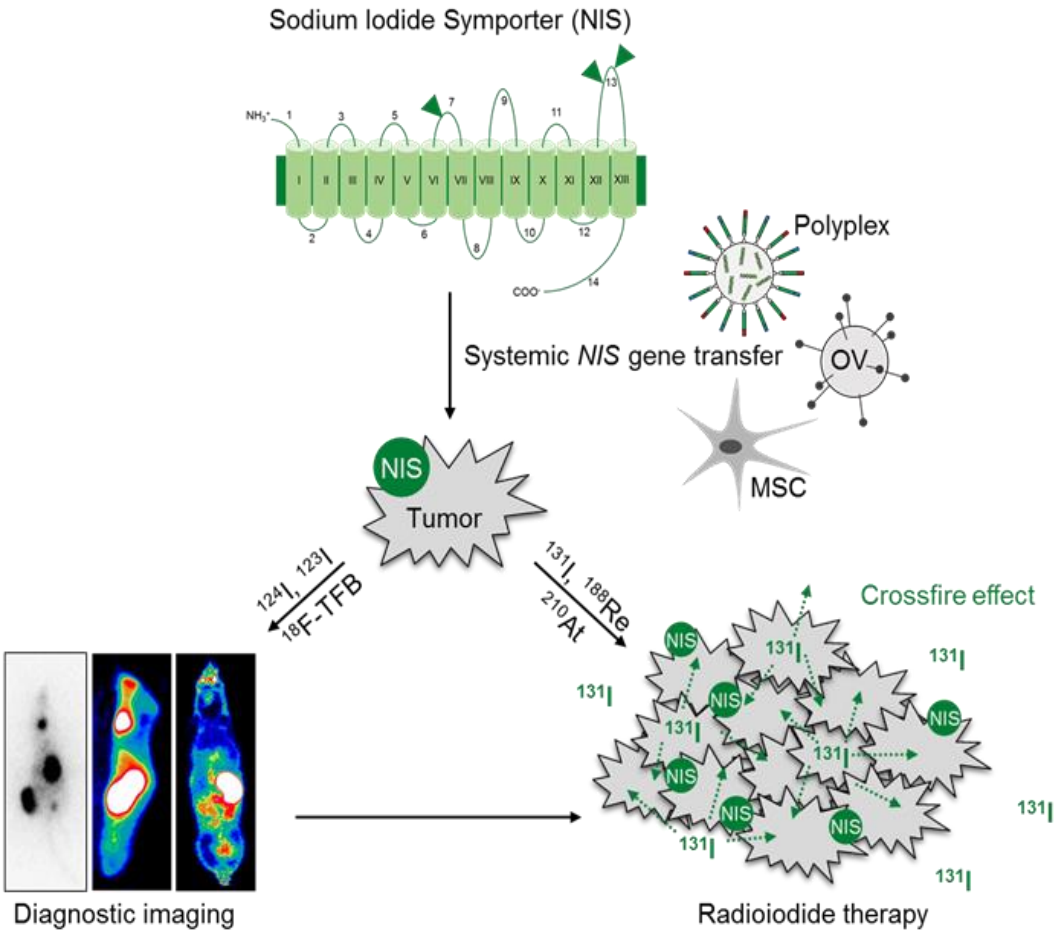

Figure 3: **Theranostic function of *NIS*.** Oncolytic viruses (OV), polyplexes or mesenchymal stem cells (MSC) can be utilized as gene vehicles for transgene expression in tumor cells. Diagnostic imaging can be performed by γ-scintigraphy or positron emission tomography. The application of β-emitters results in a therapeutic effect that is boosted by the crossfire effect (adapted from Spitzweg et al. 2021).

1.3. *NIS* gene therapy

1.3.1. Pioneering studies

Carrasco and her team cloned rat NIS cDNA in 1996[30], this was followed by the cloning of human NIS later that year by Jhiang and colleagues.[31] This milestone in thyroid physiology allowed the potential application of the well characterized NIS biology for the development of image-guided selective *NIS* gene delivery into extrathyroidal tumors followed by cytoreductive therapy by applying therapeutic radionuclides. In a pioneering study of Shimura *et al.* transformed rat thyroid epithelial cells (FRTL) that had lost the ability to accumulate iodide were transfected with rat NIS cDNA to constitutively express NIS (FRTL-TC cells). The ability to restore radioiodide accumulation was shown *in vitro* by an ^{125}I uptake assay and *in vivo* using subcutaneous FRTL-TC xenotransplants in Fischer 344 rats. The tumoral iodide accumulation was 27.3% of the total ^{125}I dose with an effective half-life of approximately 6 h.[32] As a next step in the development of NIS as a theranostic tool for non-thyroidal tumors, the selective targeting of the *NIS* gene to malignant cells was achieved through the use of tissue specific promoters to drive NIS expression to maximize potential tissue-specific cytotoxicity and minimize toxic side effects in nonmalignant cells. Spitzweg *et al.* demonstrated tissue-specific NIS expression in an androgen-sensitive human prostate cancer cell line (LNCaP) using a vector in which full-length hNIS cDNA was coupled to the prostate-specific antigen promoter.[33] The tumoral iodide uptake was confirmed *in vivo* in a LNCaP cell xenograft mouse model, and for the first time, a therapeutic effect was shown after administration of a single dose of 3 mCi ^{131}I with an average volume reduction of more than 90%.[34] Expression of functionally active NIS was demonstrated in subsequent studies using an adenovirus carrying the human *NIS* gene linked to the cytomegalovirus promoter for cell transduction. In a human glioma xenograft mouse model study by Cho *et al*., the intratumoral adenovirus injection resulted in an up to 25-fold increase in ^{125}I accumulation as compared to spleen.[35] A therapy study performed by Spitzweg *et al.* demonstrated highly active radioiodide uptake in prostate cancer xenografts after intratumoral adenovirus injection and the subsequent administration of 3 mCi ^{131}I that resulted in an average tumor volume reduction of 84%.[36] In preparation for a phase I clinical trial of adenovirus-mediated *NIS* gene therapy for locally recurrent prostate cancer, biotoxicity and efficacy studies were performed in a preclinical large animal model in beagle dogs. After intraprostatic injection of a replication-incompetent adenovirus, successful introduction of localized NIS expression in the prostate gland was seen with no vector-related toxicity observed.[37]

A large number of reports have been published in the following decades confirming the feasibility of *NIS* as a reporter and therapeutic transgene. The investigation of safe and efficient gene delivery systems is a crucial step towards clinical application of the *NIS* gene therapy concept. In this regard, the systemic administration of *NIS* gene vehicles represents an important step toward clinical translation and the treatment of primary and metastatic lesions.[24,38]

1.3.2. NIS-engineered mesenchymal stem cells

Bone marrow-derived mesenchymal stem cells (MSCs) are multipotent progenitor cells with the capability of proliferation and self-renewal. These cells are key mediators in the maintenance and regeneration of most human tissues and organs.[39] They are also linked to tumorigenesis. The process of tumor stroma formation has been described as similar to a chronic wound. The tissue signals produced by a solid tumor drive MSC recruitment to the 'damaged' tissue to effect repair. Thus MSCs show an excellent tumor-homing capacity driven by the tumoral release of soluble molecules such as inflammatory cytokines, growth factors and chemokines.[39-41] After recruitment to the tumor, MSCs differentiate into various tumor-stroma associated cell types including tumor vasculature and cancer associated fibroblast-like cells.[42,43] Due to their ease of isolation, amplification, engineering and lack of immunogenicity, genetically engineered versions of MSCs represent promising cellular vehicles for the transfer of therapeutic genes deep into growing tumors.[41]

MSCs have been genetically engineered to express NIS allowing the delivery of therapeutically effective radionuclides deep into tumor microenvironments. In initial experiments, human bone marrow-derived $CD34^-$ MSCs were stably transfected with NIS cDNA under the control of the constitutively active cytomegalovirus (CMV) promoter (CMV-NIS-MSC). *In vitro*, a clonogenic assay in mixed populations of CMV-NIS-MSCs and HuH7 cells showed a reduction of tumor cell survival of approximately 55% after ^{131}I treatment.[44] The body distribution of CMV-NIS-MSCs following injection via the tail vein was investigated by ^{123}I-scintigraphy and ^{124}I-PET imaging in a s.c. HuH7 xenograft mouse model. The results showed active MSC recruitment into the tumor stroma (7-9% ID/g). Immunohistochemistry and *ex vivo* γ-counter analysis confirmed the findings. Three cycles of systemic CMV-NIS-MSC-mediated *NIS* gene delivery followed by ^{131}I application resulted in a significant delay in tumor growth.[44]

Potential side effects of MSC-directed tumor therapy include off-target tissue damage due to MSC homing to normal tissues as part of tissue homeostasis. To increase tumor specificity of transgene expression, specific gene promoters that respond predominantly to signals present in tumor tissues have been used to drive NIS expression. An early study made use of the

promoter for CCL5 to drive NIS expression in MSCs. The chemokine RANTES/CCL5 has been shown to be upregulated in the process of MSC differentiation into CAFs.[27] In a second approach a synthetic TGFβ/SMAD promoter was used to take advantage of the pronounced tumor micromilieu-associated activation of TGFβ/SMAD signaling pathway.[45] As a further approach the HSP70B promoter was studied that allowed a more controlled activation of the *NIS* transgene by using local heat treatment of the tumor.[46] The RANTES-NIS-MSCs, SMAD-NIS-MSCs and HSP70B-NIS-MSCs were each evaluated in studies using the s.c. HuH7 xenograft mouse model. In all studies, systemic injection of NIS-MSCs under control of the specific gene promoter showed active MSC recruitment in the tumor stroma and promoter-mediated activation of the *NIS* gene as shown by tumor-selective ^{123}I accumulation, whereas non-target organs showed no functional NIS expression. In all three studies, administration of NIS-MSCs followed by a therapeutic dose of ^{131}I led to a significant delay in tumor growth and improved survival.[27,45,46] In particular, the SMAD-NIS-MSC application when coupled with a pretreatment of external beam radiation resulted in dramatic therapeutic effect as compared to other studies.[47] In addition to these proof-of-principle studies investigating MSC-based *NIS* gene delivery in s.c. xenograft mouse models, more physiologic orthotopic and metastatic tumor models have also been used. RANTES-NIS-MSCs were effective at controlling NIS expression in LS174T colon cancer liver metastases demonstrating metastasis-selective MSC recruitment and promoter activation as shown by ^{124}I PET imaging. The results were confirmed by immunohistochemistry showing strong NIS protein expression strictly confined to metastatic tissue with an absence of signal in normal liver tissue or non-target organs. Therapeutic application of ^{131}I in RANTES-NIS-MSC–treated mice resulted in a significant delay of metastatic spread mirrored by improved overall survival.[48] In a different strategy tumor-selective MSC-mediated NIS expression was driven by a synthetic gene promoter responsive to hypoxia-inducible factor-1 (HIF-1) (HIF-NIS-MSC). Efficient targeting of hypoxic tumor cells has become a central issue in cancer therapy due to their higher resistance to conventional treatment. The hypoxia induced transgene expression was demonstrated in tumor cell spheroid models and *in vivo* in intrahepatic tumor-bearing (HuH7) mice. Significant levels of tumor-selective NIS-mediated ^{123}I and ^{124}I accumulation after effective recruitment of HIF-NIS-MSCs was shown by scintigraphy and PET imaging. In line with these results, the therapy study showed a strong response to HIF-NIS-MSC + ^{131}I treatment with significantly delayed tumor growth, associated with decreased tumor perfusion assessed by contrast-enhanced ultrasound and prolonged survival of the treated animals.[49]

1.3.3. Oncolytic viruses in the *NIS* gene therapy

Oncolytic viruses (OV) are unique in their ability to amplify within the body. These viruses have developed strategies that make them efficient for the transfer of genetic information into host cells. Their antitumoral effects are based on pleiotropic modes of action including tumor-specific infection, replication, tumor cell lysis, spread and activation of antitumor immunity.[50] Endothelial cells, specifically in tumor vessels, were shown to be susceptible to OVs resulting in lysis and destruction of tumor blood vessels leading to nutrient and oxygen deprivation.[50]
In addition, the insertion of therapeutic genes into their genomes can trigger bystander killing effects by different means, depending on the gene chosen. The insertion of a therapeutic gene can lead to an antitumor immune activation, or the oncolysis can be caused by the therapeutic gene expression itself, or the therapeutic gene allows the application of reagents that are rendered cytotoxic. Bystander killing effects are capable of destroying proximal tumor cells that the virus cannot reach.[50]
In the context of *NIS* gene transfer a widely explored oncolytic replication-competent virus is the attenuated Edmonston measles virus (MV) vaccine strain that enters cells via the complement regulatory protein CD46 and therefore preferentially infects cells with an overexpression of this surface protein such as tumor cells. A recombinant MV-Edmonston strain engineered to express NIS (MV-NIS) was established for a multimodal therapy combining virus-mediated oncolysis and NIS-mediated radioiodide therapy (radiovirotherapy).[51] In a multiple myeloma xenograft mouse model, strong oncolytic activity of MV-NIS was demonstrated using *NIS* as a reporter gene to monitor the kinetics of temporal and spatial viral gene expression by ^{123}I scintigraphy. MV-sensitive KAS-6/1 myeloma xenografts were treated with a single i.v. dose of MV-NIS and subsequently showed complete regression. MV-resistant MM1 tumors completely regressed when *NIS* was additionally used as a therapy gene. The administration of ^{131}I nine days after a single i.v. injection of MV-NIS led to a significant therapeutic response.[51] Msaouel *et al.* performed a similar study in a subcutaneous prostate cancer (LNCaP) mouse model that showed a significant tumoral iodide accumulation and retention over time both in intratumorally and intravenously treated mice. These results were supported in an *in vivo* therapy trial where the injection of MV-NIS resulted in significant tumor regression and prolonged survival regardless of the route of administration. The significant oncolytic activity of MV-NIS could be further augmented by ^{131}I radiovirotherapy.[52]

1.3.4. Polyplex-mediated *NIS* gene therapy

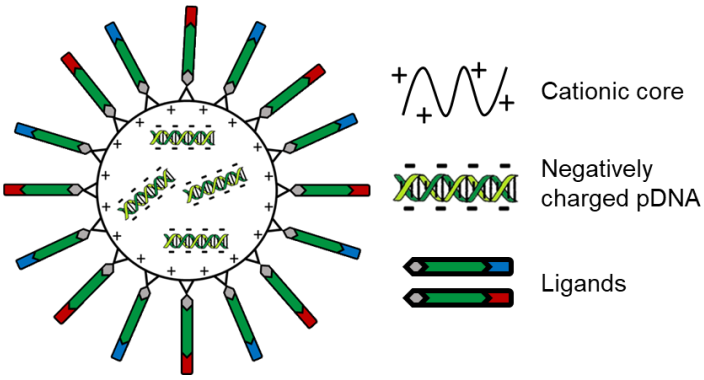

Figure 4: **Biology of polyplexes.** Cationic core packages the negatively charged pDNA through electrostatic interaction. Ligands can be used for potential surface functionalization containing a shielding and/or targeting domain.

Synthetic carriers **(Figure 4)** have been designed that mimic the targeted, dynamic, and potent nucleic acid delivery seen with viral vectors. These synthetic carriers may have advantages over viral vectors, as they overcome limitations in virus gene therapy such as immunogenicity, limited cargo capacity, rather sophisticated production, difficult manufacturing upscale and high production costs.[53]

1.3.4.1. Extra- and intracellular barriers

Before reaching the target tissue, polyplexes must overcome various extra- and intracellular barriers. Undesired issues after systemic application include dissociation of the nanoparticles caused by unspecific interactions with serum proteins or cellular surfaces, activation of serum complement proteins, inducing innate immune response, or self-aggregation or aggregation with biomacromolecules.[54] Successful accumulation at the target tissue site is achieved to some extent by passive targeting into tumor tissue that takes advantage of the enhanced permeability and retention (EPR) effect of tumors, or by the use of peptides with tissue- and cell-penetrating function leading to active tumor homing with faster and more efficient accumulation.[54] To facilitate intracellular entry **(Figure 5)** polyplexes must initially associate with the cell surface, either through electrostatic interaction, physical concentration via adsorption, or by ligand receptor binding.[55] The entry across cell surface membranes takes mainly place via endocytosis with endosomal escape desired to avoid lysosomal degradation of the nucleic acids. Carriers with pH-specific buffering capacity facilitate endosomal escape through the so-called proton sponge effect.[55] After release to the cytosol, degradation by cytosolic enzymes need to be circumvented and the nucleic acids must reach the nucleus in case of plasmid DNA (pDNA). Endosomal trafficking by microtubules transports the pDNA to the perinuclear space and nuclear import happens during cell division, which is possible in proliferating cells, or as a size-dependent phenomenon by active mechanisms through the nuclear pore complex. [54]

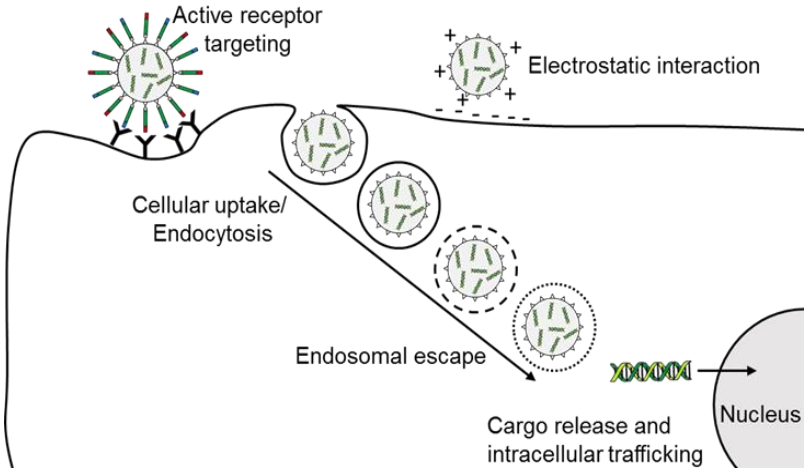

Figure 5: **Intracellular barriers**. Polyplexes interact with cell membrane by active receptor targeting or electrostatic interaction. Cellular uptake happens through endocytosis. Gene carrier are further processed for endosomal escape and nuclear trafficking of the pDNA (adapted from Lächelt et al. 2015).

1.3.4.2. Development of NIS polyplexes

The main challenges to investigate appropriate, efficient, and safe carrier systems for tissue specific gene delivery are the formation of stable polyplexes with suitable size, resistance to destabilization by serum proteins, a sufficient blood circulation, escape from removal process of liver, spleen and kidney and lack of immunogenicity. The cationic core packs the negatively charged pDNA into nanoparticles and is responsible for the balancing act between stability and endosomal release.[56]

Cationic polymers

In an early study of *NIS* gene therapy, biodegradable polycations based on oligoethylenimine (OEI)-grafted polypropylenimine dendrimers (G2-HD-OEI) **(Figure 6A)** were characterized and showed enhanced accumulation in tumor tissue based on their intrinsic tumor affinity due to the mild positive surface charge and on an enhanced permeability and retention effect due to the rather leaky tumor vasculature and decreased lymphatic drainage in the tumor environment. Tumor-selective *NIS* gene expression was shown after systemic injection of G2-HD-OEI in a syngeneic neuroblastoma (Neuro2A) mouse model and a hepatocellular cancer (HuH7) xenograft mouse model by ^{123}I scintigraphy and *ex-vivo* biodistribution studies. Using *NIS* as a therapy gene, two cycles of systemic polyplex-mediated *NIS* gene transfer followed by ^{131}I application resulted in a significant delay in tumor growth and prolonged survival in both tumor models.[57,58]

Shielding and targeting

Further development of polyplexes have included the incorporation of polyethylene glycol (PEG) as shielding domain. Efficient nucleic acid compaction through polycations usually results in the formation of nanoparticles with a positive surface charge. A positive zeta potential is desirable to ensure efficient interaction with the negatively charged cell membranes and fostering subsequent internalization.[59] At the same time, it is a balancing act to prevent undesired aggregation with negatively charged biomacromolecules in the extracellular space or self-aggregation performing potential toxicity issues, especially after intravenous application.[59] A coat of hydrophilic macromolecules can be included that effectively shields the surface potential from the exterior environment. A monodisperse PEG moiety with up to 24 oxyethylene units has been the most common shielding agent used and protects the vectors from aggregation, immune recognition and improves peripheral circulation.[59]

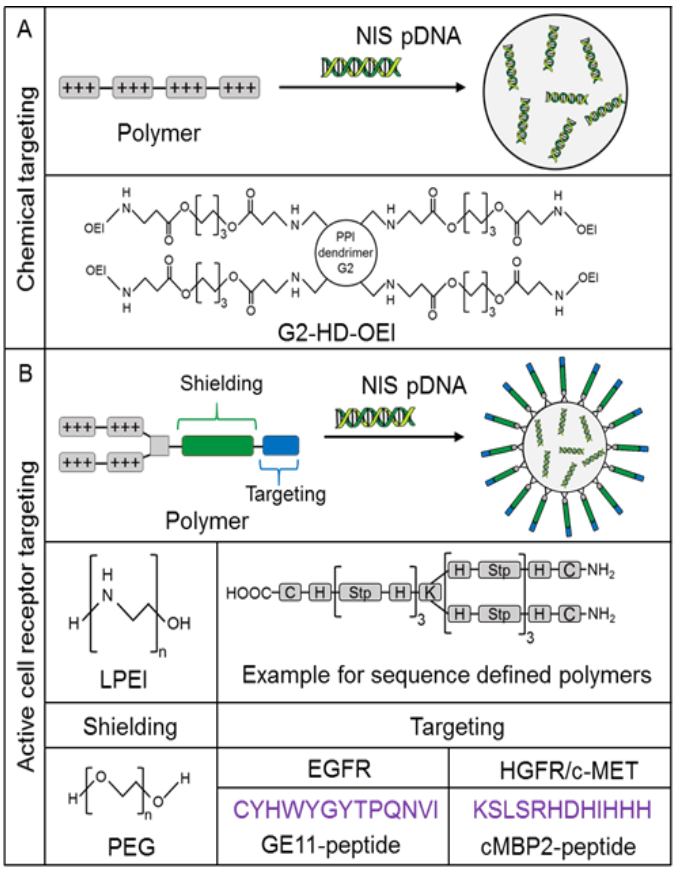

Figure 6: **pDNA polyplexes in the context of *NIS* gene therapy.** Cationic polymers complex negatively charged NIS pDNA through electrostatic interaction into nanoparticles. The mild positive surface charge of G2-HD-OEI interacts with the negatively charged cell membrane (chemical targeting) (A). Further development of polyplexes resulted in LPEI or sequence-defined backbones shielded by PEG molecules. Terminal EGFR or c-MET binding peptides were attached for active receptor targeting (B) (adapted from Spitzweg et al. 2021).

The conjugation of specific targeting ligands onto the polyplex surface enhance bioavailability, specificity, and efficiency through active receptor targeting. To investigate target-binding peptides, the phage display library screening performs a commonly used molecular biology technique. The targeting ligands identified to date comprise small chemical compounds such as vitamins, drugs, carbohydrates, peptides, and proteins.[54]

Advancements in the development of NIS-based polyplexes **(Figure 6B)** have included the integration of PEG moieties and peptides for cell targeting. The epidermal growth factor receptor (EGFR) is member of the tyrosine kinase receptor family, is upregulated in a high percentage of solid tumors, and therefore, represents an attractive surface marker for tumor-targeted delivery. GE11 has been utilized as an allosteric ligand for the EGFR and has the

advantage of no EGFR activation and no downregulation of the receptor surface expression.[60,61] GE11 was coupled via a PEG linker molecule to LPEI, a prominent carrier used for polyplex-mediated transfection (LPEI-PEG-GE11). An initial study was performed to demonstrate LPEI-PEG-GE11-mediated systemic *NIS* gene delivery into a s.c. EGFR-overexpressing hepatocellular cancer (HuH7) xenograft mouse model. Effective tumor targeting was demonstrated by scintigraphy and *ex vivo* ɣ-counting showed tumor-selective ^{123}I accumulation (6.5-9% ID/g) with an effective tumor absorbed dose of 47 mGy/MBq for ^{131}I. After pretreatment of a subset of mice with the EGFR-specific antibody cetuximab, tumoral iodide uptake was significantly reduced confirming an EGFR-dependent transfection efficiency of the polyplexes. Mice treated with LPEI-PEG-GE11 and ^{131}I showed a delay in tumor growth mirrored in prolonged survival.[62] In a further study, the LPEI-PEG-GE11 was evaluated in anaplastic thyroid cancer (ATC) models and demonstrated again high transfection efficiency and EGFR-specificity. *In vivo* ^{123}I imaging showed high radioiodide accumulation in SW1736 tumors and intermediate radioiodide accumulation in Hth74 tumors that correlated well with the EGFR expression levels seen and reflected the *in vitro* results. ^{131}I therapy performed in the SW1736 tumor model led to a significant delay in tumor growth and prolonged survival in mice treated with EGFR-targeted polyplexes.[63] Building on these results, tumor specificity and transfection efficiency of LPEI-PEG-GE11 were next investigated in a clinically highly relevant advanced genetically engineered mouse model of pancreatic ductal adenocarcinoma (Ptf1a^{+Cre};Kras$^{+/LSL-G12D}$; $^{Tp53lox/loxP}$ [Kras;p53]) (PDAC). After i.v. injection of LPEI-PEG-GE11/NIS quantitative analysis via ^{123}I gamma camera imaging showed a tumoral iodide uptake of 14.2 ± 1.4% ID/g. The significantly higher tumoral tracer uptake was confirmed by ^{124}I PET imaging, and a tumor absorbed dose of 96.5 mGy/MBq was calculated for ^{131}I. Despite the aggressive tumor model, reduced tumor growth was seen in mice treated with LPEI-PEG-GE11 followed by ^{131}I.[64] To show the potential of EGFR-targeted polyplexes for NIS-mediated radionuclide therapy in metastatic disease, a study was performed in an advanced multifocal colorectal cancer liver metastasis model, established by intrasplenic injection of LS174T human colon cancer cells. PET imaging showed high tumoral levels of NIS-mediated ^{18}F-labelled tetrafluoroborate uptake (4.8 ± 0.6% ID/g) in contrast to low levels detected in mice that received untargeted control polyplexes. The therapeutic efficacy was confirmed resulting in a marked delay in metastases spread, that was associated with prolonged animal survival.[65] In an attempt to address the complex issue of tumor heterogeneity, a major hurdle for the development of effective cancer therapy strategies, a dual-targeted polyplex was designed containing both the GE11 peptide for EGFR targeting and a cMBP2 peptide for cMET targeting. High tumor-selective transfection efficacy of the dual-targeted polyplexes was demonstrated by ^{124}I PET imaging in an orthotopic HuH7 xenograft mouse model (dual: 3.0 ± 0.4% ID, EGFR: 2.4 ± 0.5% ID, cMET: 2.3 ± 0.3% ID).[66]

Sequence-defined backbones

Based on their flexible composition allowing them to be tailor-made for tissue specific drug delivery, polyplexes composed solely of synthetic monodisperse, and sequence-defined subunits allow the chemical evolution of a precisely defined medicine. By utilizing solid phase assisted synthesis, the core oligomers obtain sequence-defined structures with monodispersity.[67] Chemical evolution strategies for intracellular macromolecule delivery have evaluated natural peptides and artificial amino acids with superior carrier properties. These molecules have been investigated with regards to their structure related activity: e.g., cationic amino acids, such as lysine, arginine or ornithine, and artificial building blocks with a cationizable motif, such as succinoyl tetraethylene pentaamine, bind the nucleic acid through electrostatic interactions. Terminal cysteines have been found to improve stability through bio-reversible disulfide crosslinking while the incorporation of histidines can enhance the buffering capacity at endosomal pH. This can increase osmotic swelling and lysis of endosomes and therefore improve endosomal escape. The use of unsaturated fatty acids help to mediate an endosomal pH specific lytic activity.[56,67]

The next generation of NIS polyplexes **(Figure 6B)** have been based on small sequence-defined biocompatible polymer backbones with precisely integrated functional groups aiming at improving efficiency and specificity with reduced toxicity. For *NIS*-mediated gene therapy of hepatocellular carcinoma, a cationic oligo(ethanamino)amide Stp core complexing NIS pDNA was functionalized with a cMET-targeting peptide (cMBP2) via a PEG linker molecule (cMBP2-PEG-Stp). High transfection efficiency and cMET-binding specificity was demonstrated *in vitro* and *in vivo* using a s.c. HuH7 xenograft mouse model. The results of the imaging study showed a tumoral ^{123}I uptake of 6.6 ± 1.6% ID/g and a calculated tumor absorbed dose of 41 mGy/MBq for ^{131}I correlating well with the therapy trial that showed a significant delay in tumor growth with prolonged survival after cMBP2-PEG-Stp/NIS injection followed by ^{131}I.[68]

1.3.5. Clinical translation

Preclinical proof of concept studies have demonstrated the flexibility of using *NIS* as imaging and/or therapy gene. These initial studies have now expanded to phase I/II clinical trials in various non-thyroidal cancer entities. The Mayo Clinic in Rochester, MN/USA has pioneered many of these studies. A non-exhaustive summary of phase I/II trials is subject of the following paragraph (Source: ClinicalTrials.gov).

Phase I trials are ongoing to determine potential side effects and the maximally tolerated dose of intratumoral administration of an Edmonston strain measles virus genetically engineered to express NIS (MV-NIS) in patients with recurrent/metastatic squamous cell head and neck

cancer (NCT01846091), malignant pleural mesothelioma (NCT01503177) or inoperable malignant peripheral nerve sheath tumor (NCT02700230).

In randomized phase II trial, the clinical efficacy of MV-NIS is being compared to standard cytotoxic chemotherapy including patients with ovarian, fallopian or peritoneal cancer. Outcome is being measured by progression free survival and overall survival. *NIS* is being used as a reporter gene to determine the course of viral gene expression, virus elimination and biodistribution of virally infected cells at various time points after infection using single-photon emission computerized tomography (SPECT) (NCT02364713).

Further phase I trials have been initiated to study the efficacy of other oncolytic viruses. An adenovirus engineered to express NIS has been intraprostatically administered to patients with recurrent adenocarcinoma of the prostate that did not respond to external-beam radiation therapy. Safety and tolerance of the engineered adenovirus has been determined with *NIS* used as reporter gene by ^{123}I application and as therapy gene by ^{131}I application afterwards. The study has been terminated but no results have been published (NCT00788307). Furthermore, the best dose and side effects of recombinant vesicular stomatitis virus carrying the human *NIS* and *IFN beta* genes in combination or without ruxolitinib phosphate therapy is being determined by SPECT in patients with multiple myeloma, acute myeloid leukemia, or recurrent or unresponsive T-cell lymphoma (NCT03017820).

Using mesenchymal stem cells as gene vehicles, a phase I/II trial is underway to study the maximally tolerated dose of intraperitoneal administration of an MV-NIS in patients with recurrent ovarian cancer, delivered by adipose tissue derived mesenchymal stem cells. The response rate, progression free survival and overall survival is being assessed (NCT02068794).

A phase I trial was initiated with the goal to perform first-in-man evaluation of ^{18}F-labelled tetrafluoroborate as a PET imaging biomarker for expression of functional NIS. Superior sensitivity and image quality could be shown in comparison to ^{99m}Tc SPECT. Myeloma patients treated with MV-NIS and endometrial cancer patients treated with vesicular stomatitis virus engineered to express IFN beta and NIS have been included. The study has been completed but data are not yet published (NCT03456908).

2. Aims of the thesis

Within the last three decades almost three-thousand gene therapy clinical trials have been performed, the majority have addressed new approaches to treat cancer and at least ten gene therapy products have now reached medical market authorization by the European Medicines Agency. In this context, nanoparticles have gained increasing attention as non-viral gene vehicles for site-specific gene delivery. The previous work of Prof. Dr. Christine Spitzweg in collaboration with Prof. Dr. Ernst Wagner have demonstrated the potential of sodium iodide symporter (NIS)-coding polyplexes in the field of nanotheranostics. As a dual function tool, *NIS* evolved as a highly promising target gene with diagnostic and therapeutic applications. To date, NIS polyplexes have been successfully introduced into a broad spectrum of cancer diseases including hepatocellular carcinoma, colorectal cancer liver metastases and pancreatic ductal adenocarcinoma. These pilot studies formed the backdrop for this thesis to refocus the technologies for the potential treatment of glioblastoma (GBM), a therapeutic challenging and aggressive tumor.

Sequence-defined lipopolyplexes combined with the post-integration concept of shielding and targeting domains were investigated with regard to safety, biocompatibility and transfection efficacy after systemic injection. The targeting peptide GE11 was chosen based on epidermal growth factor receptor (EGFR) overexpression in GBM cells. The establishment of an orthotopic GBM xenograft mouse model was aimed for *in vivo* studies. *In vivo* performance of the novel NIS lipopolyplexes was evaluated by performing high resolution positron emission tomography (PET) imaging and ^{131}I therapy studies. For clinical translation of this concept, potential complications encountered by the presence of the blood brain barrier (BBB) had to be addressed. The BBB hinders brain uptake of the majority of pharmaceutical compounds. In high-grade gliomas the blood brain tumor barrier (BBTB) can be compromised in its vascular integrity. Nevertheless, the BBTB presents an additional barrier for systemic treatment of brain tumors and EGFR-positive GBM cells can be drivers of invasive growth and are located behind an intact BBB, highlighting the importance of active transport across this biological barrier. A reengineering of the NIS lipopolyplexes was proposed to make them more suitable for receptor-mediated transcytosis across the BBB. For this purpose, a novel ligand for targeting the transferrin receptor (TfR), which is abundant in the endothelial cells lining brain vasculature, was investigated in the laboratory of Prof. Dr. Wagner. The application of this tool provided a basis for the development of a dual-targeted polyplex designed to overcome the BBB by active TfR targeting with subsequent targeting of the GBM by the EGFR-based approach. The improved efficacy of the dual-targeted polyplex was assessed in comparison to EGFR- and TfR-mono-targeted polyplexes. ^{18}F-labelled tetrafluoroborate was utilized as novel NIS PET tracer providing improved resolution and excellent target to background ratios.

3. Selective sodium iodide symporter (*NIS*) gene therapy of glioblastoma mediated by EGFR-targeted lipopolyplexes

Rebekka Spellerberg[1], Teoman Benli-Hoppe[2], Carolin Kitzberger[1], Simone Berger[2], Kathrin A Schmohl[1], Nathalie Schwenk[1], Hsi-Yu Yen[3], Christian Zach[4], Franz Schilling[5], Wolfgang A Weber[5], Roland E Kälin[6,7], Rainer Glass[6,7,8], Peter J Nelson[1], Ernst Wagner[2] and Christine Spitzweg[1,9]

[1]Department of Internal Medicine IV, University Hospital, LMU Munich, D-81377 Munich, Germany, [2]Pharmaceutical Biotechnology, Department of Pharmacy, LMU Munich, D-81377 Munich, Germany, [3]Institute of Pathology, School of Medicine, Technical University of Munich, D-81675 Munich, Germany, [4]Department of Nuclear Medicine, University Hospital, LMU Munich, D-81377 Munich, Germany, [5]Department of Nuclear Medicine, School of Medicine, Klinikum rechts der Isar, Technical University Munich, D-81675 Munich, Germany, [6]Neurosurgical Research, Department of Neurosurgery, University Hospital, LMU Munich, D-81377 Munich, Germany, [7]Walter Brendel Center of Experimental Medicine, Faculty of Medicine, LMU Munich, D-81377 Munich, Germany, [8]German Cancer Consortium (DKTK), partner site D-80336 Munich and German Cancer Research Center (DKFZ), D-69120 Heidelberg, Germany, [9]Division of Endocrinology, Diabetes, Metabolism and Nutrition, Mayo Clinic, Rochester, MN-55905, USA

This chapter is a pre-copy-edited version of a peer-reviewed article published in *Mol Ther Oncolytics* 2021;23:432-446

3.1. Abstract

Lipo-oligomers, post-functionalized with ligands to enhance targeting, represent promising new vehicles for the tumor-specific delivery of therapeutic genes such as the sodium iodide symporter (*NIS*). Due to its iodide trapping activity, NIS is a powerful theranostic tool for diagnostic imaging and the application of therapeutic radionuclides. ^{124}I PET imaging allows non-invasive monitoring of the *in vivo* biodistribution of functional NIS expression and application of ^{131}I enables cytoreduction. In our experimental design, we used epidermal growth factor receptor (EGFR)-targeted polyplexes (GE11) initially characterized *in vitro* using ^{125}I uptake assays. Mice bearing an orthotopic glioblastoma were subsequently treated with monoDBCO-PEG$_{24}$-GE11/NIS or bisDBCO-PEG$_{24}$-GE11/NIS and 24 to 48 h later ^{124}I uptake was assessed by PET imaging. The best performing polyplex in the imaging studies was then selected for ^{131}I therapy studies. The *in vitro* studies showed EGFR-dependent and NIS-specific transfection efficiency of the polyplexes. The injection of monoDBCO-PEG$_{24}$-GE11/NIS polyplexes 48 h before ^{124}I application was characterized to be the optimal regime in the imaging studies and was therefore used for an ^{131}I therapy study showing a significant decrease in tumor growth and a significant extension of survival in the therapy group. These studies demonstrate the potential of EGFR-targeted polyplex-mediated *NIS* gene therapy as a new strategy for the therapy of glioblastoma **(Figure7)**.

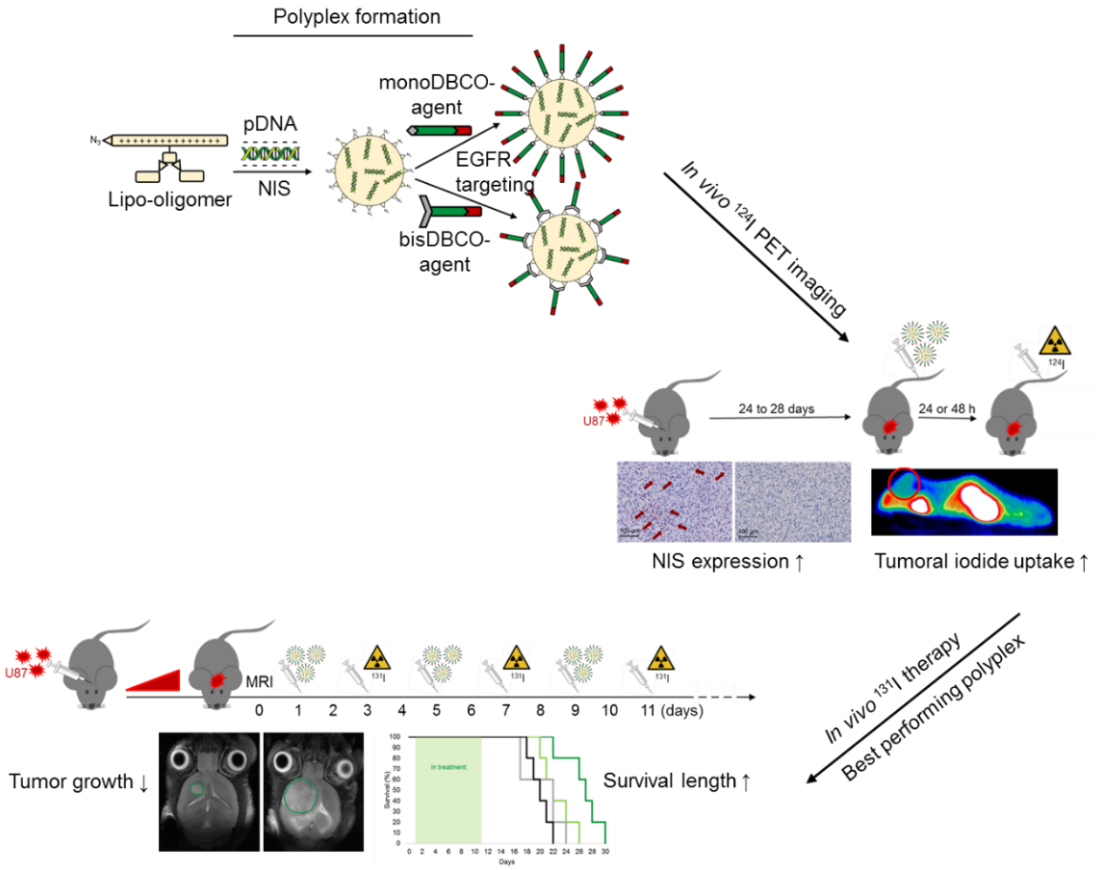

Figure 7: **Graphical abstract.**

3.2. Introduction

Glioblastoma (GBM) is a highly aggressive tumor with very limited therapeutic options. It is the most common type of malignant primary brain tumor. Presently, the median survival time after diagnosis is 12 to 15 months and less than 5% of patients survive more than 5 years.[69,70] The current clinical treatment involves surgical resection followed by external beam radiotherapy with concurrent chemotherapy.[70] Due to the infiltrating nature of GBM, local therapies or a complete resection are rarely possible and the clinical relapse of the tumor is usually unavoidable. Therefore, new postoperative therapy strategies are seen as the key for novel curative GBM treatments.[71,72]

Targeted gene therapy is a promising approach for novel therapeutics. Research in this field has been progressing for the past few decades with the majority of clinical trials focusing on cancer gene therapy.[73] The sodium iodide symporter (*NIS*) gene is a promising, efficient and safe therapy gene for systemic application. The NIS protein is an intrinsic plasma membrane glycoprotein, localized at the basolateral membrane of thyroid follicular cells that mediates the active uptake of iodide for thyroid hormone synthesis. Due to its iodide trapping activity, NIS is a powerful dual function tool with diagnostic and therapeutic applications.[74] The functional expression of NIS can be visualized by ^{123}I scintigraphy, ^{124}I or ^{18}F-TFB PET imaging (PET: positron emission tomography, TFB: tetrafluoroborate).[65,75] The application of ^{131}I or ^{188}Re and their NIS-mediated accumulation in tumor tissue allows therapeutic cytoreduction through the β-emission of these radionuclides. This therapy concept is approved, well-understood and safe, and has been in routine clinical use for over 80 years for the treatment of thyroid cancer.[26,31,76] In a pioneering preclinical study in prostate cancer, Spitzweg *et al.* took the initial step towards human *NIS* gene transfer to non-thyroidal cancer.[33,34,36] In the subsequent years, multiple groups, including our own, have established new approaches and refined diverse approaches for *NIS* gene transfer into diverse tumor models. To this end, nonviral gene delivery represents a promising technology for the transfer of genetic material into malignant primary tumors offering the advantages of safety, easy modification and enhanced biocompatibility after systemic application.[77] Besides NIS-engineered versions of mesenchymal stem cells with tumor tissue-specific promoters for selective *NIS* gene expression,[27,44-49,78-80] the potential of using targeted polyplexes for the delivery of *NIS* transgenes into tumor environments has been demonstrated by several studies by our group. These include the use of polycationic molecules based on linear polyethylenimine (LPEI) that make use of the enhanced permeability and retention effect caused by the leaky vasculature found in the tumor stroma.[57,58] A PEGylated (PEG: polyethylene glycol) and epidermal growth factor receptor (EGFR)-targeted LPEI molecule (LPEI-PEG-GE11) was demonstrated to enhance tumor-specific accumulation and could be optimized by attaching targeting

domains.[61-65] To test a broader platform of ligands targeting different tumor tissue surface receptors, ligands selectively targeting the receptor tyrosine kinase, cMET, and the transferrin receptor were developed.[66,68,81]

In the current study, we combined the theranostic *NIS* gene therapy approach with novel sequence-defined synthetic polyplexes to create an optimized, individual and powerful treatment concept for GBM. This new generation of nanosized polyplexes is based on sequence-defined cationic lipo-oligoaminoamides (OAA) synthesized by solid-phase assisted peptide synthesis (SPPS).[59] In addition to complexing plasmid DNA (pDNA) through electrostatic interactions, the OAA are azido-functionalized as a new feature that enables post-modification of the surface with targeting domains, to elicit an enhanced tumor-specific gene delivery. The functional azido group reacts with the dibenzocyclooctyne (DBCO) unit of potential ligands via copper-free click reaction.[82] PEGylation of the ligands lowers the surface charge to avoid non-specific aggregation or interaction with biomacromolecules, allowing an improved blood circulation and reducing undesired potential immune responses.[54,83] A monodisperse PEG_{24} (24 ethylene oxide units) was selected, which was already found to be suitable for *in vivo* targeting of related OAA-PEG-peptide conjugates. [68,84,85] The previously established dodecapeptide GE11, a highly specific allosteric EGFR ligand, conjugated to DBCO was used.[60] EGFR is an attractive candidate for GBM-targeting as its overexpression is a histopathological hallmark of GBM. In the GBM development, the EGFR is the most frequently amplified receptor tyrosine kinase and the receptor expression occurs early in the tumorigenesis[86,87] The peptide GE11 was selected for EGFR targeting based on its convincingly demonstrated capacity to provide EGFR-specific transfection efficiency in nanoparticle delivery both *in vitro* and *in vivo* in our previous studies.[61-65,88-92] In the present study we monitored vector biodistribution and transfection efficiency by non-invasive imaging in an orthotopic GBM mouse model and subsequently demonstrated potential therapeutic efficacy of our novel GE11-targeted NIS polyplexes after ^{131}I application.

3.3. Results

Polyplex characterization

NIS polyplexes **(Figure 8A-E)** were formed with 200 µg/ml pDNA (*in vivo* conditions) and particle sizes were measured by dynamic light scattering (DLS). We aimed at a size <200 nm to ensure unhindered blood circulation after intravenous (i.v.) injection and a sufficient cellular uptake.[93] The approximate dimensions were 120-140 nm and the polydispersity indexes (PDIs), an indicator for the heterogeneity of particle sizes in a mixture, were all below 0.2, which reflects a uniform and narrow size distribution **(Figure 8F)**. The particle sizes did not differ significantly between targeted (monoDBCO-PEG_{24}-GE11/NIS, bisDBCO-PEG_{24}-GE11/NIS) and their corresponding non-targeted polyplexes (monoDBCO-PEG_{24}/NIS, bisDBCO-PEG_{24}/NIS). Zeta potential measurements were performed to determine the surface charge of the polyplexes. A positive surface charge is achieved through the good nucleic acid compaction of the OAAs and is desirable to ensure sufficient interaction with negatively charged cell membranes and subsequent internalization.[94] However, at the same time it is a balancing act to prevent undesired aggregation with negatively charged macromolecules in the bioenvironment.[59] Taken together, a slightly positive surface charge is optimal. The zeta potentials of both PEGylated polyplexes (monoDBCO-PEG_{24}/NIS and bisDBCO-PEG_{24}/NIS) differed from those of GE11-targeted polyplexes (monoDBCO-PEG_{24}-GE11/NIS and bisDBCO-PEG_{24}-GE11/NIS). Using DBCO agents containing just the shielding domain (PEG_{24}) is more efficient in lowering the surface charge than compared to using ligands with a shielding and a targeting domain (PEG_{24} + GE11). No formulation exceeded a zeta potential of 20 mV **(Figure 8G)**.

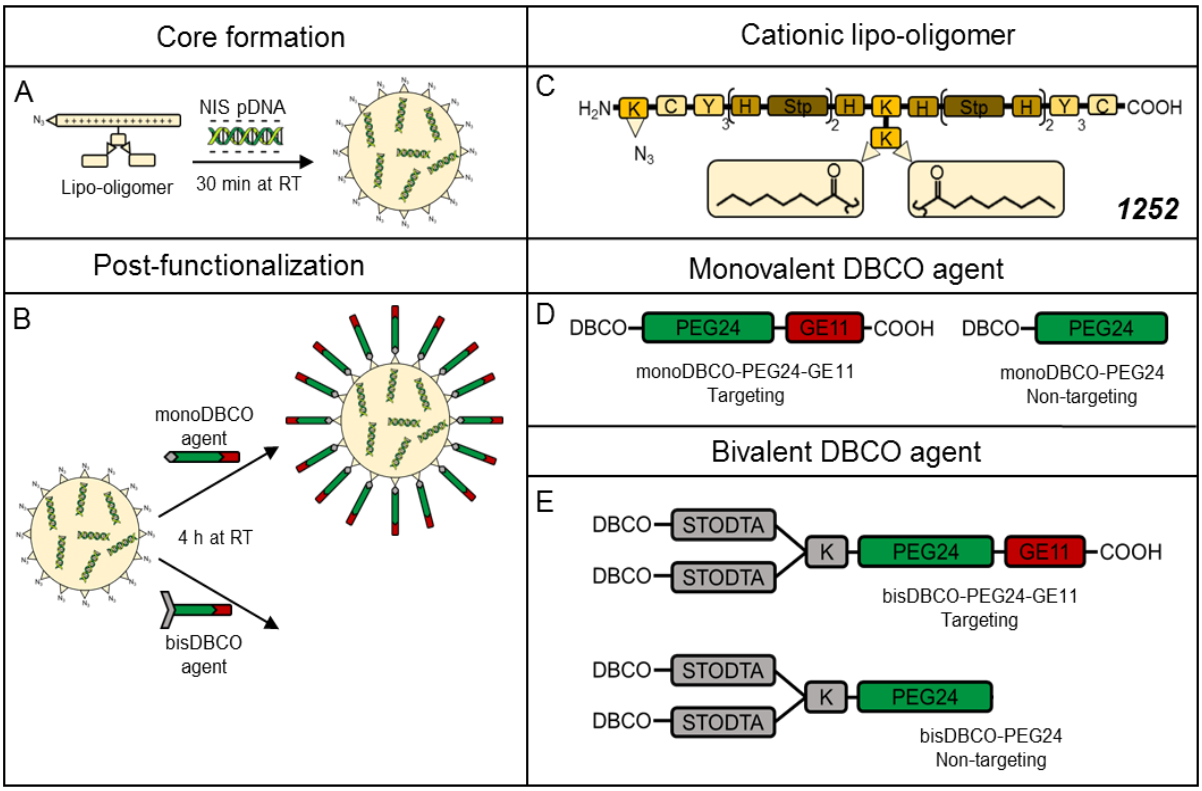

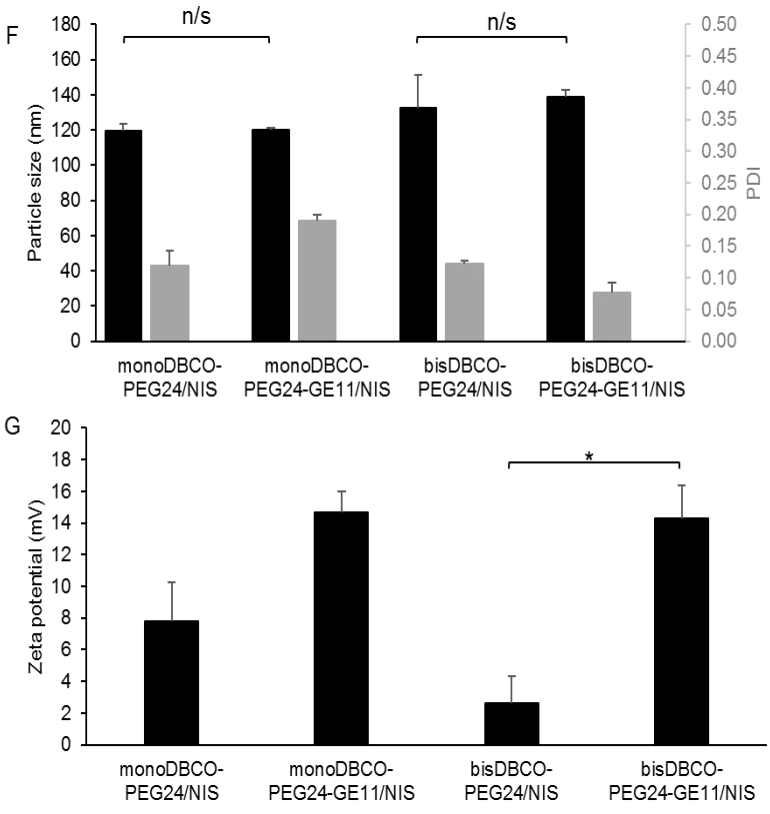

Figure 8: **Formulation of functionalized polyplexes.** The cationic lipo-OAA containing an N-terminal azido-group was mixed with pDNA at N/P 12 and incubated for 30 min at room temperature (A). Following the addition of a DBCO-agent with 0.25 equivalents, another incubation for 4 h at room temperature was performed (B). Schematic depictions are shown of the sequence-defined lipo-OAA with the compound ID ***1252*** (K: lysine, C: cysteine, Y: tyrosine, H: histidine, Stp: succinoyltetraethylene-pentamine) (C) and the structure of PEGylation agents for post-functionalization containing mono- (D) or bivalent (E) DBCO with ligand peptide GE11 for targeting of EGFR or without GE11 as negative non-targeting control. DLS measurements of formed polyplexes revealed a size of 120-140 nm with a uniform size distribution (PDI < 0.2) (F) and a zeta potential below 20 mV, whereas non-targeted PEGylated polyplexes showed more efficient surface shielding than polyplexes with targeted ligands (G) (*$p \leq 0.05$, n/s not significant). Results are reported as mean ± SEM (n=3). Experiments were performed by Teoman Benli-Hoppe (Department of Pharmacy, Pharmaceutical Biotechnology, LMU).

In vitro NIS gene transfer mediated by EGFR-targeted polyplexes

Cell surface EGFR expression levels were determined on human breast cancer cells MCF-7, human follicular thyroid carcinoma cells FTC-133 and the human glioblastoma cell lines GBM14, U87 and LN229 by flow cytometry. GBM 14 cells showed no EGFR expression, MCF-7 a very low expression level, FTC-133 a low level of EGFR expression and LN229 cells the highest EGFR density on their surface. U87 expressed an intermediate level of EGFR **(Figure 9A)**. The results indicate that the EGFR expression levels on the cells correlated with transfection efficiency after transfection with bisDBCO-PEG_{24}-GE11/NIS polyplexes. LN229 cells showed significantly higher ^{125}I uptake than U87 cells while no EGFR-expressing GBM14, very low EGFR-expressing MCF-7 and low EGFR-expressing FTC-133 cells exhibited significantly lower ^{125}I uptake **(Figure 9B)**. The transfection efficiency was higher in U87 and LN229 cells using the targeting ligand GE11: Transfection of U87 with bisDBCO-PEG_{24}-GE11/NIS polyplexes resulted in a 4-fold increase in ^{125}I uptake after 24 h as compared to transfection with non-targeting bisDBCO-PEG_{24}/NIS polyplexes **(Figure 9B)**. Transfection of U87 with monoDBCO-PEG_{24}-GE11/NIS polyplexes led to a 2.5-fold increase in ^{125}I uptake as compared to non-targeting monoDBCO-PEG_{24}/NIS polyplexes **(Figure 9C)**. The transfection of U87 with monoDBCO-PEG_{24}-GE11/NIS resulted in higher iodide uptake levels as compared to the transfection with bisDBCO-PEG_{24}-GE11/NIS indicating a higher efficiency of the monoDBCO-PEG_{24}-GE11/NIS polyplexes **(Figure 9B,C)**. In all cell lines, addition of the NIS-specific inhibitor perchlorate blocked ^{125}I uptake in NIS-transfected cells and no iodide uptake above background was seen using luciferase (LUC)-coding polyplexes **(Figure 9B,C)**. To further validate the EGFR-dependent transfection efficiency, U87 cells were simultaneously treated with increasing concentrations of the selective EGFR inhibitor cetuximab and monoDBCO-PEG_{24}-GE11/NIS polyplexes. A decrease of radioiodide uptake was shown at 2.5 mg/ml cetuximab with a complete inhibition of radioiodide uptake activity at 3.5 mg/ml cetuximab **(Figure 9D)**. All results were normalized to cell survival and U87 cell viability was not affected by polyplex treatment **(Figure 9E)**.

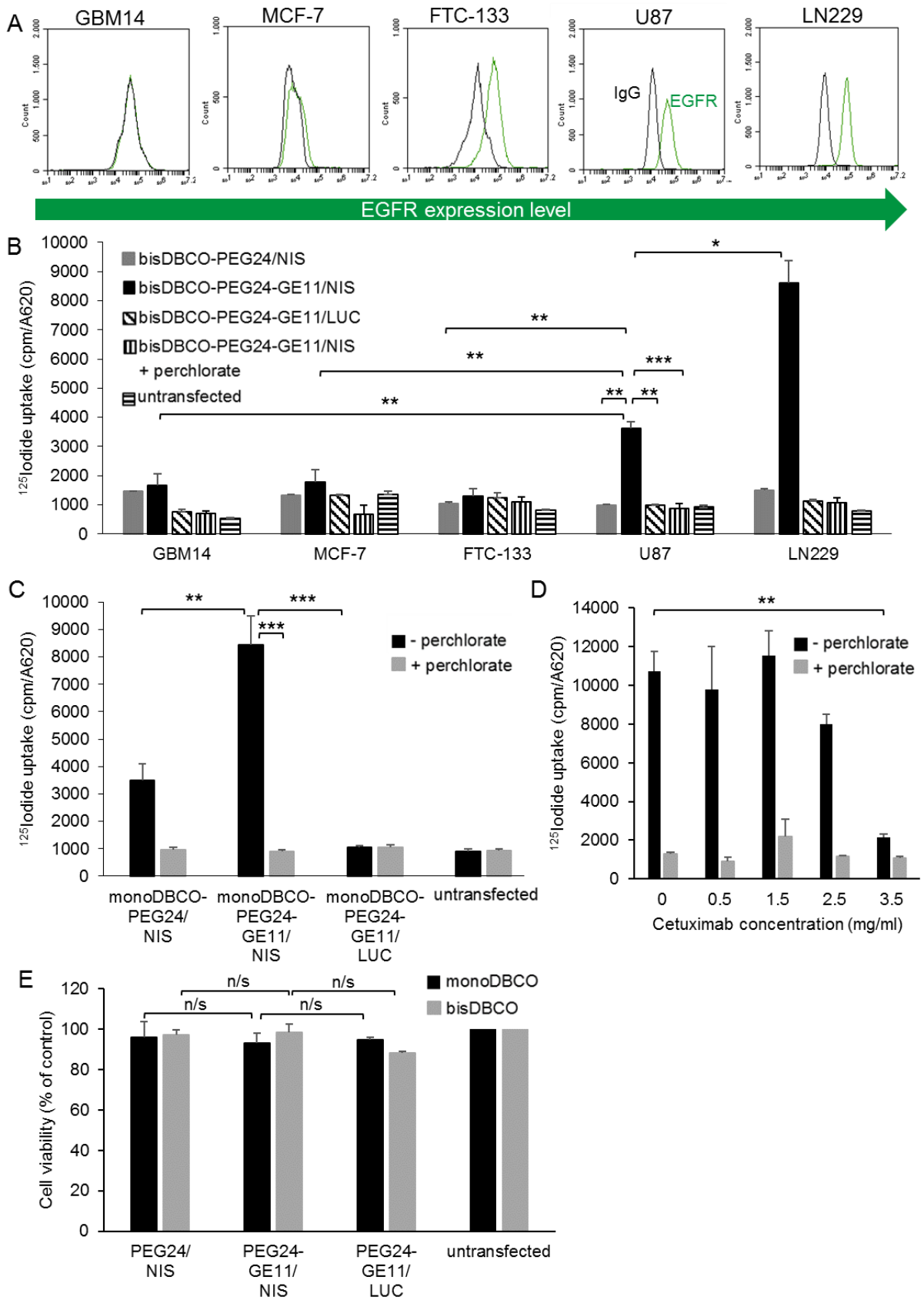

(Legend on next page)

Figure 9: **EGFR-targeted *NIS* gene transfer *in vitro*.** Cell surface expression of EGFR was measured by flow cytometry. A specific antibody detected the expression levels of human EGFR on GBM14, MCF-7, FTC-133, U87 and LN229 as compared to isotype controls (A). ^{125}I transfection studies with GBM14, MCF-7, FTC-133, U87 and LN229 (n=3) indicate a correlation between receptor expression levels and transfection efficiency of targeted polyplexes (bisDBCO-PEG$_{24}$-GE11/NIS) (B). Receptor specificity was shown by transfecting cells with untargeted polyplexes (monoDBCO-PEG$_{24}$/NIS n=6 and bisDBCO-PEG$_{24}$/NIS n=3) resulting in a significantly lower iodide uptake. Background radiation levels after control transfection with LUC-coding polyplexes (monoDBCO-PEG$_{24}$-GE11/LUC n=6 and bisDBCO-PEG$_{24}$-GE11/LUC n=3) or addition of NIS-specific inhibitor perchlorate prove NIS dependency of iodide uptake (B, C) (*p≤0.05, **p≤0.01, ***p≤0.001). Treatment with the selective EGFR inhibitor cetuximab resulted in a dose-dependent inhibition of the transfection of U87 cells using monoDBCO-PEG$_{24}$-GE11/NIS polyplexes demonstrating the EGFR dependency of transfection with GE11 polyplexes (D) (**p≤0.01). Cell viability of U87 was affected neither by monoDBCO- nor by bisDBCO-polyplex treatment (E). Results are reported as mean ± SEM.

Tumoral iodide uptake *in vivo* after systemic *NIS* gene transfer

To determine EGFR expression levels, tissue samples from an orthotopic U87 GBM xenograft mouse model **(Figure 10A)** were stained using specific antibodies. All tumors (n=7) were EGFR-positive with up to 40 % positive cells per tumor **(Figure 10B)**. GBM bearing mice received EGFR-targeted polyplexes systemically and were evaluated for functional NIS expression in the tumor tissue. Polyplex injection was scheduled 24-28 days after intracranial (i.c.) tumor cell inoculation and 24 h or 48 h later high resolution ^{124}I PET imaging was performed to quantify tumoral radioiodide uptake. The contrast between high radioiodide uptake in tumors of mice treated with EGFR-targeted polyplexes **(Figure 10C,D,G)** and low tumoral radionuclide uptake in mice injected with non-targeted polyplexes **(Figure 10E,H)** is indicated by the differences in signal strength. No tumoral iodide uptake above background **(Figure 10J)** was measured in mice that received LUC-coding polyplexes **(Figure 10F,I)**. Due to physiological NIS expression, the thyroid, salivary glands and stomach normally accumulate radioiodide. The bladder also contains radioiodide due to renal elimination **(Figure 10C-J)**.

In the quantitative analysis, tumors of mice that received monoDBCO-PEG$_{24}$-GE11/NIS showed a significantly higher ^{124}I uptake of 4.36 ± 0.65 % ID/ml (48 h) and 2.86 ± 0.24 % ID/ml (24 h) than tumors from mice that received non-targeted monoDBCO-PEG$_{24}$/NIS polyplexes, which exhibited an uptake of 1.96 ± 0.52 % ID/ml **(Figure 10K)**.

Measurements in mice that received bisDBCO-PEG$_{24}$-GE11/NIS confirmed the advantageous effect of EGFR-targeted as compared to non-targeted polyplexes. With a tumoral iodide uptake of 3.74 ± 0.83 % ID/ml, the cohort pre-treated with bisDBCO-PEG$_{24}$-GE11/NIS showed a higher signal amplification than the group injected with bisDBCO-PEG$_{24}$/NIS (1.44 ± 0.42 % ID/ml) **(Figure 10K)**.

Considering a tumor mass of 0.1 g, dosimetric calculations revealed the highest tumor-absorbed dose of 58.0 ± 18.3 mGy/MBq ^{131}I with an effective half-life of 9.6 h in the mice, treated with monoDBCO-PEG$_{24}$-GE11/NIS followed by radioiodide 48 h later. For mice, treated with non-targeted polyplexes (monoDBCO-PEG$_{24}$/NIS), a dose of 8.2 ± 1.0 mGy/MBq and an effective half-life of 2.9 h for ^{131}I were calculated. A dose of 35.0 ± 14.2 mGy/MBq ^{131}I and an

effective half-life of 5.4 h were determined for the bisDBCO-PEG$_{24}$-GE11/NIS group. Matching the *in vitro* data, monoDBCO-PEG$_{24}$-GE11/NIS polyplexes resulted in a higher tumoral iodide uptake and a higher tumor-absorbed dose as compared to the bisDBCO-PEG$_{24}$-GE11/NIS polyplexes, corroborating the higher transfection efficiency of the monoDBCO-PEG$_{24}$-GE11/NIS polyplexes, as a basis for their application in the *in vivo* therapy study.

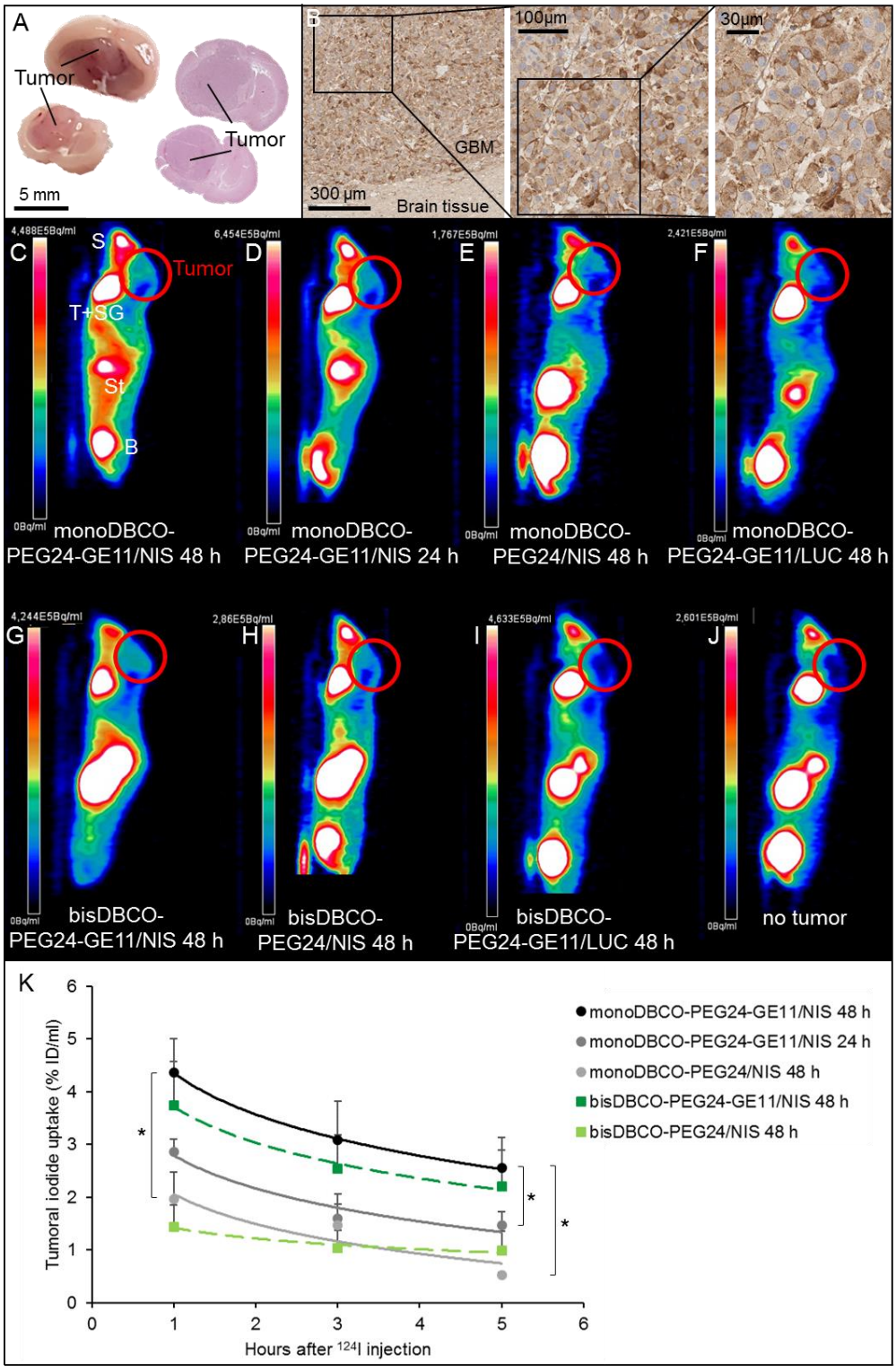

(Legend on next page)

Figure 10: **Polyplex-mediated *NIS* gene transfer *in vivo*.** U87 GBM (A) showed high membranous EGFR expression in the receptor staining compared to no EGFR expression in normal brain tissue (B). An 8x (scale bar: 1.25 cm = 300 µm), 15x (scale bar: 1 cm = 100 µm) and 40x (scale bar: 0.65 cm = 30 µm) magnification was chosen. Tumoral iodide uptake in ^{124}I PET studies was significantly higher in mice treated with monoDBCO-PEG$_{24}$-GE11/NIS (n=5) (C) as compared to non-targeting monoDBCO-PEG$_{24}$/NIS (n=4) (E). No tumoral iodide uptake above background was measured in mice that received LUC-coding monoDBCO-PEG$_{24}$-GE11/LUC polyplexes (n=3) (F) comparable to mice that did not bear a tumor (J). An interval of 48 h between systemic polyplex injection and iodide administration resulted in a higher iodide uptake than an interval of 24 h (n=5) (C,D). Analogous outcomes and reproduction of the advantageous targeting effect of GE11 polyplexes were seen in studies with bisDBCO-PEG$_{24}$-GE11/NIS (n=5) (G) for targeted, bisDBCO-PEG$_{24}$/NIS (n=3) (H) for non-targeted and bisDBCO-PEG$_{24}$-GE11/LUC (n=2) (I) for LUC-coding polyplexes. One representative image is shown for each group. Tumoral iodide uptake was measured by serial scannings over 5 h and quantified as % of the injected dose per ml tumor (K) (*p≤0.05). Results are reported as mean ± SEM. (S: snout, nasal secretion, T: thyroid, SG: salivary glands, St: stomach, B: bladder) EGFR immunohistochemistry was performed and analyzed by Hsi-Yu Yen (Institute of Pathology, Klinikum rechts der Isar, TUM).

Immunohistochemical *ex vivo* analysis of NIS protein expression

After tissue preparation, sections were stained immunohistochemically using an anti-NIS monoclonal antibody. Tumor sections derived from mice that received monoDBCO-PEG$_{24}$-GE11/NIS polyplexes 48 h **(Figure 11A)** before sacrifice showed a higher number of NIS positive cells (red) than tumor sections from the 24 h group **(Figure 11B)**. Immunohistochemical staining of tumor sections from control animals that received non-targeted monoDBCO-PEG$_{24}$/NIS **(Figure 11C)** or LUC-coding monoDBCO-PEG$_{24}$-GE11/LUC **(Figure 11D)** polyplexes showed no NIS-specific immunoreactivity that was comparable to untreated **(Figure 11E)** tumor tissue.

Immunohistochemical NIS staining of tumor sections derived from mice treated with bisDBCO-PEG$_{24}$-GE11/NIS **(Figure 11F)** polyplexes demonstrated an analogous outcome. The experimental group revealed clusters of NIS-positive cells in contrast to control groups (bisDBCO-PEG$_{24}$/NIS **(Figure 11G)** and bisDBCO-PEG$_{24}$-GE11/LUC **(Figure 11H)**) that showed no NIS detection.

In tissue sections of control organs (liver **(Figure 11I)**, lung **(Figure 11J)**, kidney **(Figure 11K)** and spleen **(Figure 11L)**), no NIS expression was detected.

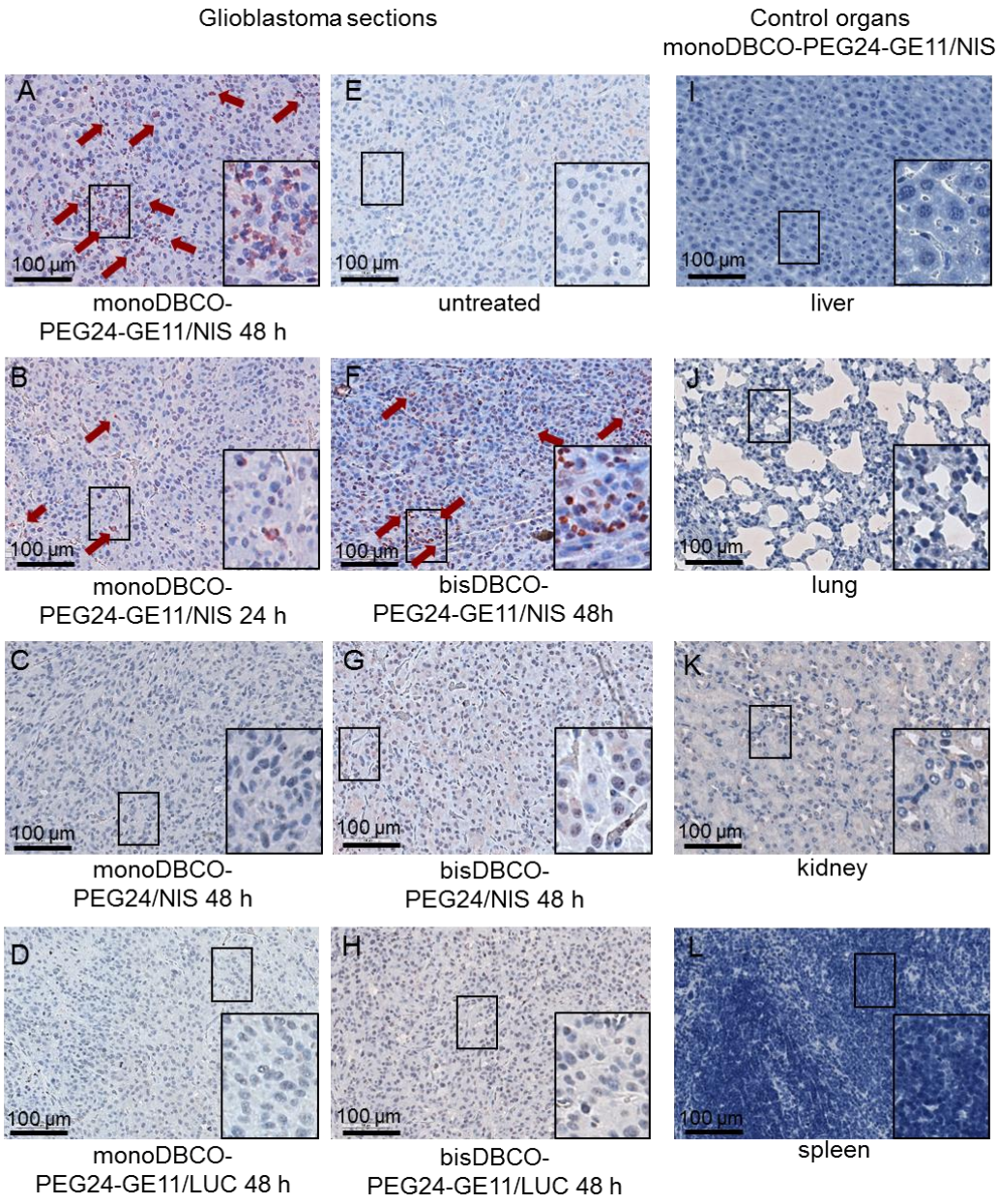

Figure 11: **Analysis of NIS protein expression in U87 tumors *ex vivo*.** Immunohistochemical staining of NIS protein in GBM xenografts embedded in paraffin revealed a higher NIS expression (red) in mice treated with targeted polyplexes (monoDBCO-PEG$_{24}$-GE11/NIS (A) and bisDBCO-PEG$_{24}$-GE11/NIS (F)) 48 h before sacrifice compared to the 24 h time point (B). No positive NIS staining in tumors of mice that received control polyplexes (C,D,G,H) or untreated (E) mice was observed. Liver (I), lung (J), kidney (K) and spleen (L) did not show any NIS expression. One representative image with 20x magnification is shown for each group (scale bar: 1 cm = 100 µm). 40x magnification was chosen for the close up (scale bar: 1 cm = 50 µm).

^{131}I therapy studies after polyplex mediated *NIS* gene transfer *in vivo*

Based on the results of the imaging studies, GBM bearing mice were then treated with monoDBCO-PEG$_{24}$-GE11/NIS followed by ^{131}I application 48 h later (therapy group). This application cycle was repeated three times. Control groups concurrently received non-targeting monoDBCO-PEG$_{24}$/NIS polyplexes followed by ^{131}I or monoDBCO-PEG$_{24}$-GE11/NIS polyplexes and then NaCl or NaCl only as a negative control. Tumor growth was monitored by high resolution magnetic resonance imaging (MRI) twice a week. The therapy group **(Figure 12A)** showed a significant delay in tumor growth as compared to the control groups. The tumor growth was only mildly reduced in the group monoDBCO-PEG$_{24}$/NIS followed by ^{131}I **(Figure 12B)** and an aggressive tumor growth was observed in the two control groups - monoDBCO-PEG$_{24}$-GE11/NIS plus NaCl **(Figure 12C)** and NaCl only **(Figure 12D)**. The enhanced therapy effect seen in tumor growth **(Figure 12E)** resulted in a significant extension of survival of the therapy group **(Figure 12F)**. On day 26, the last control mouse was sacrificed based on the animal welfare protocol while 60 % of the therapy mice were still alive. Mean survival times were 26.6 days for the therapy group, 22.6 days for the monoDBCO-PEG$_{24}$/NIS + ^{131}I group, 20.4 days for the monoDBCO-PEG$_{24}$-GE11/NIS + NaCl group and 20 days for the NaCl only group.

The results were further validated by staining of the blood vessel density and proliferation status **(Figure 13A-D)**. The therapy group showed a trend towards the lowest number of Ki67-positive cells **(Figure 13E)** and a significantly smaller area of CD31-positivity **(Figure 13F)** as compared to the control groups.

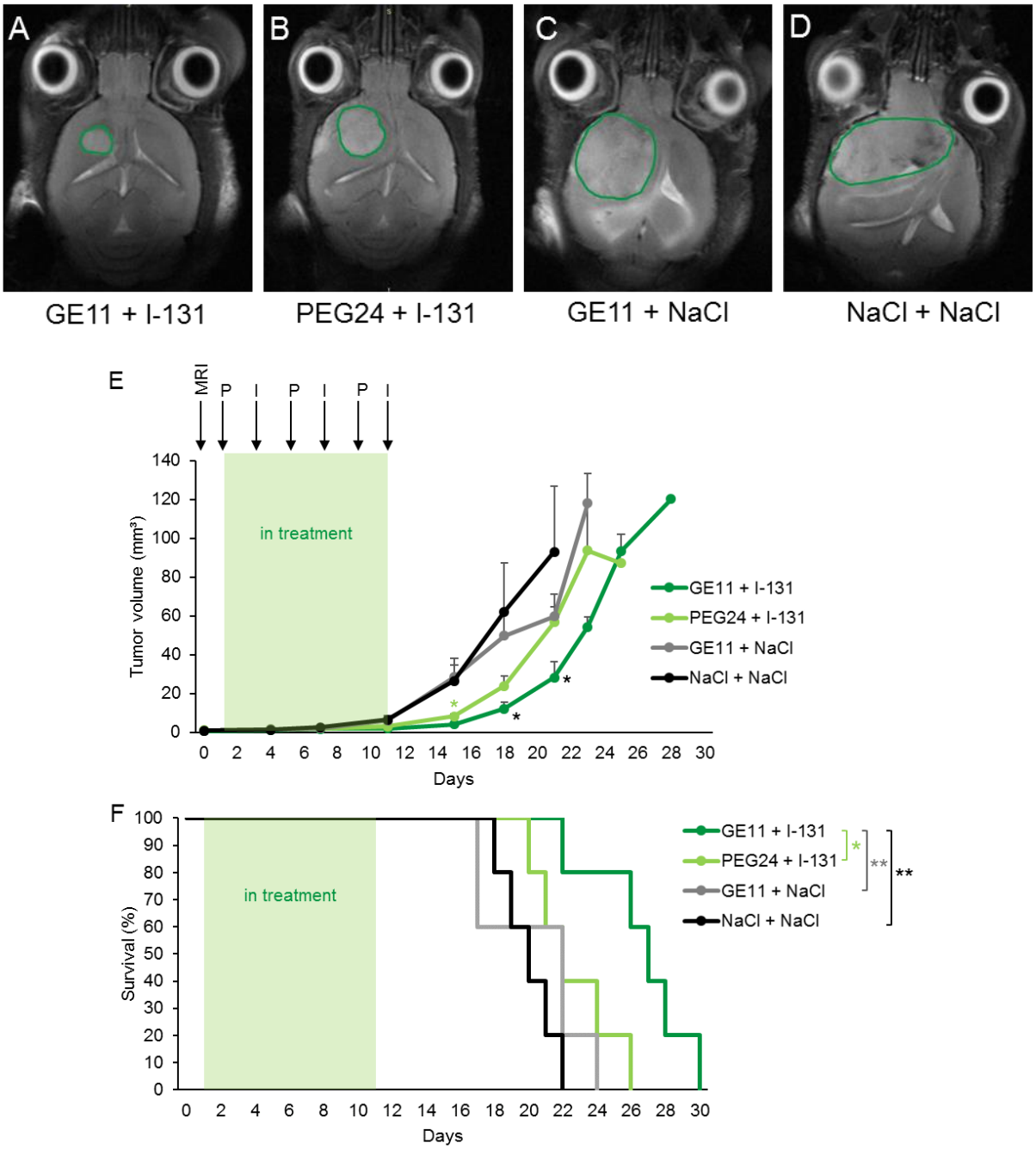

Figure 12: **^{131}I therapy studies *in vivo*.** GBM bearing mice, confirmed by MRI on day 0, were treated with three cycles of i.v. injection of polyplexes on days 1/5/9 followed by i.p. injection of 55.5 MBq ^{131}I 48 h later, on days 3/7/11. Tumor sizes were monitored twice a week by MRI. Exemplary MR images of tumor sizes on day 18 of the therapy trial from a monoDBCO-PEG$_{24}$-GE11/NIS + ^{131}I (A), a monoDBCO-PEG$_{24}$/NIS + ^{131}I (B), a monoDBCO-PEG$_{24}$-GE11/NIS + NaCl (C) and a NaCl + NaCl (D) treated mouse are shown. Tumors are highlighted by green lines. Injection of monoDBCO-PEG$_{24}$-GE11/NIS + ^{131}I led to a decrease in tumor growth in the therapy group (n=5) as compared to control groups monoDBCO-PEG$_{24}$/NIS + ^{131}I (n=5; mean ± SEM; *p<0.05 on day 15), monoDBCO-PEG$_{24}$-GE11/NIS + NaCl (n=5; mean ± SEM) and NaCl + NaCl (n=5; mean ± SEM; *p<0.05 on day 18 and 21). Therapy mice treated with monoDBCO-PEG$_{24}$-GE11/NIS + ^{131}I (n=5) showed a significant extension of survival as compared to control groups monoDBCO-PEG$_{24}$/NIS + ^{131}I (n=5; *p<0.05), monoDBCO-PEG$_{24}$-GE11/NIS + NaCl (n=5; **p<0.01) and NaCl + NaCl (n=5; **p<0.01).

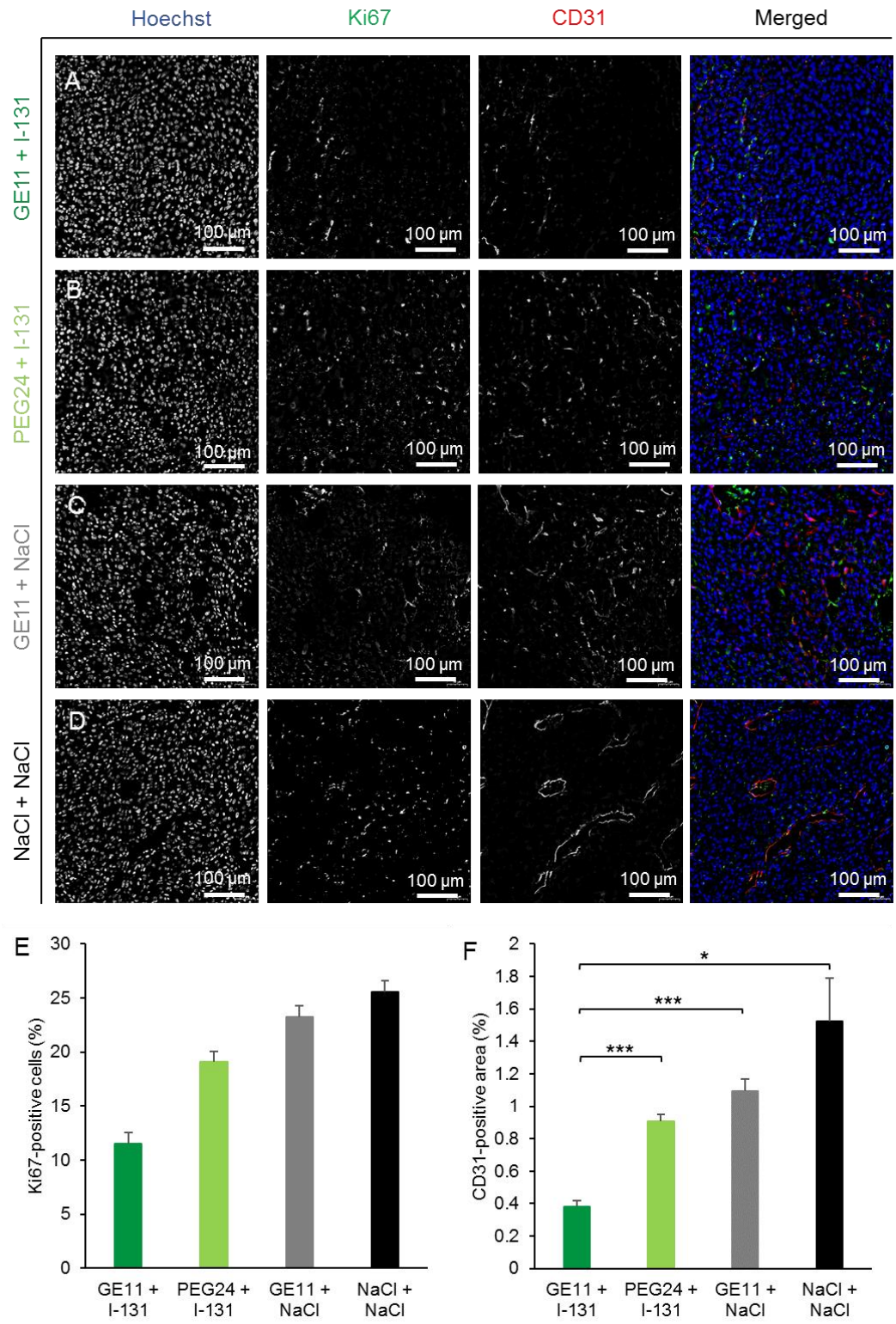

Figure 13: **Analysis of proliferation index and blood vessel density of therapy tumors *ex vivo*.** Frozen tissue sections from GBM dissected after the therapy study were stained for Ki67 (green) for proliferation index and CD31 (red) for blood vessel density. Nuclei are stained with Hoechst (blue). The therapy group that received monoDBCO-PEG$_{24}$-GE11/NIS followed by ^{131}I (A) showed less Ki67-positive cells (E) and a significantly smaller CD31-positive area (F) (*p<0.05, ***p<0.001) as compared to the control groups treated with monoDBCO-PEG$_{24}$/NIS plus ^{131}I (B), monoDBCO-PEG$_{24}$-GE11/NIS plus NaCl (C) or NaCl only (D). One representative picture of each group is shown at 20x magnification (scale bar: 0.8 cm = 100 µm). Results are reported as mean ± SEM (for each group n=4).

3.4. Discussion

As the most common malignant primary brain tumor, GBM has an incidence of 3.19 cases per 100 000 person years.[16] The remarkably poor prognosis of 15 months median survival[95] results from very limited treatment options, the diffuse-invasive nature of GBM with a remaining poor understanding of tumor pathophysiology.[11,95] The current therapy strategy is multidisciplinary. Diagnostic procedures involve MRI scan and biopsy whereas therapy involves surgical resection followed by adjuvant therapies. The gold standard of postoperative strategies is radiation therapy combined with the alkylating agent Temozolomide.[95,96] For recurrent disease that is progressive despite prior therapy, the monoclonal antibody Bevacizumab was authorized by the FDA.[12] T-cell inhibitors, peptide and dendritic cell-based vaccination, adoptive cell therapy and viral immunotherapy are new approaches currently in clinical phase studies for GBM but have not been approved by the FDA or EMA yet. To date, these therapy approaches do not differ much regarding prognosis and overall survival[16] highlighting the need for new strategies.

The cloning of *NIS* in 1996 opened up the opportunity of using this theranostic gene for non-invasive imaging and therapy purposes.[30] Due to its origin from thyroid follicular cells, it is a self-protein with no immunogenic potential and no cell toxicity.[76] Besides scintigraphic imaging, NIS facilitates tumor monitoring by PET using ^{124}I or ^{18}F-TFB as tracers.[65,75] PET allows quantitative analysis of tumoral iodide uptake mediated by functional NIS expression with high resolution and sensitivity and allows a three-dimensional reconstruction of tumors. NIS imaging allows a precise estimation of radiation dose for radioablation of the individual tumor based on dosimetric calculations.[20] Applying ^{131}I leads to radionuclide trapping within the NIS-positive cells and cell death induced by beta decay. The crossfire effect further boosts the impact of ^{131}I as neighboring cells also suffer cytotoxic destruction.[97] Off-target toxicity affects mainly the thyroid and salivary glands due to their physiologic NIS expression. Pre-treatment with LT4 causes a downregulation of thyroidal iodide uptake due to the TSH dependency of NIS expression. Should hypothyroidism nonetheless arise after therapy, it can be treated by thyroid hormone substitution.[76] The efficacy of radioiodide therapy is well established in thyroid cancer treatment, even in advanced metastatic disease.[98] This therapeutic effectiveness empowers the potential translation of NIS-mediated radioiodide therapy to other tumor diseases such as GBM. In the past, Cho *et al.* showed functional NIS expression in subcutaneous glioma tumors after intratumoral injection of NIS-expressing recombinant adenoviruses.[35] In a further step, Opyrchal *et al.* have shown a prolonged survival of orthotopic GBM bearing mice treated with intratumoral injection of measles virus engineered to express NIS followed by intraperitoneal (i.p.) injection of ^{131}I as compared to the MV-NIS-only group.[99] In the present study, we used sequence-defined polyplexes as artificial virus-like carrier systems. These synthetic carriers

may have distinct advantages over viral vectors as they overcome limitations in virus gene therapies such as immunogenicity, limited cargo capacity and difficulties in production.[53] But at the same time, this technology is inspired by virus biology in that they allow targeted, dynamic and potent nucleic acid delivery.[54] Importantly, in our study, we injected polyplexes systemically instead of intratumorally underscoring the flexibility of this approach in clinical applicability. Critical parameters for polyplexes are size, charge and surface characteristics. The T-shaped lipo-oligoaminoamide ***1252*** (OAA) packages the NIS pDNA and is responsible for the balance between stability and endosomal release.[56] Very small polyplexes (<6 nm) are rapidly eliminated by the kidney while very big polyplexes (over 400 nm) need extensive vascularization for their accumulation in solid tumors.[59] Our polyplexes have been designed for a size between 120-140 nm for optimal biodistribution and pharmacokinetics. Modification with the PEGylated ligands resulted in surface charges below 20 mV. This might be advantageous in view of avoiding self-aggregation, aggregation with biomacromolecules and to provide longer blood circulation.[59] Size and charge influence non-specific accumulation in liver, lungs and kidneys that can create toxicity issues. In *ex vivo* immunohistochemical stainings, we found no NIS expression in these healthy organs. To increase the internalization of our synthetic vectors to tumor stroma, we used GE11 ligands for specific tumor targeting.[61] We further showed EGFR dependent transfection efficiency *in vitro* and *in vivo*. The comparison of targeted polyplexes (monoDBCO-PEG_{24}-GE11/NIS and bisDBCO-PEG_{24}-GE11/NIS) to their corresponding non-targeted polyplexes (monoDBCO-PEG_{24}/NIS and bisDBCO-PEG_{24}/NIS) demonstrated the advantageous effect of using GE11 targeting ligands. In *in vitro* cell transfection and *in vivo* PET imaging experiments, the use of GE11-ligands led to a significantly higher transfection efficiency as compared to the PEG_{24}-ligands alone. Transfection resulted in background levels when using LUC-coding polyplexes (monoDBCO-PEG_{24}-GE11/LUC and bisDBCO-PEG_{24}-GE11/LUC) thus demonstrating that iodide uptake is indeed NIS-mediated. The outcome of our therapy study matched closely the results of the PET imaging study. The effective therapeutic cytoreduction achieved after treatment with targeted monoDBCO-PEG_{24}-GE11/NIS polyplexes followed by ^{131}I application resulted in a significant decrease of tumor growth as compared to the two control groups monoDBCO-PEG_{24}-GE11/NIS plus NaCl and NaCl only. The non-targeted polyplexes (monoDBCO-PEG_{24}/NIS) showed an uptake of ^{124}I only slightly above background levels in the imaging study. Accordingly, mice treated with these non-targeted polyplexes followed by ^{131}I in the therapy study showed a mild delay in tumor growth as compared to the other two control groups. These observations in tumor growth behaviour during therapy were mirrored by animal survival. The *ex vivo* analysis of NIS protein expression showed a heterogeneous, patchy transgene expression pattern *in vivo* after polyplex-mediated transfection. Nevertheless, the ^{131}I therapy resulted in a significant therapeutic effect. This is attributed to the bystander effect

of the beta-emitter ^{131}I, which is able to compensate heterogeneous tumoral NIS expression due to the range of approximately 2.4 mm of the beta particles.[26,27,100,101] This is one of the major advantages of *NIS* as therapy gene and makes the approach highly effective.[24] *Ex vivo* staining for blood vessel density demonstrated a long-term antiangiogenic therapeutic effect of ^{131}I treatment. The vascularization status of a tumor influences the growth rate. A highly vascularized tumor grows more rapidly while low vascularization decelerates tumor growth.[102] The tumors of the therapy group showed the lowest blood vessel density, delayed growth and a trend towards lower cell proliferation as determined by Ki67 staining.

In summary, our work clearly shows the potential of post-functionalized targeted polyplexes for *NIS* gene therapy of GBM using the EGFR targeting ligand GE11. During the last decade, it has been shown that glioblastomas comprise a group of highly heterogeneous tumor types including mutations, rearrangements and genetic alterations of EGFR.[87] EGFR amplification is acquired by glioblastoma cells early in tumorigenesis and substantially contributes to the invasive process.[87] In a study of van den Bent *et al.*, ~84 % of the evaluated GBMs were considered to retain their EGFR amplification at the time of tumor recurrence.[103] As amplification of tumoral EGFR is essential for the success of our personalized therapy approach, EGFR expression is optimally assessed pre-therapeutically as part of the molecular tumor profiling. The theranostic approach of the *NIS* gene therapy offers the major advantage of non-invasive monitoring of the efficacy of EGFR-targeted *NIS* gene delivery before a therapeutic dose of radioiodide is applied as demonstrated in our preclinical *in vivo* studies. Furthermore, the use of DBCO click chemistry provides the opportunity to quickly design polyplexes based on the genetic differentiation and receptor status of the individual tumor. After biopsy and analysis of the molecular tumor profile, the polyplex design can be tailored via their targeting domain to provide a personalized and individual therapy. The application of alternative targeting ligands suitable for DBCO-click chemistry, is a further subject of ongoing work and can provide a broad spectrum of polyplexes for individualized therapy.

3.5. Material and methods

Cell culture

The GBM cell line U87 (CLS 300367, Cell line service GmbH, Eppelheim, Germany) was cultured in Dulbecco's modified eagle medium (DMEM; 1g/l glucose; Sigma Aldrich, St. Louis, Missouri, USA) supplemented with 1% (v/v) MEM nonessential amino acids (Thermo Fisher Scientific, Waltham, MA, USA). The GBM cell line LN229 (ATCC CRL-2611, American Type Culture Collection, Manassas, VA) was grown in Roswell Park Memorial Institute (RPMI)-1640 culture medium (Sigma Aldrich) supplemented with 1% (v/v) sodium pyruvate (ThermoFisher Scientific). The follicular thyroid carcinoma cell line FTC-133 (94060902, Sigma-Aldrich) was cultured in DMEM/F12 (Sigma Aldrich) supplemented with 1% (v/v) L-glutamine (Sigma Aldrich). The human breast cancer cell line MCF-7 (ATCC HTB-22) was grown in minimum essential eagle medium eagle (MEM; Sigma Aldrich) supplemented with 1% (v/v) L-glutamine (Sigma Aldrich), 1% (v/v) sodium pyruvate (ThermoFisher Scientific) and 5 µg/ml insulin (Sigma Aldrich). 10% (v/v) fetal bovine serum (FBS Superior, Sigma Aldrich) and 1% (v/v) penicillin/streptomycin (Sigma-Aldrich) were added to all media. The patient-derived GBM cell line GBM14 was cultured in DMEM/F12 (Sigma Aldrich) supplemented with 1% (v/v) penicillin/streptomycin (Sigma Aldrich), B-27™ Supplement (Thermo Fisher Scientific), 10 ng/ml human EGF (PeproTech, Hamburg, Germany) and 10 ng/ml human FGF (PeproTech). All cells were passaged at 70% confluency and maintained at 37 °C, 5% CO_2 and a relative humidity of 95%. The culture medium was replaced every 48 h.

Synthesis of plasmids, carrier and DBCO agents

The NIS cDNA was synthesized and optimized by GENEART (Regensburg, Germany) based on the plasmid pCpG-hCMV-Luc. The establishment of the expression vector pCpG-hCMV-NIS has previously been described in detail.[62] The pNIS-DNA and pCMVLuc[104] (encoding a Photinus pyralis luciferase under control of the cytomegalovirus promoter) that were applied in all *in vitro* and *in vivo* experiments were produced and purified by Plasmid Factory GmbH (Bielefeld, Germany).

The T-shaped OAA ***1252*** was synthesized via standard Fmoc SPPS as described previously.[56,89]

The shielding and EGFR targeting agents, bearing one or two DBCO units as attachment sites for orthogonal click-reaction, were synthesized as described previously.[89,91]

Polyplex formation

The final pDNA concentration was 10 µg/ml for cell transfection experiments and 200 µg/ml for *in vivo* experiments. The pDNA and the calculated amount of OAA at N/P 12 (protonatable nitrogen/phosphate ratio) were diluted separately in the same volume. The solvent was 20 mM HEPES buffer with 5% (w/v) glucose at pH 7.4 (HBG buffer). The pDNA solution was mixed in OAA solution by pipetting rapidly 10 times followed by an incubation period of 30 min at room temperature to form core-polyplexes. Ligands for post-modification were diluted in HBG buffer with an equivalence of 0.25.[82] The total volume of the diluted ligand was a quarter of the volume of the OAA-pDNA mixture. The ligand was added to the core polyplex solution after the incubation period by pipetting rapidly 10 times followed by further incubation for 4 h at room temperature.

Particle size and zeta potential measurement

DLS was performed on a Zetasizer Nano ZS (Malvern Instruments, Worcestershire, U.K.) to measure particle size and zeta potential of the polyplexes. Polyplexes were formed in 100 µl HBG buffer with a final DNA concentration of 200 µg/ml (*in vivo* condition). For zeta potential measurement, 700 µl HBG was added.

EGFR expression levels *in vitro*

Flow cytometry was performed to screen for EGFR expression levels on cell surfaces. U87, LN229, MCF-7 and FTC-133 were trypsinized and GBM14 were treated with Accutase® solution (Sigma Aldrich). 8×10^5 cells of each cell line were washed and resuspended in 100 µl phosphate-buffered saline (PBS) supplemented with 10% (v/v) FBS (FACS-buffer). An antibody for human EGFR detection (monoclonal mouse IgG1, clone H11, Dako, Glostrup, Denmark) or a negative isotype control antibody (abcam, Cambridge, UK) was added at a dilution of 1:200 and the samples were incubated for 1 h on ice. Subsequently, the cells were washed with FACS buffer and stained with an AlexaFluor 488 antibody at a dilution of 1:400 (Thermo Fisher Scientific) for 1 h on ice. Propidium iodide (Sigma Aldrich) was added at a dilution of 1:100 to exclude dead cells. Analysis was performed on a BD Accuri C6 flow cytometer (BD Bioscience, Franklin Lakes, USA). Cell aggregates or fractions were excluded by appropriate gating.

Transfection studies and ^{125}I uptake assay

Cells (U87, LN229, GBM14, MCF-7 and FTC-133) were seeded in 6-well plates and grown to 60-70% confluency. Medium was replaced by 400 µl/well serum- and antibiotic-free medium. 200 µl/well monoDBCO-PEG$_{24}$-GE11/NIS or bisDBCO-PEG$_{24}$-GE11/NIS polyplex solutions with a DNA concentration of 10 µg/ml were added and the cells were incubated for 4 h at 37 °C before medium was changed to normal growth medium. As negative controls, ligands without the targeting domain (monoDBCO-PEG$_{24}$/NIS or bisDBCO-PEG$_{24}$/NIS) or LUC-coding polyplexes (monoDBCO-PEG$_{24}$-GE11/LUC or bisDBCO-PEG$_{24}$-GE11/LUC) were applied. The EGFR-specific antibody cetuximab (Erbitux®, Merck, Darmstadt, Germany) was added in different concentrations (0.5, 1.5, 2.5, 3.5 mg/ml) 15 min prior to the cell treatment with monoDBCO-PEG$_{24}$-GE11/NIS polyplexes. Furthermore, the NIS-specific inhibitor perchlorate (1 mM of potassium perchlorate; Merck) was added as an additional control. 24 h after transfection, NIS-mediated ^{125}I uptake was examined as described previously [26,33]. Results are normalized to cell survival and specified as cpm/A620 (cpm: counts per minute) (for cell viability assay see below).

Cell viability assay

Commercially available MTT-reagent (3-(4,5-dimethylthiazol-2-yl)-2,5-diphenyltetrazolium bromide) (Sigma Aldrich) was added 24 h after transfection and cells were incubated for 1 h at 37 °C. For cell lysis, 10% dimethyl sulfoxide in isopropanol with an incubation time of 15 min at room temperature was used. The measurement was performed on a Sunrise microplate absorbance reader (Tecan, Männedorf, Switzerland) at a wavelength of 620 nm.

Establishment of intracranial U87 tumors *in vivo*

6- to 7-week-old female CD-1 nu/nu mice (Charles River, Sulzfeld, Germany) were anesthetized and immobilized and a skin incision was made on the top of the skull. Mice were mounted onto a stereotactic head holder (David Kopf Instruments, Tujunga, Canada) in the flat-skull position. A hole was carefully drilled into the skullcap 1 mm anterior and 1.5 mm lateral to the bregma with a 21G cannula. A blunt syringe with an injection volume of 1 µl (22G Hamilton syringe, Hamilton, Reno, Nevada, USA) was inserted 4 mm deep and retracted to 3 mm depth. 1 µl U87 cell suspension (1×10^5 cells/µl PBS) was injected slowly (over 2 min) into the brain before the syringe was removed carefully within 2 further minutes. The area of injection was the right caudate putamen. The skin incision was stitched with surgical thread (Johnson & Johnson, New Brunswick, New Jersey, USA) and mice were kept warm while

awaking. Mice were treated with Metacam (0.5 mg/kg) pre- and postoperatively to reduce pain and the risk of inflammation. Animals were maintained with access to mouse chow and water *ad libitum* and under specific pathogen-free conditions. More than 15% weight loss or signs of ill health (impairment of breathing, drinking, eating or cleaning behavior) led to sacrifice. All experimental protocols were authorized by the regional governmental commission for animals (Regierung von Oberbayern) and meet the requirements of the German Animal Welfare Act.

In vivo PET imaging studies after systemic *NIS* gene transfer

3.5-4 weeks after i.c. tumor cell inoculation, polyplexes (monoDBCO-PEG_{24}-GE11/NIS and bisDBCO-PEG_{24}-GE11/NIS polyplexes for EGFR targeting, non-targeted monoDBCO-PEG_{24}/NIS and bisDBCO-PEG_{24}/NIS polyplexes, monoDBCO-PEG_{24}-GE11/LUC and bisDBCO-PEG_{24}-GE11/LUC containing pCMVLuc as additional negative control) with a DNA dose of 2.5 mg/kg (for a 20 g mouse: 50 µg DNA in a total volume of 250 µl, solvent: HBG) were applied systemically via the tail vein. 24 h or 48 h later, mice received 10 MBq of ^{124}I (Perkin Elmer, Waltham, Massachusetts, USA or DSD Pharma, Purkersdorf, Austria) as NIS PET tracer by i.v. injection and NIS-mediated iodide accumulation in tumor areas was determined by small-animal PET (Inveon, SIEMENS Preclinical Solutions, Erlangen, Germany). Serial scanning took place 1 h, 3 h and 5 h after ^{124}I application. Results were assessed with the software Inveon Acquisition Workplace (Siemens, Munich, Germany), analyzed using Inveon Research Workplace (Siemens) and are represented as percentage of the injected dose per ml tumor (% ID/ml). Mice were pretreated with L-thyroxine (L-T4; 5mg/ml, Sigma Aldrich) in their drinking water 10 days before imaging to reduce thyroidal iodide uptake and at the same time mouse chow was changed to low iodine diet (ssniff Spezialdiäten GmbH, Soest, Germany).

Mouse brain tissue preparation

After anesthesia and thorax incision, mice were perfused transcardially with 1× PBS followed by 4 % formaldehyde solution. The brain was explanted and fixed in 4 % formaldehyde solution for 48 h at room temperature and stored in 1× PBS at 4 °C for further preparation. Liver, spleen, kidney and lung were collected as control organs under the same procedure.

Immunohistochemical EGFR staining

Immunohistochemistry of tumor tissues derived from mice used for the imaging study, was performed using a Bond RXm system (Leica, Wetzlar, Germany, all reagents from Leica) with

an EGFR antibody (clone E235, 1:100, ab32077, abcam). Briefly, slides were deparaffinized and pretreated with Epitope retrieval solution 1 (EDTA buffer pH 6) before the diluted primary antibody was applied for 15 min. Antibody binding was detected with a polymer refine detection kit without post primary agent and visualized with Diaminobenzidin as a dark brown precipitate. Counterstaining was done with hematoxylin. A positive control was included in each run. The stained slides were scanned with an automated slide scanner (Leica Biosystems, Wetzlar, Germany, AT-2) and the Aperio Imagescope software (version 12.3, Leica Biosystems) was used to take representative images. The receptor expression level was evaluated by a veterinary pathologist.

Tumor volume estimation *ex vivo*

Tumors were cut in axial sections with a microtome. Twenty transverse layers with defined anatomical characteristics were selected with the help of a mouse brain atlas.[105] The interval between selected brain sections was 0.32-0.52 mm. Hematoxylin and Eosin (H&E) staining was performed according to standard protocol, slides were scanned, all sections containing tumor were taken into consideration and the tumor area (A) was determined by encircling the tumor (Aperio Imagescope software). The average area was calculated ($A_{average}=A_{total}/N$ (number of selected sections)) and the height of the tumor (H) was considered as the interval between the first and last section containing tumor. The final tumor volume (mm^3) is the multiplication of $A_{average}$ (mm^2) and H (mm).[106]

Only mice bearing a GBM with a size >30 mm^3 were considered in the *in vivo* PET imaging studies. There was no significant difference in mean tumor sizes between control and experimental groups: The groups that received targeted polyplexes had a mean tumor size of 44.6 ± 5.1 mm^3 (monoDBCO-PEG_{24}-GE11/NIS 48 h), 51.2 ± 6.0 mm^3 (monoDBCO-PEG_{24}-GE11/NIS 24 h) and 57.6 ± 8.6 mm^3 (bisDBCO-PEG_{24}-GE11/NIS), while those treated with non-targeted polyplexes developed tumors of 43.9 ± 2.9 mm^3 (monoDBCO-PEG_{24}/NIS) and 43.9 ± 6.2 mm^3 (bisDBCO-PEG_{24}/NIS) in size. Animals treated with LUC-coding polyplexes had tumors with a mean size of 71.5 ± 10.0 mm^3 (monoDBCO-PEG_{24}-GE11/LUC) and 42.7 ± 8.9 mm^3 (bisDBCO-PEG_{24}-GE11/LUC).

Immunohistochemical staining of NIS protein

Paraffin-embedded tumor and control organ samples were immunohistochemically stained as described previously.[107] A primary mouse monoclonal NIS-specific antibody (Merck Millipore; dilution 1:500) was incubated on tissue samples for 60 min at room temperature, followed by a biotin-SP-conjugated goat antimouse IgG antibody (Jackson ImmunoResearch, West Grove,

Pennsylvania, USA; dilution 1:200) for 20 min and peroxidase-conjugated streptavidin (Jackson ImmunoResearch; dilution 1:300) for a further 20 min. Scanning was performed as described above.

Radioiodide therapy study *in vivo*

Starting 5 days after i.c. tumor cell inoculation, tumor growth was assessed twice a week by high resolution MRI. A visible tumor in one slice with a diameter between 0.8-1.3 mm was used as inclusion parameter (day 0). Therapy trials were started the day after. To this end, therapy mice were treated systemically with monoDBCO-PEG_{24}-GE11/NIS followed by an i.p. injection of 55.5 MBq ^{131}I (GE Healthcare, Braunschweig, Germany) 48 h later. The therapy trial was repeated for three times, thus i.v. polyplex injection took place on days 1/5/9 and i.p. ^{131}I injections were performed on days 3/7/11. Accordingly, control mice received monoDBCO-PEG_{24}/NIS followed by ^{131}I or monoDBCO-PEG_{24}-GE11/NIS followed by saline (NaCl), or NaCl i.v. followed by NaCl i.p., respectively. Once, at least one endpoint criterion was met (>15 % weight loss, impairment of breathing, drinking, eating or cleaning behavior, self-isolation from the group), monitored by independent animal care personnel blind to treatment and hypothesis, mice were sacrificed.

MRI was acquired with a small animal 7 T preclinical scanner (Agilent Discovery MR901 magnet and gradient system, Bruker AVANCE III HD electronics running ParaVision software release 6.0.1). A birdcage quadrature volume resonator (inner diameter 72 mm, RAPID Biomedical, Rimpar, Germany) was used for 300 MHz RF transmission and a rigid-housing two-channel surface receiver coil array (RAPID Biomedical) was placed over the mouse heads. Animals were screened for tumor growth with a T2-weighted RARE (rapid acquisition with relaxation enhancement) sequence, with a repetition time of 2.5 s, an effective echo time of 40 ms, 8 echoes per excitation, an acquisition matrix 192×192, an in-plane resolution of 0.104×0.104 mm^2, 1 average, and 7 slices with a thickness of 1 mm. The oblique coronal (horizontal) slices were tilted to be parallel with the brain anterior-posterior axis, which was tilted anterior-down due to mouse positioning under the coil. Images were exported in a Digital Imaging and Communications in Medicine (DICOM) format for analysis with the DICOM viewer RadiAnt (Medixant, Poznan, Poland). The tumor area of each slice was encircled and RadiAnt provided the size in mm^2. The tumor volume was calculated using the same formula as for *ex vivo* tumor volume estimation (see above).

Ex vivo immunofluorescence assay

U87 GBMs from therapy mice were prepared as described above. 2 days after post-fixation in PFA, the brains were left in 30 % sucrose at least for 24 h at 4 °C. Freezing was performed by embedding the tissue in Cryomatrix (Leica). Frozen tumor sections were stained with an antibody against Ki67 (abcam; dilution 1:200) for cell proliferation and CD31 (BD Pharmingen, Heidelberg, Germany; dilution 1:100) for blood vessel density as described previously.[66] The stained tumor sections were scanned with the Pannoramic MIDI digital slide scanner and pictures were taken using Caseviewer software (3DHISTECH Ltd., Budapest, Hungary). For quantification 4 visual fields (20× magnification) per tumor were chosen and analyzed with ImageJ software (NIH, Bethesda, MD).

Statistical methods

All *in vitro* experiments were performed at least in triplicates and results are shown as mean ± SEM, mean fold change ± SEM and percent for survival plots. Two-tailed Student's *t*-test was used to prove statistical significance.

For therapy studies, differences in tumor growth were tested by one-way ANOVA followed by post-hoc Fisher's LSD or Games Howell. Mouse survival is presented in a Kaplan-Meier-plot and statistical significance was tested by log-rank. Statistical significance was defined as *p* values <0.05 (**p*<0.05; ***p*<0.01; ****p*<0.001).

3.6. Acknowledgements

The authors want to thank Dr. Sissy M Jhiang (Ohio State University, Columbus, OH, USA) for supplying the full length human NIS cDNA. We owe special thanks to Sybille Reder, Markus Mittelhäuser, Hannes Rolbieski, Sandra Sühnel, Dr. Geoffrey Topping and Jakob Allmann (Department of Nuclear Medicine, Klinikum rechts der Isar, Technical University of Munich, Munich, Germany) for their assistance and support in performing the imaging and therapy studies. We are grateful to Olga Seelbach and her team (Institute of Pathology, School of Medicine, Technical University of Munich, Munich, Germany) for preparation of paraffin embedded slides and the H&E and EGFR staining. We appreciate the help from Prof. Dr. Gabriele Multhoff and Dr. Stefan Stangl (Center for Translational Cancer Research, Klinikum rechts der Isar, Technical University of Munich, Munich, Germany) for establishing the orthotopic glioblastoma mouse model in our group. Furthermore, we thank Prof. Dr. Julia Mayerle, Dr. Ivonne Regel and Dr. Ujjwal Mahajan for allowing us to use their lab equipment.
This work was supported by a grant from the Deutsche Forschungsgemeinschaft within the Collaborative Research Center SFB 824 to C.S. (project C8) and to F.S. (project Z3), SFB 1032 to E.W. (project B4), as well as within the Priority Program SPP1629 to C.S. and P.J.N. and by a grant form the Wilhelm Sander-Stiftung to C.S. and P.J.N. (2014.129.1). R.G. and R.E.K. gratefully acknowledge funding by the DFG (GL691/2; SFB824-B2) and the Anni-Hofmann Stiftung.

4. Dual EGFR- and TfR-targeted gene transfer improves efficacy of sodium iodide symporter (*NIS*) gene therapy of glioblastoma

Rebekka Spellerberg[1], Teoman Benli-Hoppe[2], Carolin Kitzberger[1], Nathalie Schwenk[1], Özgür Öztürk[2], Katja Steiger[3], Gabriele Multhoff[4], Matthias Eiber[5], Franz Schilling[5], Wolfgang A Weber[5], Roland E Kälin[6,7], Rainer Glass[6,7,8], Peter J Nelson[1], Ernst Wagner[2], Christine Spitzweg[1,9,*]

[1]Department of Internal Medicine IV, LMU University Hospital Munich, LMU Munich, Munich, Germany, [2]Pharmaceutical Biotechnology, Department of Pharmacy, Centre for System-Based Drug Research, and Centre for Nanoscience, LMU Munich, Munich, Germany, [3]Institute of Pathology, School of Medicine, Technical University of Munich, Munich, Germany, [4]Center for Translational Cancer Research, Radiation Immuno-Oncology Group, School of Medicine, Klinikum rechts der Isar, Technical University Munich, Munich, Germany, [5]Department of Nuclear Medicine, School of Medicine, Klinikum rechts der Isar, Technical University Munich, Munich, Germany, [6]Neurosurgical Research, Department of Neurosurgery, University Hospital, LMU Munich, Munich, Germany, [7]Walter Brendel Center of Experimental Medicine, Faculty of Medicine, LMU Munich, Munich, Germany, [8]German Cancer Consortium (DKTK), partner site Munich and German Cancer Research Center (DKFZ), Heidelberg, Germany, [9]Division of Endocrinology, Diabetes, Metabolism and Nutrition, Mayo Clinic, Rochester, Minnesota, USA

[Manuscript submitted]

4.1. Abstract

Sodium iodide symporter (*NIS*) gene transfer for active accumulation of iodide in tumor cells is a powerful theranostic strategy facilitating both diagnostic and therapeutic application of radioiodide. In glioblastoma (GBM), the blood brain barrier (BBB) presents an additional delivery barrier for nucleic acid nanoparticles. In the present study, we designed dual-targeted NIS plasmid DNA complexes containing targeting ligands for the transferrin receptor (TfR) and the epidermal growth factor receptor (EGFR), thus providing the potential for active transport across the BBB followed by targeting of tumor cells. *In vitro* ^{125}I transfection studies confirmed TfR- and EGFR-dependent transfection efficiency and NIS-specific iodide uptake of dual-targeted polyplexes. *In vivo* gene transfer in mice bearing orthotopic U87 GBM xenografts was assessed at 48 h after intravenous polyplex injection by PET imaging using ^{18}F-labelled tetrafluoroborate (TFB) as tracer. The tumoral ^{18}F-TFB uptake of mice treated with dual-targeted polyplexes (0.56 ± 0.08% ID/ml) was significantly higher as compared to mice treated with EGFR-mono-targeted (0.33 ± 0.03% ID/ml) or TfR-mono-targeted (0.27 ± 0.04% ID/ml) polyplexes. In therapy studies, application of ^{131}I induced a superior therapeutic effect of the dual-targeted therapy, demonstrated by a significant delay in tumor growth and prolonged survival **(Figure 14)**.

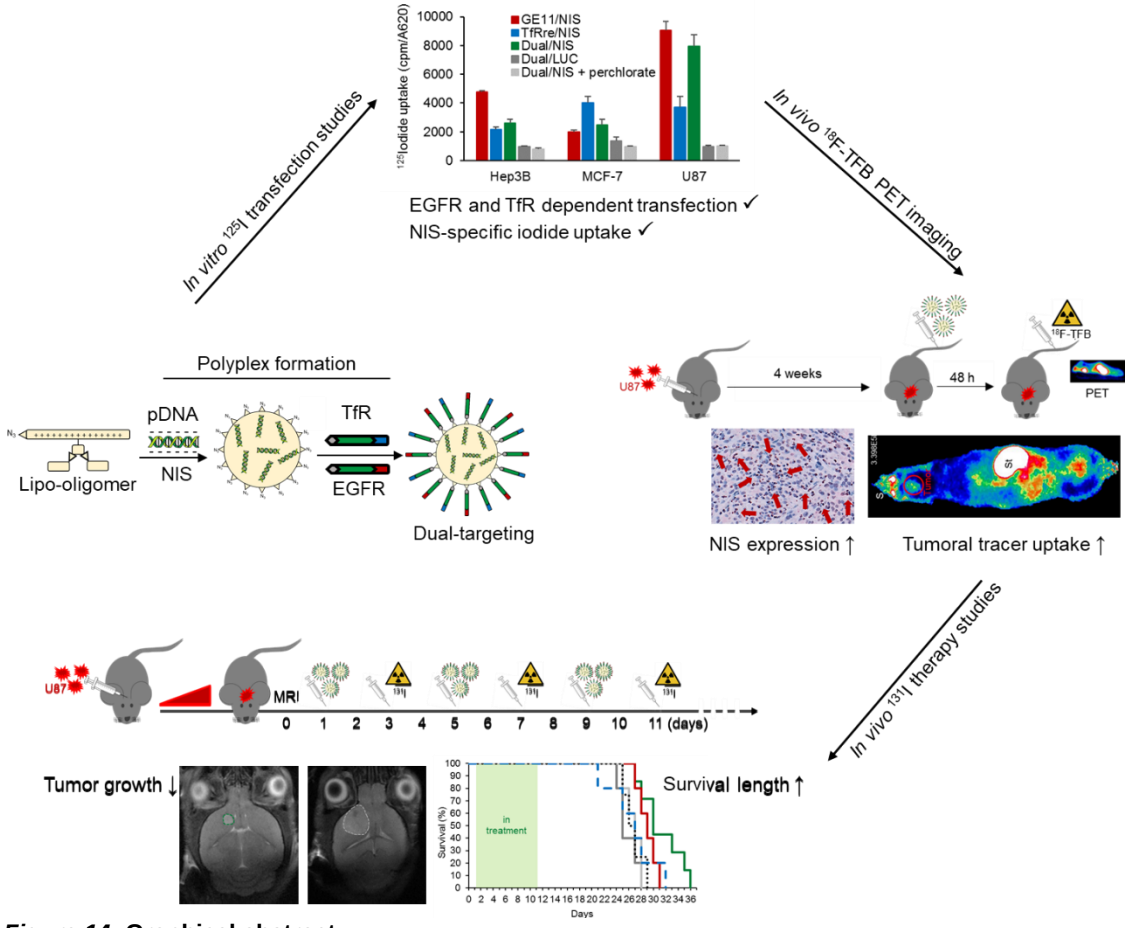

Figure 14: **Graphical abstract.**

4.2. Introduction

Cloning of the sodium iodide symporter (*NIS*) gene in 1996 provided a powerful tool for cytoreductive gene therapy. As an intrinsic plasma glycoprotein NIS imports iodide into thyroid follicular cells by an active transport mechanism.[30] The use of *NIS* as a theranostic gene has been applied for over 80 years in the management of differentiated thyroid cancer.[108] Functional NIS expression allows the accumulation of radionuclides such as ^{123}I, ^{124}I, ^{99m}Tc or ^{18}F-TFB (TFB: tetrafluoroborate) that facilitates non-invasive diagnostic imaging through scintigraphic or positron emission tomography (PET) imaging techniques and provides the possibility of dosimetric calculations.[24] In addition to serving as a reporter gene, *NIS* allows the application of therapeutic radionuclides (^{131}I, ^{188}Re) that facilitates cytotoxic destruction of tumor tissue through the radionuclide trapping activity of NIS expressing cells and the bystander effect induced by the crossfire effect of beta emission.[21,25] The extensive clinical experience with radioiodide imaging and treatment in differentiated thyroid cancer patients is now being translated to non-thyroidal cancers. Our initial studies focused on prostate cancer using adenovirus-mediated human *NIS* gene delivery *in vivo.*[33,34,36] Since then, our group has focussed on the optimization and expansion of *NIS*-based gene therapy, establishing modified viruses, mesenchymal stem cells and targeted polyplexes as effective gene delivery vehicles for systemic application. To date, we have successfully introduced *NIS* into hepatocellular carcinoma, neuroblastoma, colorectal cancer liver metastases, anaplastic thyroid carcinoma and pancreatic ductal adenocarcinoma.[27,44-49,57,58,62-66,68,78-81,100,109-111] In these studies, high levels of *NIS* transgene expression resulted in a delay in tumor growth and prolonged survival in *in vivo* ^{131}I or ^{188}Re therapy trials. These pilot studies formed the backdrop for refocusing these technologies for the potential treatment of glioblastoma (GBM), a therapeutically challenging and aggressive tumor.

GBM is the most common and a highly aggressive primary brain tumor. Current GBM therapy involves surgical resection, external beam radiation and temozolomide, however, theses approaches remain largely palliative.[112] Due to its aggressive nature, patient survival is on average less than 15 months after diagnosis, with a survival of more than 3 years considered long-term survival.[70,113] One of the challenges that make GBM notoriously difficult to target is the blood brain barrier (BBB) that limits the effectiveness of systemic therapies. The BBB is characterized by tight junctions between the endothelial cells in brain capillaries, low vesicular transport, high metabolic activity and an extensive variety of efflux pumps.[114] This environment represents an active and highly restrictive barrier that protects the central nervous system and provides the basis for optimal neuronal function. Most biotechnologically produced therapeutics are not able to cross the BBB.[115] In high-grade gliomas and brain metastases the blood brain tumor barrier (BBTB) can be compromised in its integrity and might be more leaky

as compared to the intact BBB. Nevertheless, the BBTB presents an additional barrier for systemic treatment of brain tumors.[116] By reengineering pharmaceutical compounds to make them suitable for receptor- mediated transcytosis (RMT), a well-known mechanism for crossing the BBB, the active uptake from blood into brain becomes possible.[117] The transferrin receptor (TfR) is expressed on brain endothelial cells to import iron conjugated with transferrin and is one of the major targeting receptors for RMT. Synthetic non-viral gene delivery systems can be functionalized with a specific TfR ligand for BBB penetration to introduce the *NIS* gene therapy as a therapy concept to GBM.[118-120]

The gene shuttle system used here includes sequence-defined cationic lipo-oligoaminoamides (OAAs) required for stable plasmid DNA (pDNA) complexation through electrostatic interaction.[56] Due to their novel design incorporating an azido functional group, ligands containing dibenzocyclooctyne (DBCO) can be added for potential functionalization via copper-free click reaction. In addition to the masking of positive charges using monodisperse polyethylene glycol (PEG), the surface functionalization by addition of peptidic ligands is used for targeting purposes.[89] In earlier studies, we have convincingly demonstrated the enormous potential of epidermal growth factor receptor (EGFR)-targeted polyplexes for tumor-specific delivery.[58,62-66] In our most recent study, we have already shown successful GBM targeting using EGFR-mono-targeted polyplexes that led to a significant increase in tumoral iodide uptake as evidenced by *in vivo* PET imaging, and a sharp decrease in tumor growth that was accompanied by a significant prolongation of survival in the therapy group.[121] The present study evaluated a combinatorial strategy to generate a dual-targeted gene transfer vehicle. It was designed to overcome the BBB through inclusion of the ligand TfRre, a 12-amino acid small protease-resistant retro-enantio peptide that binds the TfR,[120] thereby facilitating transport across the BBB which was recently applied as a targeting agent for pDNA and siRNA delivery by Benli-Hoppe *et al.*[122] The combination of this technology with EGFR targeting using the allosteric EGFR-specific ligand GE11 led to enhanced targeting and therapeutic potential.

4.3. Results

Polyplex formation and characterization

NIS polyplexes **(Figure 15)** were formed with 10 µg/ml pDNA by first complexing with the T-shaped lipo-OAA *1252* into nanoparticles **(Figure 15A)**,[56] followed by surface modification with shielding and targeting reagents DBCO-PEG_{24}-GE11 and/or DBCO-PEG_{24}-TfRre **(Figure 15B)** using azido/DBCO click chemistry as previously described.[91,122] For surface shielding a monodisperse PEG moiety with 24 oxyethylene units (PEG_{24}) was introduced and the GE11 peptide was applied for EGFR targeting and the TfRre peptide for TfR targeting. In this manner, either mono-targeted NIS polyplexes (GE11/NIS, TfRre/NIS) **(Figure 15C,D)** or dual-targeted polyplexes containing both ligands (Dual/NIS) **(Figure 15E)** were prepared. Transmission electron microscopy (TEM) images were taken of Dual/NIS **(Figure 15F)**, GE11/NIS **(Figure 15G)** and TfRre/NIS **(Figure 15H)** polyplexes. Polyplexes were generally spherical **(Figure 15F-H)** and sizes as measured by TEM revealed a range of 25-32 nm **(Figure 15I)**. The characterization by dynamic light scattering (DLS) yielded approximate dimensions of 42-48 nm (size by numbers) and the polydispersity indexes (PDIs), an indicator of the heterogeneity of particle sizes, were all below 0.3 reflecting a narrow and uniform size distribution **(Figure 15I)**. Zeta potential measurements were assessed by DLS to determine surface charge of polyplexes. A slightly positive surface charge is desired to meet the balancing act between sufficient cellular uptake and no aggregation with biomacromolecules. All formulation displayed a zeta potential of 13-17 mV **(Figure 15J)**.

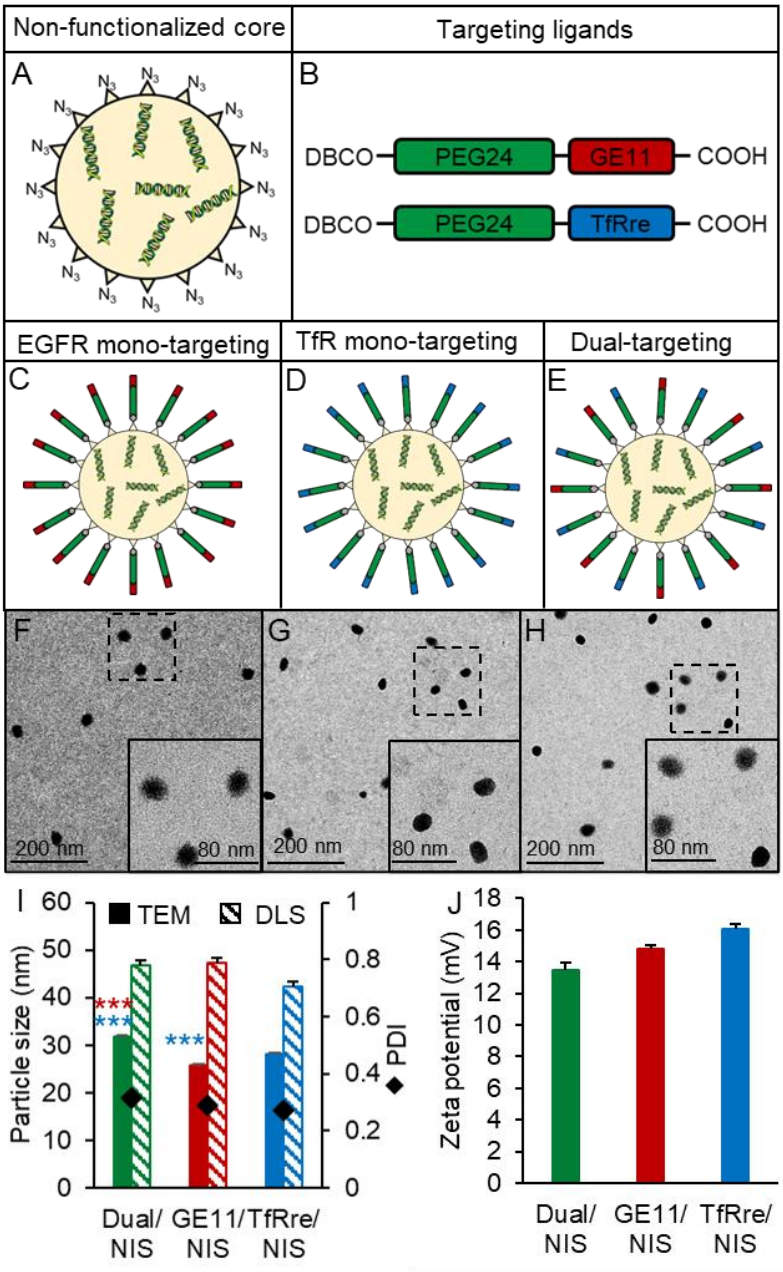

***Figure 15*: Polyplex characterization.** The sequence-defined cationic lipo-OAA containing an N-terminal azido group complexed NIS pDNA (N/P ratio of 12) to build an azido bearing core (A). Structures are shown of PEGylated DBCO-agents containing the GE11 peptide to target tumoral EGFR or TfRre peptide to target transferrin receptors (B). Ligands were added with 0.25 equivalents to build EGFR mono-targeted (C) or TfR mono-targeted polyplexes (D). For dual-targeted polyplexes 0.125 equivalents of DBCO-PEG$_{24}$-GE11 and 0.125 equivalents of DBCO-PEG$_{24}$-TfRre were used (E). TEM images are shown of DBCO-PEG$_{24}$-Dual/NIS (F), DBCO-PEG$_{24}$-GE11/NIS (G) and DBCO-PEG$_{24}$-TfRre/NIS polyplexes (H) revealing spherical shapes and narrow size distribution. One representative image of each group is shown (scale bar 200 µm, close-up 80 µm). TEM measurements revealed a size of 25-32 nm and DLS measurements a size of 42-48 nm (size by numbers) with a uniform size distribution (PDI ≤ 0.3) (I) and a positive surface charge below 20 mV (J) (*p ≤ 0.05, ***p ≤ 0.001). Results are reported as mean ± SEM (n=3). DLS measurements were performed by Teoman Benli-Hoppe (Department of Pharmacy, Pharmaceutical Biotechnology, LMU) and TEM measurements by Özgür Öztürk (Department of Pharmacy, Pharmaceutical Biotechnology, LMU).

Polyplex-mediated *NIS* gene transfer *in vitro*

Cell-surface EGFR and TfR expression levels were determined on the human hepatocellular cancer cell line Hep3B, human breast cancer cell line MCF-7, and human GBM cell line U87 by flow cytometry. Hep3B cells showed positive EGFR expression and a minor level of TfR expression, the MCF-7 cells expressed very low levels of EGFR and a high density of TfR. The U87 cells showed high expression levels for both receptors **(Figure 16A)**. Cell transfection studies were performed using GE11/NIS polyplexes for EGFR-targeted transfection, TfRre/NIS polyplexes for TfR-targeted transfection, Dual/NIS polyplexes for dual-targeted transfection and Dual/LUC polyplexes as negative control containing a non-NIS expressing plasmid. Results of the ^{125}I uptake studies indicated that transfection efficiency of the polyplexes

correlated with levels of cell surface receptor expression. EGFR-positive Hep3B cells showed 6.1-fold higher iodide uptake 24 h after GE11/NIS polyplex treatment as compared to background levels, while TfRre/NIS polyplex treatment resulted in 2.5-fold uptake levels **(Figure 16B)**. Respective outcomes were observed using TfR-positive MCF-7 cells: No efficient transfection was observed using GE11/NIS polyplexes, but ^{125}I uptake was 4.4-fold increased after transfection with TfRre/NIS polyplexes **(Figure 16B)**. U87 cells, expressing both surface receptors, showed 9.5-fold increased ^{125}I uptake after GE11/NIS polyplex treatment and a 3.8-fold increase after TfRre/NIS polyplex transfection. The treatment with GE11/NIS led to a 2.4-fold increased iodide uptake as compared to TfRre/NIS **(Figure 16B)**. Dual/NIS polyplexes showed high transfection efficiency in U87 cells with a 7.9-fold increased iodide uptake and moderate transfection efficiency in Hep3B cells with a 3.5-increased iodide uptake **(Figure 16B)**. Using luciferase (LUC)-coding polyplexes (Dual/LUC) or adding the NIS-specific inhibitor perchlorate iodide uptake resulted in background levels **(Figure 16B)**. All results were normalized to cell survival and polyplex treatment of cells had no impact on cell survival **(Figure 16C)**.

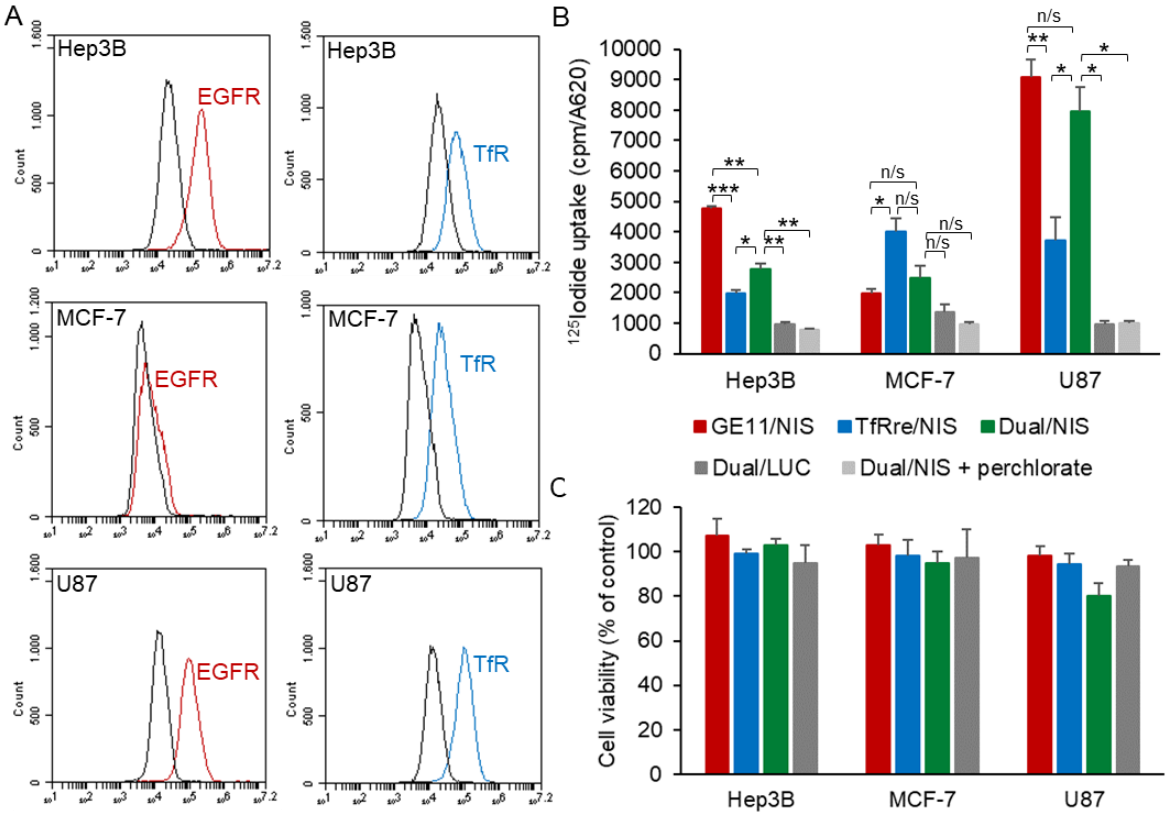

Figure 16: **Polyplex-mediated *NIS* gene transfer *in vitro*.** Cell surface receptor expression of EGFR and TfR was measured by flow cytometry. A specific antibody monitored the expression levels of human EGFR and TfR on Hep3B, MCF-7, and U87 cells as compared to isotype controls (A). ^{125}I cell transfection studies (n=3 for each cell line) showed EGFR- and TfR-specific transfection efficiency of targeted polyplexes (GE11/NIS, TfRre/NIS) (B). Dual/NIS polyplexes showed transfection efficiency in Hep3B and U87 cells (B). Background radiation levels after control transfection with LUC-coding polyplexes (Dual/LUC) or the addition of NIS specific inhibitor perchlorate proved NIS dependency of iodide uptake (B) (*p ≤ 0.05, **p ≤ 0.01). Cell viability of Hep3B, MCF-7, and U87 was not affected by polyplex treatment (C). Results are reported as mean ± SEM.

Systemic *NIS* gene transfer *in vivo*

Functional tumoral NIS expression was assessed in an orthotopic GBM (U87) xenograft mouse model after systemic polyplex injection. Mice received polyplexes 23-26 days after intracranial U87 cell inoculation and 48 h later high-resolution PET was performed using in-house synthesized ^{18}F-labelled TFB as tracer. Robust tumoral radionuclide uptake was found in mice treated with Dual/NIS **(Figure 17A)**, GE11/NIS **(Figure 17B)**, and TfRre/NIS polyplexes **(Figure 17C)**, as evidenced by strong signals in the brain area. The strongest signal was seen in the group that received dual-targeted polyplexes **(Figure 17A)**. No tumoral ^{18}F-TFB uptake above background levels was measured in mice that were injected with LUC-coding polyplexes as control (Dual/LUC) **(Figure 17D)**. Due to physiological NIS expression, the salivary glands, stomach, and mammary glands normally accumulate NIS substrates. In the quantitative analysis, tumors of mice that received dual-targeted NIS polyplexes showed a significantly higher tracer uptake of 0.56 ± 0.08% ID/ml as compared to tumors from mice injected with GE11/NIS polyplexes, which exhibited an uptake of 0.33 ± 0.03% ID/ml, or injected with TfRre/NIS polyplexes, revealing an uptake of 0.27 ± 0.04% ID/ml **(Figure 17E)**. MR **(Figure 17F)** and PET images **(Figure 17G)** of axial tumor slices are shown and their co-registration **(Figure 17H)** displayed the high congruence of PET signal localization in the tumor area assessed by MRI.

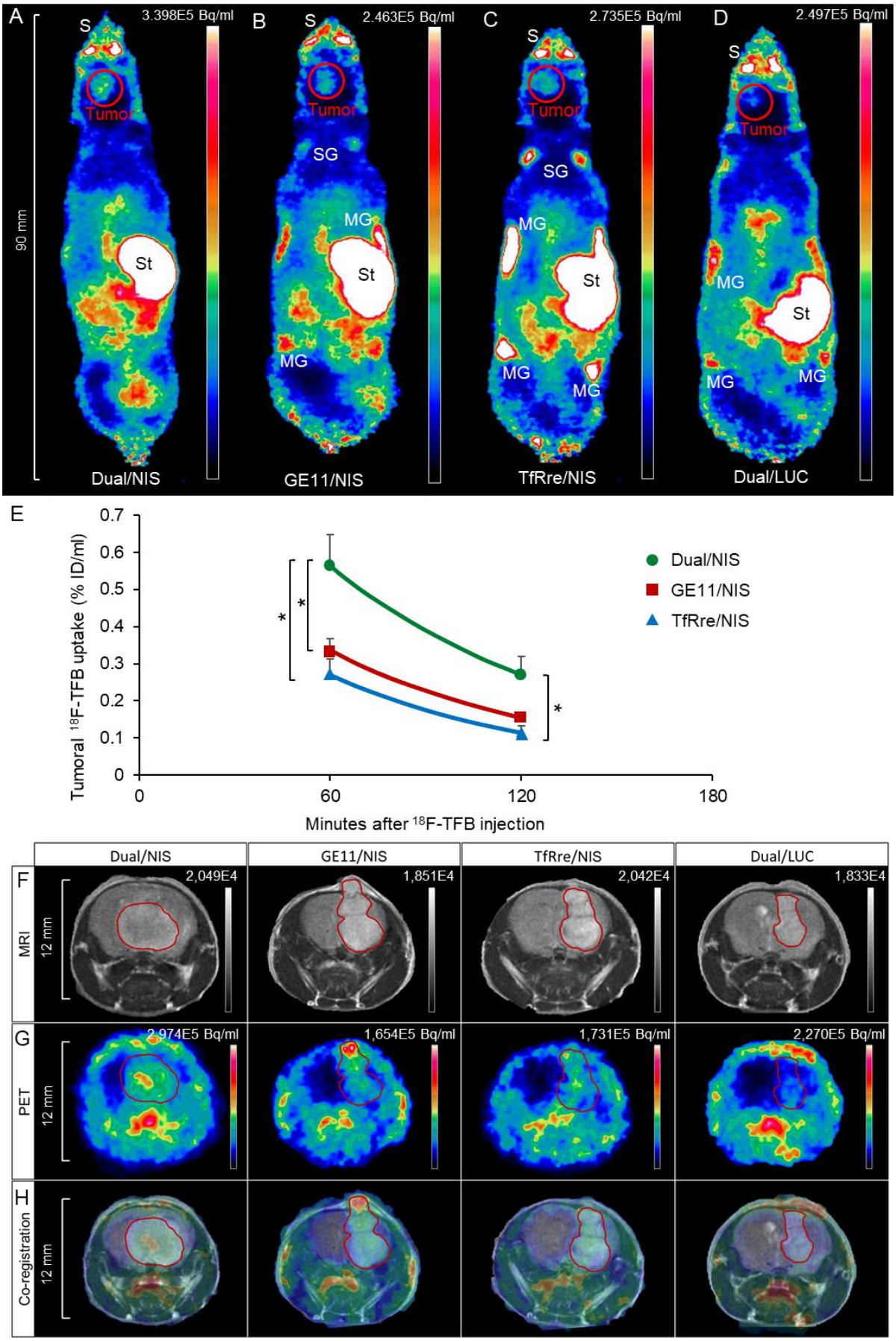

(Legend on next page)

Figure 17: **Polyplex-mediated *NIS* gene transfer *in vivo.*** U87 GBM bearing mice were treated with polyplexes and 48 h later ^{18}F-TFB PET imaging was performed by serial scannings over 120 min. Tumoral tracer uptake was significantly higher in mice treated with Dual/NIS polyplexes (n=6) (A) as compared to GE11/NIS (n=6) (B) or TfRre/NIS (n=5) polyplexes (C). Mice treated with GE11/NIS showed a trend towards higher tumoral tracer accumulation as compared to mice administered with TfRre/NIS (B,C). No tumoral tracer uptake above background levels was measured in mice injected with Dual/LUC polyplexes (n=3) (D). One representative image is shown for each group. Quantitative analysis is presented as the percentage of the injected dose per milliliter tumor (E) (*p ≤ 0.05). Axial MR images (F), and axial PET images (G) of GBMs are shown and co-registrated (H) to demonstrate signal localization in the tumor area. One representative tumor slice is shown for each group. Results are reported as mean ± SEM. Tumor signal is encircled in red. (S, nasal secretion, snout; St, stomach; SG, salivary glands; MG, mammary glands)

Ex vivo analysis of NIS protein expression by immunohistochemistry

After tissue preparation, tumor sections were analyzed by immunohistochemical staining using an anti-NIS monoclonal antibody. Tumor sections derived from mice that received Dual/NIS **(Figure 18A)**, GE11/NIS **(Figure 18B)**, or TfRre/NIS **(Figure 18C)** polyplexes showed NIS-expressing tumor cells throughout the tumor sections (red), with the dual-targeted polyplex-treated tumors showing a trend toward higher number and expanded areas of NIS protein expression. Quantitative analysis of four visual fields per tumor revealed 3.73 ± 1.46% NIS expressing cells in tumor sections of mice that received Dual/NIS polyplexes, 1.75 ± 0.24% in tumor sections of GE11/NIS treated mice and 0.58 ± 0.28% in tumor sections of TfRre/NIS injected mice. Immunohistochemical staining of tumor sections from control animals that received Dual/LUC polyplexes showed no NIS-specific immunoreactivity **(Figure 18D)**. In tissue sections of control organs (liver **(Figure 18E)**, spleen **(Figure 18F)**, kidney **(Figure 18G)** and lung **(Figure 18H)** of mice treated with Dual/NIS polyplexes, no NIS expression was detected.

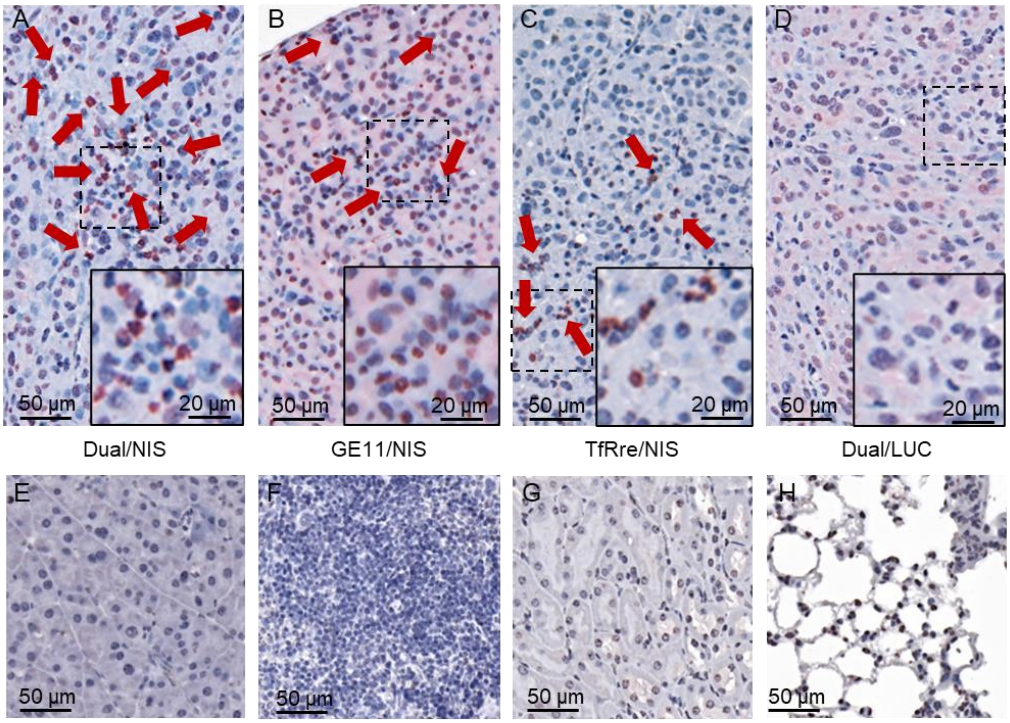

(Legend on next page)

Figure 18: ***Ex vivo*** **analysis of NIS protein expression.** Immunohistochemical staining of NIS protein in GBM xenografts embedded in paraffin showed positive NIS expression (red) in mice treated with targeted NIS polyplexes (A-C). GBM sections of mice treated with Dual/NIS polyplexes revealed a trend towards higher amounts of NIS positive cells (A) as compared to mice injected with GE11/NIS (B) or TfRre/NIS polyplexes (C). No positive NIS staining in tumors of mice that received Dual/LUC as control polyplexes (D). Liver (E), spleen (F), kidney (G) and lung (H) sections of a mouse treated with Dual/NIS did not show any NIS expression. One representative image with 20× original magnification is shown for each group (scale bar: 50 µm). A 40× original magnification was chosen for the close up (scale bar: 20 µm).

^{131}I therapy studies *in vivo*

Based on the results of the imaging studies, GBM bearing mice were then injected i.v. with Dual/NIS (n=7), GE11/NIS (n=5) or TfRre/NIS (n=5) followed by ^{131}I application (55.5 MBq) 48 h later. This application cycle was repeated three times in 4-day intervals. In parallel, control groups received LUC-coding Dual/LUC polyplexes plus ^{131}I, Dual/NIS polyplexes followed by saline or saline only. Tumor growth was monitored by high-resolution magnetic resonance imaging (MRI) twice a week. All three therapy groups showed a significant delay in tumor growth as compared to control groups with the dual-targeted NIS polyplex therapy group showing the most prominent tumor growth inhibition **(Figure 19A**, day 21 of therapy trial is shown) as compared to mice treated with GE11/NIS polyplexes **(Figure 19B**; non-significant) or mice injected with TfRre/NIS polyplexes **(Figure 19C**, significant, $*p \leq 0.05$). All control groups showed an aggressive tumor growth (Dual/LUC + ^{131}I **(Figure 19D)**, Dual/NIS + NaCl **(Figure 19E)** and NaCl + NaCl **(Figure 19F)**). The significant delay of tumor growth **(Figure 19G)** resulted in a significant extension of survival of the Dual/NIS + ^{131}I and GE11/NIS + ^{131}I group **(Figure 19H)** with a trend toward survival advantage of mice treated with Dual/NIS polyplexes followed by ^{131}I as compared to animals which received GE11/NIS polyplexes followed by ^{131}I. The slight delay in tumor growth in mice administered with TfRre/NIS + ^{131}I had no impact on survival time. On day 29, the last control mouse was sacrificed based on the animal welfare protocol, while 40% of the GE11/NIS and 57% of the Dual/NIS therapy group were still alive.

The results were further validated by staining of proliferation status and blood vessel density **(Figure 20A-F)**. The two therapy groups Dual/NIS and GE11/NIS showed a significantly lower number of Ki67-positive cells **(Figure 20G)** and a significantly smaller area of CD31 positivity **(Figure 20H)** as compared to TfRre/NIS and negative control groups.

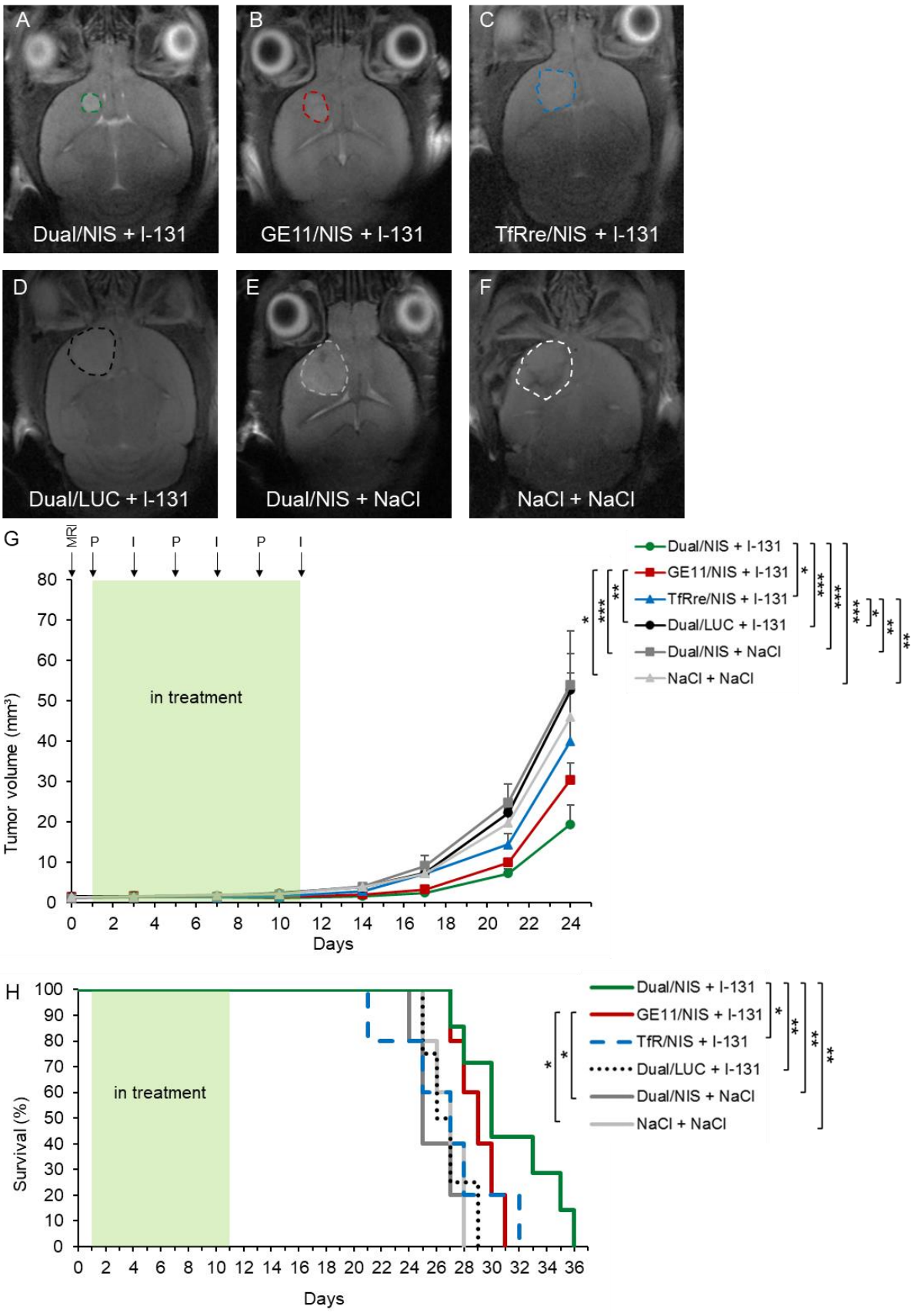

(Legend on next page)

Figure 19: **^{131}I therapy studies *in vivo*.** GBM-bearing mice were included in therapy trial once tumor volume reached ≥ 1mm³, confirmed by MRI on day 0. Mice were treated with three cycles of i.v. injection of polyplexes on days 1, 5, and 9 followed by i.p. injection of 55.5 MBq ^{131}I 48 h later (respectively days 3, 7, and 11). Tumor volume was monitored twice a week by MRI. Exemplary MR images of tumor sizes on day 21 of the therapy trial from each group are shown: Dual/NIS + ^{131}I (n=7) (A), GE11/NIS + ^{131}I (n=5) (B), TfRre + ^{131}I (n=5) (C), Dual/LUC + ^{131}I (n=4) (D), Dual/NIS + NaCl (n=5) (E) and NaCl + NaCl (n=5) (F). Tumors are encircled. Injection of Dual/NIS, GE11/NIS and TfRre/NIS polyplexes followed by ^{131}I led to significant delay in tumor growth as compared to the negative control groups Dual/LUC + ^{131}I, Dual/NIS + NaCl or Saline only (G). Administration of Dual/NIS + ^{131}I revealed a trend towards a delay in tumor growth as compared to GE11/NIS + ^{131}I and a significant delay as compared to TfRre + ^{131}I (G) (*p ≤ 0.05, **p ≤ 0.01, ***p ≤ 0.001). Therapy mice treated with Dual/NIS + ^{131}I showed a significant extension of survival as compared to TfRre/NIS + ^{131}I and all three negative control groups. Administration of GE11/NIS + ^{131}I led to a significant extension as compared to injection of Dual/NIS + NaCl and NaCl + NaCl (**p ≤ 0.05, **p ≤ 0.01). Results are reported as mean ± SEM.

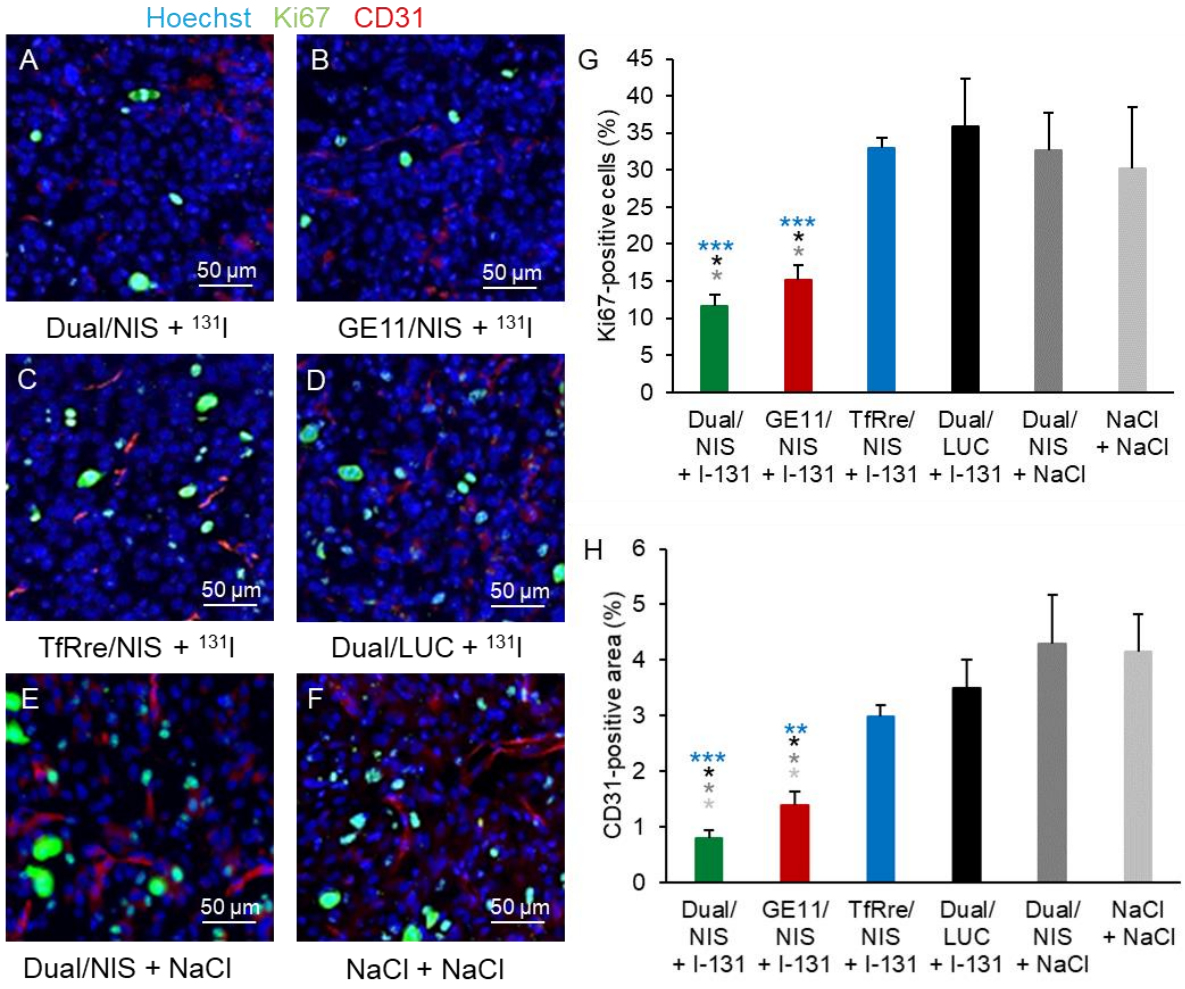

Figure 20: ***Ex vivo* analysis of cell proliferation index and blood vessel density of therapy tumors.** Frozen tissue sections from GBM of the therapy study were prepared and stained for Ki67 (green) for cell proliferation index and CD31 (red) for blood vessel density. Hoechst (blue) was used for nuclei staining. The two therapy groups Dual/NIS (A) and GE11/NIS (B) followed by ^{131}I showed significantly less Ki67-positive cells and significantly smaller CD31-positive area as compared to TfRre/NIS + ^{131}I (C) and negative control groups (Dual/LUC + ^{131}I (D), Dual/NIS + NaCl (E), NaCl only (F)). Quantitative analysis for cell proliferation index (G) and blood vessel density (H) are shown (*p ≤ 0.05, **p ≤ 0.01, ***p ≤ 0.001). One representative picture of each group is shown at 20× magnification (scale bar 50 µm). Results are reported as mean ± SEM (for each group n=4).

4.4. Discussion

The blood brain barrier (BBB) represents a major challenge in developing effective therapeutics for brain diseases. This is true not only for neurodegenerative diseases, such as Alzheimer's, Huntington's, and Parkinson's diseases, but also for brain malignancies, such as glioblastoma. Brain microvascular endothelial cells supported by pericytes, astrocytes, tight junctions, neurons, and the basement membrane ensure the blockage of all large molecules and 98% of small molecules into the brain at sufficient therapeutic levels.[115] During GBM development, tumor neo-vasculature is formed and neo-capillaries exhibit small fenestrations. Therefore, the permeability of the blood brain tumor barrier (BBTB) is altered and small sized nanocarriers may pass through such areas. With further tumor growth, inter-endothelial gaps are formed and the BBTB is progressively disrupted compromising the vascular integrity.[123] However, it is suggested that initially occurring GBM cells and residual tumor cells infiltrating to brain parenchyma are populated behind an intact BBB and are not barely reached by passive targeting.[124] These invasive tumor cells and tumor associated stromal cells are drivers of tumor recurrence, highlighting the urgent need of active BBB transfer of therapeutic compounds to treat early-stage tumors and reach invasive cell populations.[125,126]

In the past decade nanoparticles have become a major research focus based on their flexible composition allowing them to be tailor-made for site specific drug delivery. Polyplexes, i.e. complexes of pDNA with synthetic sequence-defined cationic subunits, as used in the present study, enable the chemical evolution of a precisely defined medicine.[122]

Targeted delivery of nucleic acid polyplexes is a complicated process involving multiple extracellular and intracellular barriers.[116] Physiochemical characteristics of polyplexes can affect biological distribution, cellular uptake, penetration into biological barriers, and resultant therapeutic effects, highlighting the importance of size, surface charge, and shape of the nanoparticles. Optimally designed polyplexes show a size of around 20 -75 nm to ensure sufficient blood circulation and escape from the removal processes found in lung, liver, spleen, and kidney and also allow efficient tissue penetration.[12] Larger particles and agglomerates above 2 µm are captured by pulmonary capillary vessels leading to toxicity issues.[93] In our studies, TEM images showed homogenous and spherical-shaped nanoparticles for Dual/NIS, GE11/NIS and TfRre/NIS in the range of 25-32 nm. The characterization by DLS showed a size ranged between 42-48 nm and a low PDI (≤ 0.3) confirming a narrow size distribution. The apparent discrepancy in size, identified by TEM and DLS, was previously observed and can be explained by fixation/dehydration for TEM and the high sensitivity of DLS for minor fractions of aggregates. No NIS positive cells were detected off-target in liver, spleen, kidney, or lung tissue by immunohistochemical staining. To avoid self-aggregation and aggregation with biomacromolecules, a monodisperse PEG moiety with 24 oxyethylene units was introduced

for surface shielding, which was previously shown to be suitable for the *in vivo* targeting of related polyplexes.[68,84,85] Positively charged nanoparticles are more easily internalized than neutral and negatively charged nanoparticles. They are also more efficiently taken up by proliferating cells. Interestingly, cationic nanoparticles were found to specifically attach to tumor vasculature due to negatively charged glycoproteins on the luminal side of tumor endothelium.[127,128] Therefore, a slightly positive surface charge (< 20 mV) is desired.[93] DLS characterization of Dual/NIS, GE11/NIS and TfRre/NIS polyplexes displayed a zeta potential of 13-17 mV.

The polyplexes encapsulated an expression plasmid for the sodium iodide symporter (*NIS*) gene. NIS is a well-characterized iodide symporter and implemented as standard care in the treatment of differentiated thyroid cancer for more than 80 years.[23] It is a self-protein, originated in thyrocytes, with no cell toxicity or immunogenicity. NIS actively accumulates a wide range of substrates, such as ^{123}I,^{124}I, ^{99m}Tc, TFB, ^{131}I and ^{188}Re.[24] Therefore, NIS polyplexes are part of nanotheranostics facilitating diagnostic and monitoring features, such as γ-scintigraphy, single-photon emission computed tomography and positron emission tomography (PET), as well as the application of beta emitting radionuclides for a therapeutic purpose.[24] In our study, we took advantage of the imaging function of NIS expression using three-dimensional ^{18}F-TFB PET offering to visualize NIS-expressing cells with high resolution and sensitivity. The ^{18}F-labelled TFB represents a novel PET-based tracer that can deliver clear images with an excellent target-to-background ratio.[24,38] A well delineated tumor signal in the PET images displayed high congruence with localization of the tumor area using MR images.

A further notable characteristic of nanoparticles is the ability to enhance its bioavailability by the conjugation of specific targeting ligands onto the surface of the polyplexes.[12] In the present study, we used the well-characterized ligand GE11 for EGFR targeting and the TfRre peptide for TfR targeting. Both ligands proved to be highly specific and effective in single targeting experiments.[58,62-65,120-122]

In *in vitro* cell transfection, we showed EGFR- and TfR-dependent transfection efficiency. GE11/NIS polyplexes showed high transfection efficiency in EGFR-positive Hep3B and U87 cells while there was an only minor iodide uptake in EGFR-negative MCF-7 cells. Similar specificity was observed when using the TfRre/NIS peptide: High transfection efficiency was seen in the TfR-positive MCF-7 and U87 cells, while a low transfection efficiency was found in the low TfR expressing Hep3B cells. The results of U87 cell transfection using GE11/NIS and TfRre/NIS indicate an advantageous transfection efficacy of GE11 polyplexes as compared to TfRre polyplexes. Dual-targeted polyplexes showed high transfection efficiency in U87 cells and moderate transfection efficiency in Hep3B cells suggesting that in the context of the dual targeting approach the main effect of tumor cell transfection may arise from the EGFR targeting by the GE11 ligand. For all three cell lines transfection resulted in only background levels when

using LUC-coding control polyplexes or in the presence of the NIS-specific inhibitor perchlorate, thus demonstrating that iodide uptake is indeed NIS mediated.

The TfR is abundant in the endothelial cells lining brain vasculature and has been shown to be a suitable receptor for transcytosis.[117] The biodistribution of radiolabeled transferrin conjugated liposomes for 5-fluorouracil delivery was previously investigated in rats and brain uptake was increased by 13 times as compared to non-conjugated liposomes.[129] Pardridge et al. demonstrated BBB transfer of a tritium engineered humanized monoclonal antibody against the human TfR1 ([^{3}H]-hTfRMAb), which crossreacted with the primate TfR, in a primate model. The brain uptake at 2 h after i.v. injection of [^{3}H]-hTfRMAb was 1.1% ID/100 g. Capillary depletion analysis showed that the majority of the vascular bond antibody had passaged across the BBB into brain parenchyma by 2 h after administration.[119] The TfR targeting peptide TfRre used in our present study was initially identified by phage display, interacts with the receptor at a binding site different from that of transferrin to avoid competition, in order to increase metabolic stability a retro-enantio version of the peptide was used.[120] Prades et al. showed the capacity of TfRre to travel through the BBB using an *in vitro* cellular transwell model. Various types of cargos have been attached to the N-terminal region of the peptide and the capacity of the constructs to cross the cellular BBB model was evaluated. Further validation of the penetration of the cargo-peptide constructs was performed in living mice using intravital two-photon microscopy and confirmed by *ex vivo* confocal laser scanning microscopy of sectioned brain slices.[120]

Successful *NIS* gene therapy of GBM mediated by EGFR-mono-targeted GE11 polyplexes was recently shown by our group.[121] Building on these results, we refined the surface functionalization by adding the TfR targeting peptide TfRre to facilitate active transport of the NIS polyplexes across the BBB. EGFR-amplified glioblastoma cells can be highly invasive and therefore, they are partly detected in areas with an intact BBB[87] emphasizing the promising concept of combining the GE11 peptide with the TfRre peptide for sequential targeting.

Quantitative analysis of PET imaging revealed a significantly higher tumoral tracer uptake in mice treated with dual-targeted polyplexes as compared to groups injected with mono-targeted GE11 or TfRre polyplexes. Immunohistochemical staining confirmed tumoral NIS protein expression in the groups treated with Dual/NIS, GE11/NIS or TfRre/NIS with the highest number of NIS positive cells and expanded areas of NIS-specific immunostaining in tumor sections of mice treated with dual-targeted polyplexes. The results obtained from the imaging studies were mirrored by the outcome of the therapy study. Mice treated with Dual/NIS, GE11/NIS or TfRre/NIS polyplexes followed by ^{131}I 48 h later showed a significant delay in tumor growth as compared to negative controls (Dual/LUC + ^{131}I, Dual/NIS + NaCl, NaCl only). Dual-targeted polyplexes led to a significantly slower tumor growth as compared to TfR-targeted polyplexes and a trend toward slower tumor growth as compared to EGFR-targeted

polyplexes. The delay in tumor growth also led to a significantly prolonged survival for Dual/NIS and GE11/NIS treated mice. The slightly decreased tumor growth in the TfR-targeted polyplex-treated group had no impact on survival time, thus matching the lowest *in vivo* transfection efficiency as demonstrated by the non-invasive PET imaging studies. In accordance with these findings, mice treated with Dual/NIS and GE11/NIS polyplexes followed by ^{131}I showed less proliferating cells as determined by Ki67 staining and reduced blood vessel density measured at the end of the therapy study suggesting a long term-antiangiogenic effect of ^{131}I.

The beneficial effect of the dual targeting strategy may further arise in parts from simultaneously targeting of two receptors resulting in enhanced particle uptake by receptor crosslinking and triggering enhanced endocytosis and particle uptake into the lysosome.[66,130] Therefore, the dual-targeted polyplexes address concurrently two major obstacles in optimizing GBM treatment strategies, crossing actively the BBB and addressing tumor heterogeneity.

However, TfR-mono-targeted polyplexes can potentially act as both a BBB crossing and a glioma targeting nanocarrier, but they showed the lowest tumoral tracer uptake in PET imaging despite high TfR expression in U87 cells, suggesting that in the context of the dual targeting approach the TfRre peptide worked mainly as a BBB shuttle and the GE11 peptide was indeed required for a solid antitumoral effect.

Although, the U87 mouse model is a widely used GBM mouse xenograft model for proof-of-principle studies, it does not faithfully represent BBTB characteristics of the majority of GBM patients due to a relatively large extent of BBTB disruption.[131] In order to have a more accurate prediction of clinical outcome of novel therapeutic strategies, mouse models using patient derived GBM cells better mimic the invasive and infiltrative nature of human GBM.[132] Also, genetically engineered mouse models, which allow *de novo* tumor formation, more accurately provide functional tight junction proteins, transporters, or ECM components that are essential in BBB development and biology.[133] For a more robust and quantitative analysis of the superior efficacy of cascade targeting polyplexes in the context of *NIS* gene therapy, further experiments have to be performed in tumor models that more reliably reflect the invasive nature of GBM with a reproducible BBB. Optionally, other well described BBB ligands might be evaluated,[116] which, however, is beyond the scope of the current study.

In conclusion, this novel approach of dual targeting of TfR and EGFR for polyplex-mediated *NIS* gene delivery to GBM combines two crucial dual approaches: sequential targeting of two cascades in context of site-specific drug delivery resulting in increased *NIS* gene expression in the tumor lesion, in synergy with the theranostic function of NIS enhancing safety by molecular imaging of biodistribution and gene expression levels and allowing targeted NIS-based radioiodide therapy. Our results highlight the potential of the efficient dual-targeted NIS

lipopolyplexes as a promising concept for future clinical translation of the *NIS* gene therapy in the field of nanotheranostics.

4.5. Material and methods

Cell lines

The human GBM cell line U87 (CLS 300367, Cell Line Service GmbH, Eppelheim, Germany) was cultured in Dulbecco's modified Eagle's medium (DMEM; 1 g/L glucose; Sigma Aldrich, St. Louis, MO) supplemented with 1% (v/v) MEM non-essential amino acids (Thermo Fisher Scientific, Waltham, MA). The human breast cancer cell line MCF-7 (ATCC HTB-22) was grown in minimum essential Eagle's medium (MEM; Sigma Aldrich) and 1% (v/v) L-glutamine (Sigma Aldrich), 1% (v/v) sodium pyruvate (Thermo Fisher Scientific), and 5 µg/ml insulin (Sigma Aldrich) were added. The human hepatocellular cancer cell line Hep3B (HB-8064; American Type Culture Collection (ATCC), Manassas, VA, UDA) was cultured in Dulbecco's modified Eagle's medium (DMEM; 1 g/L glucose; Sigma Aldrich) supplemented with 1% (v/v) MEM nonessential amino acids (Thermo Fisher Scientific), 1% (v/v) sodium pyruvate (Thermo Fisher Scientific), and 1% (v/v) L-glutamine (Sigma-Aldrich). We added 10% (v/v) fetal bovine serum (FBS Superior, Sigma Aldrich) and 1% (v/v) penicillin/streptomycin (Sigma Aldrich) to all media. All cells were maintained at 37° C, 5% CO2, and a relative humidity of 95%. The culture medium was replaced every 48 h and cells were passaged at 70% confluency.

Plasmid, carrier and DBCO-agents synthesis

The synthesis and optimization of the NIS cDNA was performed by GENEART (Regensburg, Germany) based on the plasmid pCpG-hCMV-Luc. The establishment of the expression vector pCpG-hCMV-NIS has been described in detail previously.[62] The production and purification of the plasmids pNIS-DNA and pCMVLuc (encoding a Photinus pyralis LUC under control of the cytomegalo-virus promoter) was operated by Plasmid Factory GmbH (Bielefeld, Germany). The T-shaped lipo-OAA *1252* was synthesized via standard Fmoc SPPS as described previously.[56] The EGFR and TfR targeting agents containing PEG_{24} as shielding domain and one DBCO unit as attachment site for orthogonal click reaction were synthesized as described previously.[91,122]

Polyplex formation

The final pDNA concentration was 10 µg/ml for *in vitro* experiments and 200 µg/ml for *in vivo* studies. The amount of OAA was calculated at N/P 12 (protonatable nitrogen/phosphate ratio). The solvent was 20 mM HEPES (Sigma Aldrich) buffer with 5% (w/v) glucose (Roth, Karlsruhe, Germany) at pH 7.4 (HBG buffer). pDNA and OAA were diluted in HBG buffer to the same volume. The pDNA solution was mixed in OAA solution by pipetting rapidly 10 times, followed by 30 min incubation at room temperature to form core polyplexes. Ligands for post-modification were diluted in HBG buffer with an equivalence of 0.25. For the dual-targeted polyplex, the equivalence of 0.25 was composed of 0.125 eq. GE11 and 0.125 eq TfRre. The total volume of the diluted ligand was one-quarter of the volume of the OAA-pDNA mixture. The ligand was added to the core polyplex solution by pipetting rapidly 10 times, followed by further incubation for 4 h at room temperature.

Particle imaging by Transmission Electron Microscopy (TEM)

Polyplexes (pDNA concentration 10 µg/ml) were formed in water instead of HBG. The preparation of carbon coated copper grids (Ted Pella, Inc. USA, 300 mesh, 3.0 mm O.D.) and the staining procedure was performed as described previously.[122] All grids were analyzed with a JEOL JEM-1100 (JEOL, Tokyo, Japan) electron microscope at 80 kV acceleration voltage.

Particle size and zeta potential measurements

Particle size and zeta potential of polyplexes were measured by dynamic light scattering on a Zetasizer Nano ZS (Malvern Instruments, Worcestershire, UK). Polyplexes were formed in 100 µl HBG buffer with a final pDNA concentration of 10 µg/ml. 700 µl HBG was added before zeta potential measurement. Detailed measurement parameters were described previously.[122] Results are presented by analysis of size by numbers.

Flow cytometry analysis

Flow cytometry was performed to analyze EGFR and TfR expression levels on cell surfaces. U87, MCF-7, and Hep3B were trypsinized and 8×10^5 cells each were washed and resuspended in 100 µl PBS containing 10% (v/v) FBS (FACS buffer). For EGFR expression, an antibody for human EGFR detection (monoclonal mouse IgG1, clone H11; Dako, Glostrup, Denmark) or a negative isotype control antibody (abcam, Cambridge, UK) was added at a dilution of 1:200 and the samples were incubated for 1 h on ice. Afterwards, the cells were

washed with FACS buffer and stained with an Alexa Fluor 488 anitbody at a dilution of 1:400 (Thermo Fisher Scientific) for 1 h on ice. For TfR expression, a FITC-labelled antibody for human CD71 detection (monoclonal mouse IgG1k, clone Ber-T9, Milli-Mark™, Millipore Corporation, Temecula, CA) or a FITC-labelled negative isotype control antibody (abcam) was added at a dilution of 1:10 and an incubation time of 1 h on ice was following. Propidium iodide (Sigma Aldrich) was utilized at a dilution of 1:100 to exclude dead cells. BD Accuri C6 flow cytometer (BD Bioscience, Franklin Lakes, NJ) was used for analysis and appropriate gating was conducted for exclusion of aggregated or fragmented cells.

^{125}I uptake assay

U87, MCF-7 and Hep3B cells were seeded in six-well plates and grown to 60%-70% confluency. Medium was changed to serum-, antibiotic- and supplement-free medium. 200 µl/well polyplex solution was added with a pDNA concentration of 10 µg/ml. DBCO-PEG-Dual/NIS, DBCO-PEG-GE11/NIS and DBCO-PEG-TfRre/NIS were added as targeting polyplexes, DBCO-PEG-Dual/LUC was added as negative control. Cells were incubated for 4 h at 37° C and subsequently the medium was replaced by normal growth medium. Cells were maintained overnight and 24 h after transfection, NIS mediated ^{125}I uptake was evaluated as described previously.[33] The NIS-specific inhibitor perchlorate (1mM potassium perchlorate; Merck, Darmstadt, Germany) was added as an additional control. Results are normalized to cell survival and specified as counts per minute (cpm/A620).

Cell viability assay

24 h after transfection, 3-(4,5-dimethylthiazol-2-yl)-2,5-diphenyl-tetrazolium bromide (MTT) reagent (commercially available, Sigma Aldrich) was applied followed by an incubation time of 1 h at 37° C. 10% dimethyl sulfoxide in isopropanol with an incubation time of 15 min at room temperature was used for cell lysis. The measurement was performed on a Sunrise microplate absorbance reader (Tecan, Männedorf, Switzerland) at a wavelength of 620 nm. Cell viability is presented as % of control (HBG).

Establishment of orthotopic U87 xenografts

U87 cells were intracranially implanted in six- to 7-week-old female CD-1 nu/nu mice (Charles River, Sulzfeld, Germany) using a stereotactic head holder (David Kopf Instruments, Tujunga, CA) as described in detail previously.[121] Animals were maintained with access to mouse chow and water ad libitum and under specific-pathogen-free conditions. More than 15% weight loss

or signs of ill health (impairment of breathing, drinking, eating, or cleaning behavior) led to sacrifice. All experimental protocols were authorized by the regional governmental commission for animals (Regierung von Oberbayern) and meet the requirements of the German Animal Welfare Act.

^{18}F-TFB synthesis

For synthesis of ^{18}F-TFB, the protocol published by Khoshnevisan et al. was followed.[134] Briefly, [18F]F^- in H_2O (starting activity 6 GBq), trapped on a preconditioned (first 0.9% NaCl (5 ml), then H_2O (10 ml)) quaternary methyl ammonium (QMA) ion exchange column (Sep-Pak® Light, Accell™ Plus QMA Carbonate, Waters, Wilmslow, UK), was eluted with 0.9% NaCl (0.5 ml) and dried under an argon stream at 95 °C and azeotropic distillation with acetonitrile (MeCN; Merck) (3 × 0.5 ml) was performed. 15-Crown-5 (24 mg) (Sigma Aldrich) in MeCN (0.5 ml) and Boron trifluoride diethyl etherate ($BF_3 \cdot OEt_2$; Sigma Aldrich) (1 µL) in MeCN (0.5 ml) were added and the mixture was heated to 80 °C for 10 min. After quenching with H_2O (8 ml), the reaction mixture was passed over preconditioned (H_2O (20 ml), acetone (20 mL), air (20 ml)) neutral alumina (Sep-Pak® Plus, Alumina N Cartridges, Waters, Wilmslow, UK) and QMA (preconditioning see above) cartridges in tandem. QMA cartridge was washed with H_2O (4 ml) and afterwards, the product was eluted from the QMA cartridge using 0.9% NaCl (0.5 ml). Quality check was performed using radio thin layer chromatography on a neutral alumina stationary phase (TLC aluminium sheets aluminium oxide 60 F254 neutral (type E) pre-coated, Merck) with methanol (100%) (J.T.Baker®, Avantor, Radnor, Pennsylvania, USA) as mobile phase. The TLC plates were scanned using a radioTLC imaging scanner (Mini-Scan, Eckert & Ziegler Radiopharma, Wilmington, Massachusetts, USA). The yield was 14.2 ± 1.2% with a purity of 97.5 ± 0.95%.

Tumoral ^{18}F-TFB uptake *in vivo*

25-30 days after i.c. U87 cell inoculation, mice were systemically i.v. injected with polyplexes (DBCO-PEG-Dual/NIS for dual-targeted *NIS* gene transfer, DBCO-PEG-GE11/NIS and DBCO-PEG-TfRre/NIS for mono-targeted *NIS* gene transfer, and DBCO-PEG-Dual/LUC as negative control). The pDNA dose was 2.5 mg/kg in a total volume of 250 µl and HBG was the solvent. 48 h later mice received 10 MBq of in-house synthesized ^{18}F-TFB as a NIS PET tracer via the tail vein. NIS-mediated ^{18}F-TFB accumulation in GBM areas was determined by small-animal PET/MRI (nanoScan®, Mediso, Budapest, Hungary). Serial scanning was performed 60 and 120 min after ^{18}F-TFB application. Results were assessed using Nucline Acquisition Software (Mediso) and were analyzed with Inveon Research Workplace (SIEMENS Preclinical

Solutions, Erlangen, Germany). 10 days before imaging, L-thyroxine (LT4; 5 mg/ml, Sigma Aldrich) was added to the drinking water of the mice to downregulate thyroidal NIS expression, and at the same time the mouse chow was changed to a low-iodine diet (ssniff Spezialdiäten GmbH, Soest, Germany).

Tumor volume was assessed by MRI during the scan. The tumor area of each slice was encircled and the size was provided in square millimeters. The average tumor area and tumor height were calculated ($A_{average}$ (mm^2) = A_{total} (mm^2) /$N_{number\ of\ sections\ containing\ tumor}$; H (mm) = $N_{number\ of\ sections\ containing\ tumor}$ * $T_{slice\ thickness}$ (mm)) followed by the calculation of the tumor volume: V_{tumor} (mm^3) = $A_{average}$ (mm^2) * H (mm). Only mice bearing a GBM with a size of >30 mm^3 were considered for the PET imaging analysis. There was no significant difference in the mean tumor sizes between the experimental groups: mice that received DBCO-PEG-Dual/NIS had a mean tumor size of 69.3 ± 11.8 mm^3, the group that was injected with DBCO-PEG-GE11/NIS had a mean tumor volume of 70.0 ± 13.5 mm^3 and DBCO-PEG-TfRre treated mice were bearing tumors with the mean size of 61.4 ± 10.9 mm^3.

Tissue preparation

After anesthesia and thorax incision, mice were perfused transcardially with 1× PBS followed by a 4% formaldehyde solution (PFA). Brain, liver, spleen, kidney, and lungs were explanted and fixed in 4% PFA for 48 h at room temperature and stored in 1× PBS at 4° C until paraffin embedding.

***Ex vivo* immunohistochemical NIS protein staining**

Paraffin-embedded tissue were rehydrated and incubated with a primary mouse monoclonal NIS-specific antibody (Merck Millipore; dilution 1:500) for 60 min at room temperature. Subsequently, a biotin-SP-conjugated goat antimouse IgG antibody (Jackson ImmunoResearch; West Grove, PA; dilution 1:200) was applied for 20min, followed by peroxidase-conjugated streptavidin (Jackson ImmunoResearch; dilution 1:300) for a further 20 min. The detailed protocol was described previously.[107] Scanning of stained sections was performed with the Pannoramic MIDI digital slide scanner and pictures were taken using Caseviewer software (3DHISTECH Ltd., Budapest, Hungary). Four visual fields (20× magnification) per tumor were chosen and analyzed with ImageJ software (NIH, Bethesda, MD) for quantification.

^{131}I therapy studies

Starting 5 days after i.c. U87 cell implantation, tumor growth was assessed twice a week by high-resolution MRI. A tumor volume of ≥ 1 mm³ was defined as inclusion parameter (day 0). Therapy trials were started 24 h later with a polyplex injection via the tail vein followed by an i.p. injection of 55.5 MBq ^{131}I (Rotop Pharmaka GmbH, Dresden, Germany) 48 h later. The therapy trial was repeated three times; i.v. polyplex injections were performed on days 1, 5 and 9 and i.p. ^{131}I injections were performed on days 3, 7 and 11. Therapy mice received DBCO-PEG-Dual/NIS, DBCO-PEG-GE11/NIS or DBCO-PEG-TfRre/NIS followed by ^{131}I. Control mice were treated with DBCO-PEG-Dual/LUC followed by ^{131}I or with DBCO-PEG-Dual/NIS followed by saline (NaCl), or with NaCl i.v. followed by NaCl i.p., respectively. >15% weight loss, impairment of breathing, drinking, eating, or cleaning behaviour, and self-isolation from the group were defined as endpoint criteria. Once at least one of those endpoint criteria was met, the mice were sacrificed.

MR-imaging was performed as described previously.[121] Briefly, MRI was acquired with a small animal 7T preclinical scanner (Agilent Discovery MR901 magnet and gradient system, Bruker AVANCE III HD electronics running ParaVision software release 6.0.1). A birdcage quadrature volume resonator (RAPID Biomedical, Rimpar, Germany) was used for 300 MHz RF transmission, and a rigid-housing two channel surface receiver coil array (RAPID Biomedical) was placed over the mouse's head. Animals were screened for tumor growth with a T2-weightened rapid acquisition with relaxation enhancement (RARE) sequence. 7 slices with a thickness of 1 mm were generated and images were exported in a Digital Imaging and Communications in Medicine (DICOM) format for analysis with the DICOM viewer RadiAnt (Medixant, Poznan, Poland). ROIs were visually determined. The tumor volume was calculated as described above.

Indirect immunofluorescence assay

The brains of therapy and control mice were prepared as described in the chapter tissue preparation. 48 hours after post-fixation in PFA, the organs were left in 30% sucrose for at least 24 h at 4°C. Afterwards, tissue was embedded in Cryomatrix (Leica) for freezing. Frozen tumor sections were stained with an antibody against Ki67 (abcam, dilution 1:200) for cell proliferation and CD31 (BD Pharmingen, Heidelberg, Germany; dilution 1:50) for blood vessel density as described previously.[66] Scanning was performed with the Pannoramic MIDI digital slide scanner and pictures were taken using Caseviewer software (3DHISZTECH Ltd.). Four visual fields (20× magnification) per tumor were chosen and analyzed with ImageJ software (NIH) for quantification.

Statistics

In vitro experiments were performed at least in triplicates and results are shown as mean ± SEM, mean fold change ± SEM, and percentage for survival plots. Two tailed Student's t test was used to prove statistical significance. Results of imaging studies are presented as % of injected dose per ml tumor and Two tailed Student's t test was used to prove statistical significance. For therapy studies, differences in tumor growth were tested by one-way ANOVA followed by post hoc Fisher's LSD. Mouse survival is presented in a Kaplan-Meier-plot and statistical significance was tested by log rank. Statistical significance was defined as a p value of <0.05 ($^*p < 0.05$; $^{**}p < 0.01$; $^{***}p < 0.001$).

4.6. Acknowledgements

The authors want to thank Markus Mittelhäuser, Sandra Sühnel, Sybille Reder and Jakob Allmann (Department of Nuclear Medicine, Klinikum rechts der Isar, Technical University of Munich, Munich,Germany) for their assistance and support in performing the imaging and therapy studies. We are grateful to Olga Seelbach and her team (Institute of Pathology, School of Medicine, Technical University of Munich, Munich, Germany) for preparation of paraffin-embedded slides. We want to acknowledge Susanne Kempter (Department of Physics, LMU Munich, Munich, Germany) for TEM measurements. We owe thanks to Dr. Stefan Stangl (Center of Translational Cancer Research, Klinikum rechts der Isar, Technical University of Munich, Munich Germany) for his help to establish the orthotopic glioblastoma mouse model in our group. Furthermore, we are grateful for the permission of Prof. Dr. Julia Mayerle, Dr. Yvonne Regel, and Dr. Ujjwal Mahajan to use their laboratory equipment and we thank Sissy M. Jhiang (Ohio State University, Columbus, OH, USA) for supplying the full-length human NIS cDNA.

This work was supported by a grant from the Deutsche Forschungsgemeinschaft within the Collaborative Research Center SFB 824 to C.S. (project C8), K.S. (project Z2) and F.S. (project Z3), as well as within the Priority Program SPP1629 to C.S. and P.J.N., and by the DFG research project WA 1648/7-1 to E.W., and by a grant from the Wilhelm Sander-Stiftung to C.S. and P.J.N. (2014.129.1). Ö.Ö. appreciate receiving a YLSY fellowship granted by Turkish Ministry of Education as support to his Ph.D. study.

This work was performed as partial fulfillment of the doctoral thesis of R.S. at the Faculty of Chemistry and Pharmacy of the LMU Munich.

5. Summary

Glioblastoma (GBM) is the most common and malignant type of primary brain tumors with a very poor prognosis and an urgent need for novel therapy options. Treatment difficulties encountered include the infiltrative nature of GBM, tumor heterogeneity and presence of the blood brain barrier (BBB) / blood brain tumor barrier (BBTB). Sequence-defined nanocarriers have become a major research focus for cancer therapy based in part on their flexible composition allowing them to be tailor-made for site specific drug delivery and to enable the chemical evolution of a precisely defined medicine. Functional expression of the theranostic sodium iodide symporter (*NIS*) gene allows non-invasive positron emission tomography (PET) imaging by application of ^{124}I or ^{18}F-labelled tetrafluoroborate and enables a cytoreductive therapy by application of β-emitters, such as ^{131}I. In the course of this thesis, novel targeted lipopolyplexes were established and applied in the context of the *NIS* gene therapy of GBM.

Initially, sequence-defined lipopolyplexes combined with the post-integration concept of shielding and targeting domains taking advantage of copper-free click chemistry were investigated in Prof. Dr. Wagner's laboratory. For the *NIS* gene therapy concept of GBM, epidermal growth factor receptor (EGFR)-targeted NIS lipopolyplexes were generated by utilizing the GE11 peptide domain and the resulting polyplexes were characterized and tested by dynamic light scattering and *in vitro* ^{125}I transfection studies using multiple cell lines expressing different levels of EGFR. EGFR-dependent transfection efficiency, an advantageous targeting effect by using GE11 and NIS-mediated iodide uptake were confirmed. To perform *in vivo* studies, an orthotopic xenograft mouse model was established for adequate reflection of the tumor milieu and thus allowing a realistic evaluation of the efficacy of the *NIS* gene therapy approach as a crucial prerequisite for clinical translation. In the ^{124}I PET imaging, tumor-selective transfection, the advantageous targeting effect of GE11 polyplexes and NIS dependent iodide uptake was shown and further confirmed by *ex vivo* NIS protein immunohistochemistry of GBM sections. The outcome of the therapy study matched closely the results of the PET imaging study. The effective therapeutic cytoreduction achieved after treatment with EGFR-targeted polyplexes followed by ^{131}I application resulted in a significant decrease of tumor growth as compared to control groups. These observations in tumor growth behaviour during therapy were mirrored by animal survival.

As a next step, the polyplexes were reengineered and a second targeting domain was added utilizing the retro-enantio peptide TfRre that targets the transferrin receptor that should be suitable for receptor-mediated transcytosis across the BBB. A dual-targeted polyplex was generated to overcome the BBB by active TfR targeting and to subsequently target the GBM by EGFR targeting. The polyplexes were characterized by transemission electron microscopy

and dynamic light scattering showing sufficient size, surface charge and spherical shapes. *In vitro* transfection studies showed high transfection efficiency of the dual-targeted polyplexes in EGFR-positive cells. ^{18}F-labelled tetrafluoroborate was utilized as a novel PET tracer and delivered clear images with improved resolution and excellent target-to-background ratios. Quantitative analysis of PET imaging revealed a significantly higher tumoral tracer uptake in mice treated with dual-targeted polyplexes as compared to groups injected with mono-targeted GE11 or TfRre polyplexes. The results obtained from the imaging studies were mirrored by the outcome of the therapy study. Mice treated with dual-targeted polyplexes followed by ^{131}I 48 h later showed a significant delay in tumor growth as compared to negative controls and a trend toward slower tumor growth as compared to EGFR- and TfR-mono-targeted polyplexes. The delay in tumor growth led to a significantly prolonged survival of Dual/NIS and GE11/NIS treated mice.

In conclusion, the results of this thesis highlight the potential of targeted NIS lipopolyplexes for the *NIS* gene therapy of glioblastoma. Two crucial dual approaches were combined: The theranostic function of NIS enhancing safety by molecular imaging of biodistribution and gene expression levels, in synergy with efficient sequential targeting strategies in context of nanocarrier-mediated site specific gene delivery resulting in increased *NIS* gene expression in the GBM lesion. These highly efficient and tumor-specific sequence-defined NIS lipopolyplexes represent a promising concept for future clinical translation of the *NIS* gene therapy in the field of nanotheranostics.

6. Publications

6.1. Original papers

Spellerberg R, Benli-Hoppe T, Kitzberger C, Schwenk N, Steiger K, Öztürk Ö, Eiber M, Schilling F, Weber WA, Kälin RE, Glass R, Nelson PJ, Wagner E, Spitzweg C. Dual EGFR- and TfR-targeted gene transfer improves efficacy of sodium iodide symporter (*NIS*) gene therapy of glioblastoma. [Manuscript submitted].

Spellerberg R, Benli-Hoppe T, Kitzberger C, Berger S, Schmohl KA, Schwenk N, Yen HY, Zach C, Schilling F, Weber WA, Kälin RE, Glass R, Nelson PJ, Wagner E and Spitzweg C. Selective sodium iodide symporter (*NIS*) gene therapy of glioblastoma mediated by EGFR-targeted lipopolyplexes. *Mol Ther Oncolytics* 2021. 23:432-446.

Kitzberger C, **Spellerberg R**, Han Y, Schmohl KA, Stauss C, Zach C, Kälin RE, Schilling F, Glass R, Weber WA, Wagner E, Nelson PJ, Spitzweg C. Mesenchymal stem cell-mediated image-guided sodium iodide symporter (*NIS*) gene therapy improves survival of glioblastoma bearing mice. [Manuscript submitted].

Schmohl KA, Müller AM, Dohmann M, **Spellerberg R**, Urnauer S, Schwenk N, Ziegler S, Bartenstein P, Nelson PJ, Spitzweg C. Integrin αvβ3-mediated effects of thyroid hormones on mesenchymal stem cells in tumour angiogenesis. *Thyroid* 2019. 29(12):1843-1857.

Schug C, Kitzberger C, Sievert W, **Spellerberg R**, Tutter M, Schmohl KA, Eberlein B, Biedermann T, Steiger K, Zach C, Schwaiger M, Multhoff G, Wagner E, Nelson PJ, Spitzweg C. Radiation-induced amplification of TGFB1-induced mesenchymal stem cell-mediated sodium iodide symporter (*NIS*) gene ^{131}I therapy. *Clin Cancer Res* 2019. 25:5997-6008.

6.2. Manuscripts in preparation

Han Y, Koehler VF, Schwenk N, Schmohl KA, **Spellerberg R**, Kitzberger C, Zach C, Nelson PJ, Spitzweg C. Using TGFB1 biology in radioiodine refractory differentiated thyroid cancer to re-establish sodium iodide symporter (NIS) expression using engineered mesenchymal stem cells as therapy vehicles.

Kitzberger C, Shehzad K, Morath V, **Spellerberg R**, Kälin RE, Glass R, Multhoff G, Eiber M, Schilling F, Weber WA, Wagner E, Nelson PJ, Spitzweg C. Tumor-selective interleukin-6 targeted mesenchymal stem cell-mediated sodium iodide symporter (*NIS*) gene therapy of glioblastoma

6.3. Reviews

Kitzberger C, **Spellerberg R**, Morath V, Schwenk N, Schmohl KA, Stauss C, Urnauer S, Tutter M, Eiber M, Schilling F, Weber WA, Ziegler S, Bartenstein P, Wagner E, Nelson PJ, Spitzweg C. The sodium iodide symporter (NIS) as theranostic gene: its emerging role in new imaging modalities and non-viral gene therapy. *EJNMMI Research* 2022.12:25

6.4. Oral presentations

65th Annual meeting of the German Society of Endocrinology, online, March 2022. **Spellerberg R**, Benli-Hoppe T, Kitzberger C, Schwenk N, Steiger K, Öztürk Ö, Eiber M, Schilling F, Weber WA, Kälin RE, Glass R, Nelson PJ, Wagner E, Spitzweg C. Dual-targeted sodium iodide symporter (NIS) polyplexes: a cascade-targeting strategy for the *NIS* gene therapy of glioblastoma.

64th Annual meeting of the German Society of Endocrinology, online, March 2021. **Spellerberg R**, Benli-Hoppe T, Kitzberger C, Berger S, Schwenk N, Schilling F, Weber WA, Kälin RE, Glass R, Nelson PJ, Wagner E, Spitzweg C. Targeted polyplex-mediated sodium iodide symporter (*NIS*) gene therapy in glioblastoma.

22nd Annual meeting of Young Active Research in Endocrinology (YARE), online, January 2021. **Spellerberg R**, Benli-Hoppe T, Kitzberger C, Berger S, Schwenk N, Kälin RE, Glass R, Nelson PJ, Wagner E, Spitzweg C. Polyplex-mediated sodium iodide symporter (*NIS*) gene transfer in glioblastoma.

Jahrestagung Sektion Schilddrüse, online, November 2020. **Spellerberg R**, Benli-Hoppe T, Kitzberger C, Berger S, Schwenk N, Kälin RE, Glass R, Nelson PJ, Wagner E, Spitzweg C. Polyplex-mediated sodium iodide symporter (*NIS*) gene transfer in glioblastoma.

Local Chapter Meeting Controlled Release Society, Munich, Germany, February 2020. **Spellerberg R**, Benli-Hoppe T, Kitzberger C, Hager S, Kälin RE, Glass R, Wagner E, Spitzweg C. Nanocarrier-mediated sodium iodide symporter (*NIS*) gene transfer in glioblastoma.

18th Symposium Gentianum, Klausurtagung der Medizinischen Klinik und Poliklinik IV, Frauenchiemsee, Germany, February 2019. **Spellerberg R**, Kitzberger C. Non-viral sodium iodide symporter (*NIS*) gene transfer in glioblastoma.

6.5. Poster presentations

90th Annual Meeting of the American Thyroid Association, online, September 2021. Kitzberger C, **Spellerberg R**, Morath V, Schwenk N, Glass R, Weber WA, Wagner E, Nelson PJ, Spitzweg C. ^{18}F-TFB-PET imaging of the sodium iodide symporter (*NIS*) as a molecular reporter gene in an orthotopic glioblastoma xenograft mouse model. Highlighted poster presentation.

42nd Annual Meeting of the European Thyroid Association, Budapest, Hungary, September 2019. **Spellerberg R**, Benli-Hoppe T, Kitzberger C, Hager S, Schwenk N, Kälin RE, Glass R, Wagner E, Spitzweg C. Nanocarrier-mediated sodium iodide symporter (*NIS*) gene transfer in glioblastoma.

6.5. Awards

Best-Mini-Video Award, 64th Annual meeting of the German Society of Endocrinology, online, March 2021. Supported by Pfizer Deutschland GmbH. **Spellerberg R**, Benli-Hoppe T, Kitzberger C, Berger S, Schwenk N, Schilling F, Weber WA, Kälin RE, Glass R, Nelson PJ, Wagner E, Spitzweg C. Targeted polyplex-mediated sodium iodide symporter (*NIS*) gene therapy in glioblastoma.

Travel Grant, German Society of Endocrinology: 42nd Annual Meeting of the European Thyroid Association, Budapest, Hungary, September 2019

7. References

1. Hanahan, D., and Weinberg, R.A. (2000). The hallmarks of cancer. Cell *100*, 57-70.
2. Hanahan, D., and Weinberg, R.A. (2011). Hallmarks of cancer: the next generation. Cell *144*, 646-674.
3. Clarke, M.F., Dick, J.E., Dirks, P.B., Eaves, C.J., Jamieson, C.H., Jones, D.L., Visvader, J., Weissman, I.L., and Wahl, G.M. (2006). Cancer stem cells--perspectives on current status and future directions: AACR Workshop on cancer stem cells. Cancer research *66*, 9339-9344.
4. Atashzar, M.R., Baharlou, R., Karami, J., Abdollahi, H., Rezaei, R., Pourramezan, F., and Zoljalali Moghaddam, S.H. (2020). Cancer stem cells: A review from origin to therapeutic implications. Journal of cellular physiology *235*, 790-803.
5. Chiaverina, G., di Blasio, L., Monica, V., Accardo, M., Palmiero, M., Peracino, B., Vara-Messler, M., Puliafito, A., and Primo, L. (2019). Dynamic Interplay between Pericytes and Endothelial Cells during Sprouting Angiogenesis. Cells *8*.
6. De Palma, M., Biziato, D., and Petrova, T.V. (2017). Microenvironmental regulation of tumour angiogenesis. Nature reviews. Cancer *17*, 457-474.
7. Xing, F., Saidou, J., and Watabe, K. (2010). Cancer associated fibroblasts (CAFs) in tumor microenvironment. Front Biosci (Landmark Ed) *15*, 166-179.
8. Zeltz, C., Primac, I., Erusappan, P., Alam, J., Noel, A., and Gullberg, D. (2020). Cancer-associated fibroblasts in desmoplastic tumors: emerging role of integrins. Seminars in cancer biology *62*, 166-181.
9. Gonzalez, H., Hagerling, C., and Werb, Z. (2018). Roles of the immune system in cancer: from tumor initiation to metastatic progression. Genes Dev *32*, 1267-1284.
10. Galli, F., Aguilera, J.V., Palermo, B., Markovic, S.N., Nisticò, P., and Signore, A. (2020). Relevance of immune cell and tumor microenvironment imaging in the new era of immunotherapy. Journal of Experimental & Clinical Cancer Research *39*, 89.
11. Rajesh, Y., Pal, I., Banik, P., Chakraborty, S., Borkar, S.A., Dey, G., Mukherjee, A., and Mandal, M. (2017). Insights into molecular therapy of glioma: current challenges and next generation blueprint. Acta pharmacologica Sinica *38*, 591-613.
12. Zhao, M., van Straten, D., Broekman, M.L.D., Préat, V., and Schiffelers, R.M. (2020). Nanocarrier-based drug combination therapy for glioblastoma. Theranostics *10*, 1355-1372.
13. DeCordova, S., Shastri, A., Tsolaki, A.G., Yasmin, H., Klein, L., Singh, S.K., and Kishore, U. (2020). Molecular Heterogeneity and Immunosuppressive Microenvironment in Glioblastoma. Frontiers in immunology *11*, 1402.
14. van den Bent, M.J., Afra, D., de Witte, O., Ben Hassel, M., Schraub, S., Hoang-Xuan, K., Malmström, P.O., Collette, L., Piérart, M., Mirimanoff, R., et al. (2005). Long-term efficacy of early versus delayed radiotherapy for low-grade astrocytoma and oligodendroglioma in adults: the EORTC 22845 randomised trial. Lancet (London, England) *366*, 985-990.
15. Karim, R., Palazzo, C., Evrard, B., and Piel, G. (2016). Nanocarriers for the treatment of glioblastoma multiforme: Current state-of-the-art. Journal of controlled release : official journal of the Controlled Release Society *227*, 23-37.
16. Batash, R., Asna, N., Schaffer, P., Francis, N., and Schaffer, M. (2017). Glioblastoma Multiforme, Diagnosis and Treatment; Recent Literature Review. Current medicinal chemistry *24*, 3002-3009.
17. Pardridge, W.M. (2019). Blood-Brain Barrier and Delivery of Protein and Gene Therapeutics to Brain. Frontiers in aging neuroscience *11*, 373.
18. Portulano, C., Paroder-Belenitsky, M., and Carrasco, N. (2014). The Na+/I- symporter (NIS): mechanism and medical impact. Endocrine reviews *35*, 106-149.
19. Ravera, S., Reyna-Neyra, A., Ferrandino, G., Amzel, L.M., and Carrasco, N. (2017). The Sodium/Iodide Symporter (NIS): Molecular Physiology and Preclinical and Clinical Applications. Annual review of physiology *79*, 261-289.

20. Baril, P., Martin-Duque, P., and Vassaux, G. (2010). Visualization of gene expression in the live subject using the Na/I symporter as a reporter gene: applications in biotherapy. British journal of pharmacology *159*, 761-771.
21. Hingorani, M., Spitzweg, C., Vassaux, G., Newbold, K., Melcher, A., Pandha, H., Vile, R., and Harrington, K. (2010). The biology of the sodium iodide symporter and its potential for targeted gene delivery. Current cancer drug targets *10*, 242-267.
22. Hertz, S., Roberts, A., and Salter, W.T. (1942). RADIOACTIVE IODINE AS AN INDICATOR IN THYROID PHYSIOLOGY. IV. THE METABOLISM OF IODINE IN GRAVES' DISEASE. The Journal of clinical investigation *21*, 25-29.
23. Borges de Souza, P., and McCabe, C.J. (2021). Radioiodine treatment: an historical and future perspective. Endocrine-related cancer *28*, T121-t124.
24. Spitzweg, C., Nelson, P.J., Wagner, E., Bartenstein, P., Weber, W.A., Schwaiger, M., and Morris, J.C. (2021). The sodium iodide symporter (NIS): novel applications for radionuclide imaging and treatment. Endocrine-related cancer *28*, T193-t213.
25. Guo, R., Zhang, M., Xi, Y., Ma, Y., Liang, S., Shi, S., Miao, Y., and Li, B. (2014). Theranostic studies of human sodium iodide symporter imaging and therapy using 188Re: a human glioma study in mice. PloS one *9*, e102011.
26. Willhauck, M.J., Sharif Samani, B.R., Gildehaus, F.J., Wolf, I., Senekowitsch-Schmidtke, R., Stark, H.J., Göke, B., Morris, J.C., and Spitzweg, C. (2007). Application of 188rhenium as an alternative radionuclide for treatment of prostate cancer after tumor-specific sodium iodide symporter gene expression. The Journal of clinical endocrinology and metabolism *92*, 4451-4458.
27. Knoop, K., Schwenk, N., Dolp, P., Willhauck, M.J., Zischek, C., Zach, C., Hacker, M., Göke, B., Wagner, E., Nelson, P.J., et al. (2013). Stromal targeting of sodium iodide symporter using mesenchymal stem cells allows enhanced imaging and therapy of hepatocellular carcinoma. Human gene therapy *24*, 306-316.
28. Willhauck, M.J., Samani, B.R., Wolf, I., Senekowitsch-Schmidtke, R., Stark, H.J., Meyer, G.J., Knapp, W.H., Göke, B., Morris, J.C., and Spitzweg, C. (2008). The potential of 211Astatine for NIS-mediated radionuclide therapy in prostate cancer. European journal of nuclear medicine and molecular imaging *35*, 1272-1281.
29. Llorente-Esteban, A., Manville, R.W., Reyna-Neyra, A., Abbott, G.W., Amzel, L.M., and Carrasco, N. (2020). Allosteric regulation of mammalian Na(+)/I(-) symporter activity by perchlorate. Nature structural & molecular biology *27*, 533-539.
30. Dai, G., Levy, O., and Carrasco, N. (1996). Cloning and characterization of the thyroid iodide transporter. Nature *379*, 458-460.
31. Smanik, P.A., Liu, Q., Furminger, T.L., Ryu, K., Xing, S., Mazzaferri, E.L., and Jhiang, S.M. (1996). Cloning of the human sodium lodide symporter. Biochemical and biophysical research communications *226*, 339-345.
32. Shimura, H., Haraguchi, K., Miyazaki, A., Endo, T., and Onaya, T. (1997). Iodide uptake and experimental 131I therapy in transplanted undifferentiated thyroid cancer cells expressing the Na+/I- symporter gene. Endocrinology *138*, 4493-4496.
33. Spitzweg, C., Zhang, S., Bergert, E.R., Castro, M.R., McIver, B., Heufelder, A.E., Tindall, D.J., Young, C.Y., and Morris, J.C. (1999). Prostate-specific antigen (PSA) promoter-driven androgen-inducible expression of sodium iodide symporter in prostate cancer cell lines. Cancer research *59*, 2136-2141.
34. Spitzweg, C., O'Connor, M.K., Bergert, E.R., Tindall, D.J., Young, C.Y., and Morris, J.C. (2000). Treatment of prostate cancer by radioiodine therapy after tissue-specific expression of the sodium iodide symporter. Cancer research *60*, 6526-6530.
35. Cho, J.Y., Xing, S., Liu, X., Buckwalter, T.L., Hwa, L., Sferra, T.J., Chiu, I.M., and Jhiang, S.M. (2000). Expression and activity of human Na+/I- symporter in human glioma cells by adenovirus-mediated gene delivery. Gene therapy *7*, 740-749.
36. Spitzweg, C., Dietz, A.B., O'Connor, M.K., Bergert, E.R., Tindall, D.J., Young, C.Y., and Morris, J.C. (2001). In vivo sodium iodide symporter gene therapy of prostate cancer. Gene therapy *8*, 1524-1531.

37. Dwyer, R.M., Schatz, S.M., Bergert, E.R., Myers, R.M., Harvey, M.E., Classic, K.L., Blanco, M.C., Frisk, C.S., Marler, R.J., Davis, B.J., et al. (2005). A preclinical large animal model of adenovirus-mediated expression of the sodium-iodide symporter for radioiodide imaging and therapy of locally recurrent prostate cancer. Molecular therapy : the journal of the American Society of Gene Therapy *12*, 835-841.
38. Kitzberger, C., Spellerberg, R., Morath, V., Schwenk, N., Schmohl, K.A., Schug, C., Urnauer, S., Tutter, M., Eiber, M., Schilling, F., et al. (2022). The sodium iodide symporter (NIS) as theranostic gene: its emerging role in new imaging modalities and non-viral gene therapy. EJNMMI research *12*, 25.
39. Birnbaum, T., Roider, J., Schankin, C.J., Padovan, C.S., Schichor, C., Goldbrunner, R., and Straube, A. (2007). Malignant gliomas actively recruit bone marrow stromal cells by secreting angiogenic cytokines. Journal of neuro-oncology *83*, 241-247.
40. Melzer, C., Yang, Y., and Hass, R. (2016). Interaction of MSC with tumor cells. Cell communication and signaling : CCS *14*, 20.
41. Hagenhoff, A., Bruns, C.J., Zhao, Y., von Lüttichau, I., Niess, H., Spitzweg, C., and Nelson, P.J. (2016). Harnessing mesenchymal stem cell homing as an anticancer therapy. Expert opinion on biological therapy *16*, 1079-1092.
42. Schmohl, K.A., Müller, A.M., Wechselberger, A., Rühland, S., Salb, N., Schwenk, N., Heuer, H., Carlsen, J., Göke, B., Nelson, P.J., et al. (2015). Thyroid hormones and tetrac: new regulators of tumour stroma formation via integrin αvβ3. Endocrine-related cancer *22*, 941-952.
43. Droujinine, I.A., Eckert, M.A., and Zhao, W. (2013). To grab the stroma by the horns: from biology to cancer therapy with mesenchymal stem cells. Oncotarget *4*, 651-664.
44. Knoop, K., Kolokythas, M., Klutz, K., Willhauck, M.J., Wunderlich, N., Draganovici, D., Zach, C., Gildehaus, F.J., Böning, G., Göke, B., et al. (2011). Image-guided, tumor stroma-targeted 131I therapy of hepatocellular cancer after systemic mesenchymal stem cell-mediated NIS gene delivery. Molecular therapy : the journal of the American Society of Gene Therapy *19*, 1704-1713.
45. Schug, C., Urnauer, S., Jaeckel, C., Schmohl, K.A., Tutter, M., Steiger, K., Schwenk, N., Schwaiger, M., Wagner, E., Nelson, P.J., et al. (2019). TGFB1-driven mesenchymal stem cell-mediated NIS gene transfer. Endocrine-related cancer *26*, 89-101.
46. Tutter, M., Schug, C., Schmohl, K.A., Urnauer, S., Schwenk, N., Petrini, M., Lokerse, W.J.M., Zach, C., Ziegler, S., Bartenstein, P., et al. (2020). Effective control of tumor growth through spatial and temporal control of theranostic sodium iodide symporter (NIS) gene expression using a heat-inducible gene promoter in engineered mesenchymal stem cells. Theranostics *10*, 4490-4506.
47. Schug, C., Kitzberger, C., Sievert, W., Spellerberg, R., Tutter, M., Schmohl, K.A., Eberlein, B., Biedermann, T., Steiger, K., Zach, C., et al. (2019). Radiation-Induced Amplification of TGFB1-Induced Mesenchymal Stem Cell-Mediated Sodium Iodide Symporter (NIS) Gene (131)I Therapy. Clinical cancer research : an official journal of the American Association for Cancer Research *25*, 5997-6008.
48. Knoop, K., Schwenk, N., Schmohl, K., Müller, A., Zach, C., Cyran, C., Carlsen, J., Böning, G., Bartenstein, P., Göke, B., et al. (2015). Mesenchymal stem cell-mediated, tumor stroma-targeted radioiodine therapy of metastatic colon cancer using the sodium iodide symporter as theranostic gene. Journal of nuclear medicine : official publication, Society of Nuclear Medicine *56*, 600-606.
49. Müller, A.M., Schmohl, K.A., Knoop, K., Schug, C., Urnauer, S., Hagenhoff, A., Clevert, D.A., Ingrisch, M., Niess, H., Carlsen, J., et al. (2016). Hypoxia-targeted 131I therapy of hepatocellular cancer after systemic mesenchymal stem cell-mediated sodium iodide symporter gene delivery. Oncotarget *7*, 54795-54810.
50. Ungerechts, G., Bossow, S., Leuchs, B., Holm, P.S., Rommelaere, J., Coffey, M., Coffin, R., Bell, J., and Nettelbeck, D.M. (2016). Moving oncolytic viruses into the clinic: clinical-grade production, purification, and characterization of diverse oncolytic viruses. Molecular therapy. Methods & clinical development *3*, 16018.

51. Dingli, D., Peng, K.W., Harvey, M.E., Greipp, P.R., O'Connor, M.K., Cattaneo, R., Morris, J.C., and Russell, S.J. (2004). Image-guided radiovirotherapy for multiple myeloma using a recombinant measles virus expressing the thyroidal sodium iodide symporter. Blood *103*, 1641-1646.
52. Msaouel, P., Iankov, I.D., Allen, C., Aderca, I., Federspiel, M.J., Tindall, D.J., Morris, J.C., Koutsilieris, M., Russell, S.J., and Galanis, E. (2009). Noninvasive imaging and radiovirotherapy of prostate cancer using an oncolytic measles virus expressing the sodium iodide symporter. Molecular therapy : the journal of the American Society of Gene Therapy *17*, 2041-2048.
53. Zhang, P., and Wagner, E. (2017). History of Polymeric Gene Delivery Systems. Topics in current chemistry (Cham) *375*, 26.
54. Hager, S., and Wagner, E. (2018). Bioresponsive polyplexes - chemically programmed for nucleic acid delivery. Expert opinion on drug delivery *15*, 1067-1083.
55. He, D., and Wagner, E. (2015). Defined polymeric materials for gene delivery. Macromolecular bioscience *15*, 600-612.
56. Berger, S., Krhač Levačić, A., Hörterer, E., Wilk, U., Benli-Hoppe, T., Wang, Y., Öztürk, Ö., Luo, J., and Wagner, E. (2021). Optimizing pDNA Lipo-polyplexes: A Balancing Act between Stability and Cargo Release. Biomacromolecules *22*, 1282-1296.
57. Klutz, K., Russ, V., Willhauck, M.J., Wunderlich, N., Zach, C., Gildehaus, F.J., Göke, B., Wagner, E., Ogris, M., and Spitzweg, C. (2009). Targeted radioiodine therapy of neuroblastoma tumors following systemic nonviral delivery of the sodium iodide symporter gene. Clinical cancer research : an official journal of the American Association for Cancer Research *15*, 6079-6086.
58. Klutz, K., Willhauck, M.J., Dohmen, C., Wunderlich, N., Knoop, K., Zach, C., Senekowitsch-Schmidtke, R., Gildehaus, F.J., Ziegler, S., Fürst, S., et al. (2011). Image-guided tumor-selective radioiodine therapy of liver cancer after systemic nonviral delivery of the sodium iodide symporter gene. Human gene therapy *22*, 1563-1574.
59. Lächelt, U., and Wagner, E. (2015). Nucleic Acid Therapeutics Using Polyplexes: A Journey of 50 Years (and Beyond). Chemical reviews *115*, 11043-11078.
60. Li, Z., Zhao, R., Wu, X., Sun, Y., Yao, M., Li, J., Xu, Y., and Gu, J. (2005). Identification and characterization of a novel peptide ligand of epidermal growth factor receptor for targeted delivery of therapeutics. FASEB journal : official publication of the Federation of American Societies for Experimental Biology *19*, 1978-1985.
61. Schäfer, A., Pahnke, A., Schaffert, D., van Weerden, W.M., de Ridder, C.M., Rödl, W., Vetter, A., Spitzweg, C., Kraaij, R., Wagner, E., et al. (2011). Disconnecting the yin and yang relation of epidermal growth factor receptor (EGFR)-mediated delivery: a fully synthetic, EGFR-targeted gene transfer system avoiding receptor activation. Human gene therapy *22*, 1463-1473.
62. Klutz, K., Schaffert, D., Willhauck, M.J., Grünwald, G.K., Haase, R., Wunderlich, N., Zach, C., Gildehaus, F.J., Senekowitsch-Schmidtke, R., Göke, B., et al. (2011). Epidermal growth factor receptor-targeted (131)I-therapy of liver cancer following systemic delivery of the sodium iodide symporter gene. Molecular therapy : the journal of the American Society of Gene Therapy *19*, 676-685.
63. Schmohl, K.A., Dolp, P., Schug, C., Knoop, K., Klutz, K., Schwenk, N., Bartenstein, P., Nelson, P.J., Ogris, M., Wagner, E., et al. (2017). Reintroducing the Sodium-Iodide Symporter to Anaplastic Thyroid Carcinoma. Thyroid : official journal of the American Thyroid Association *27*, 1534-1543.
64. Schmohl, K.A., Gupta, A., Grünwald, G.K., Trajkovic-Arsic, M., Klutz, K., Braren, R., Schwaiger, M., Nelson, P.J., Ogris, M., Wagner, E., et al. (2017). Imaging and targeted therapy of pancreatic ductal adenocarcinoma using the theranostic sodium iodide symporter (NIS) gene. Oncotarget *8*, 33393-33404.
65. Urnauer, S., Müller, A.M., Schug, C., Schmohl, K.A., Tutter, M., Schwenk, N., Rödl, W., Morys, S., Ingrisch, M., Bertram, J., et al. (2017). EGFR-targeted nonviral NIS gene

transfer for bioimaging and therapy of disseminated colon cancer metastases. Oncotarget *8*, 92195-92208.

66. Urnauer, S., Schmohl, K.A., Tutter, M., Schug, C., Schwenk, N., Morys, S., Ziegler, S., Bartenstein, P., Clevert, D.A., Wagner, E., et al. (2019). Dual-targeted NIS polyplexes-a theranostic strategy toward tumors with heterogeneous receptor expression. Gene therapy *26*, 93-108.
67. Freitag, F., and Wagner, E. (2021). Optimizing synthetic nucleic acid and protein nanocarriers: The chemical evolution approach. Advanced drug delivery reviews *168*, 30-54.
68. Urnauer, S., Morys, S., Krhac Levacic, A., Müller, A.M., Schug, C., Schmohl, K.A., Schwenk, N., Zach, C., Carlsen, J., Bartenstein, P., et al. (2016). Sequence-defined cMET/HGFR-targeted Polymers as Gene Delivery Vehicles for the Theranostic Sodium Iodide Symporter (NIS) Gene. Molecular therapy : the journal of the American Society of Gene Therapy *24*, 1395-1404.
69. Aum, D.J., Kim, D.H., Beaumont, T.L., Leuthardt, E.C., Dunn, G.P., and Kim, A.H. (2014). Molecular and cellular heterogeneity: the hallmark of glioblastoma. Neurosurgical focus *37*, E11.
70. Louis, D.N., Perry, A., Reifenberger, G., von Deimling, A., Figarella-Branger, D., Cavenee, W.K., Ohgaki, H., Wiestler, O.D., Kleihues, P., and Ellison, D.W. (2016). The 2016 World Health Organization Classification of Tumors of the Central Nervous System: a summary. Acta neuropathologica *131*, 803-820.
71. Bastien, J.I., McNeill, K.A., and Fine, H.A. (2015). Molecular characterizations of glioblastoma, targeted therapy, and clinical results to date. Cancer *121*, 502-516.
72. Aldape, K., Brindle, K.M., Chesler, L., Chopra, R., Gajjar, A., Gilbert, M.R., Gottardo, N., Gutmann, D.H., Hargrave, D., Holland, E.C., et al. (2019). Challenges to curing primary brain tumours. Nature reviews. Clinical oncology *16*, 509-520.
73. Ginn, S.L., Amaya, A.K., Alexander, I.E., Edelstein, M., and Abedi, M.R. (2018). Gene therapy clinical trials worldwide to 2017: An update. The journal of gene medicine *20*, e3015.
74. Spitzweg, C., and Morris, J.C. (2002). The sodium iodide symporter: its pathophysiological and therapeutic implications. Clinical endocrinology *57*, 559-574.
75. Penheiter, A.R., Russell, S.J., and Carlson, S.K. (2012). The sodium iodide symporter (NIS) as an imaging reporter for gene, viral, and cell-based therapies. Current gene therapy *12*, 33-47.
76. Spitzweg, C. (2009). Gene therapy in thyroid cancer. Hormone and metabolic research = Hormon- und Stoffwechselforschung = Hormones et metabolisme *41*, 500-509.
77. Amer, M.H. (2014). Gene therapy for cancer: present status and future perspective. Molecular and cellular therapies *2*, 27.
78. Schug, C., Gupta, A., Urnauer, S., Steiger, K., Cheung, P.F., Neander, C., Savvatakis, K., Schmohl, K.A., Trajkovic-Arsic, M., Schwenk, N., et al. (2019). A Novel Approach for Image-Guided (131)I Therapy of Pancreatic Ductal Adenocarcinoma Using Mesenchymal Stem Cell-Mediated NIS Gene Delivery. Molecular cancer research : MCR *17*, 310-320.
79. Schug, C., Sievert, W., Urnauer, S., Müller, A.M., Schmohl, K.A., Wechselberger, A., Schwenk, N., Lauber, K., Schwaiger, M., Multhoff, G., et al. (2018). External Beam Radiation Therapy Enhances Mesenchymal Stem Cell-Mediated Sodium-Iodide Symporter Gene Delivery. Human gene therapy *29*, 1287-1300.
80. Tutter, M., Schug, C., Schmohl, K.A., Urnauer, S., Kitzberger, C., Schwenk, N., Petrini, M., Zach, C., Ziegler, S., Bartenstein, P., et al. (2021). Regional Hyperthermia Enhances Mesenchymal Stem Cell Recruitment to Tumor Stroma: Implications for Mesenchymal Stem Cell-Based Tumor Therapy. Molecular therapy : the journal of the American Society of Gene Therapy *29*, 788-803.
81. Urnauer, S., Klutz, K., Grünwald, G.K., Morys, S., Schwenk, N., Zach, C., Gildehaus, F.J., Rödl, W., Ogris, M., Wagner, E., et al. (2017). Systemic tumor-targeted sodium

iodide symporter (NIS) gene therapy of hepatocellular carcinoma mediated by B6 peptide polyplexes. The journal of gene medicine *19*.

82. Klein, P.M., Kern, S., Lee, D.J., Schmaus, J., Höhn, M., Gorges, J., Kazmaier, U., and Wagner, E. (2018). Folate receptor-directed orthogonal click-functionalization of siRNA lipopolyplexes for tumor cell killing in vivo. Biomaterials *178*, 630-642.
83. Ogris, M., Brunner, S., Schüller, S., Kircheis, R., and Wagner, E. (1999). PEGylated DNA/transferrin-PEI complexes: reduced interaction with blood components, extended circulation in blood and potential for systemic gene delivery. Gene therapy *6*, 595-605.
84. Wang, S., Reinhard, S., Li, C., Qian, M., Jiang, H., Du, Y., Lächelt, U., Lu, W., Wagner, E., and Huang, R. (2017). Antitumoral Cascade-Targeting Ligand for IL-6 Receptor-Mediated Gene Delivery to Glioma. Molecular therapy : the journal of the American Society of Gene Therapy *25*, 1556-1566.
85. Kos, P., Lächelt, U., He, D., Nie, Y., Gu, Z., and Wagner, E. (2015). Dual-targeted polyplexes based on sequence-defined peptide-PEG-oligoamino amides. Journal of pharmaceutical sciences *104*, 464-475.
86. Rao, S.A., Arimappamagan, A., Pandey, P., Santosh, V., Hegde, A.S., Chandramouli, B.A., and Somasundaram, K. (2013). miR-219-5p inhibits receptor tyrosine kinase pathway by targeting EGFR in glioblastoma. PloS one *8*, e63164.
87. Eskilsson, E., Røsland, G.V., Solecki, G., Wang, Q., Harter, P.N., Graziani, G., Verhaak, R.G.W., Winkler, F., Bjerkvig, R., and Miletic, H. (2018). EGFR heterogeneity and implications for therapeutic intervention in glioblastoma. Neuro-oncology *20*, 743-752.
88. Mickler, F.M., Möckl, L., Ruthardt, N., Ogris, M., Wagner, E., and Bräuchle, C. (2012). Tuning nanoparticle uptake: live-cell imaging reveals two distinct endocytosis mechanisms mediated by natural and artificial EGFR targeting ligand. Nano letters *12*, 3417-3423.
89. Wang, Y., Luo, J., Truebenbach, I., Reinhard, S., Klein, P.M., Höhn, M., Kern, S., Morys, S., Loy, D.M., Wagner, E., et al. (2020). Double Click-Functionalized siRNA Polyplexes for Gene Silencing in Epidermal Growth Factor Receptor-Positive Tumor Cells. ACS Biomaterials Science & Engineering *6*, 1074-1089.
90. Morys, S., Urnauer, S., Spitzweg, C., and Wagner, E. (2018). EGFR Targeting and Shielding of pDNA Lipopolyplexes via Bivalent Attachment of a Sequence-Defined PEG Agent. Macromolecular bioscience *18*.
91. Truebenbach, I., Zhang, W., Wang, Y., Kern, S., Höhn, M., Reinhard, S., Gorges, J., Kazmaier, U., and Wagner, E. (2019). Co-delivery of pretubulysin and siEG5 to EGFR overexpressing carcinoma cells. International journal of pharmaceutics *569*, 118570.
92. Steinborn, B., Truebenbach, I., Morys, S., Lächelt, U., Wagner, E., and Zhang, W. (2018). Epidermal growth factor receptor targeted methotrexate and small interfering RNA co-delivery. The journal of gene medicine *20*, e3041.
93. Jo, D.H., Kim, J.H., Lee, T.G., and Kim, J.H. (2015). Size, surface charge, and shape determine therapeutic effects of nanoparticles on brain and retinal diseases. Nanomedicine : nanotechnology, biology, and medicine *11*, 1603-1611.
94. Boeckle, S., von Gersdorff, K., van der Piepen, S., Culmsee, C., Wagner, E., and Ogris, M. (2004). Purification of polyethylenimine polyplexes highlights the role of free polycations in gene transfer. The journal of gene medicine *6*, 1102-1111.
95. Šamec, N., Zottel, A., Videtič Paska, A., and Jovčevska, I. (2020). Nanomedicine and Immunotherapy: A Step Further towards Precision Medicine for Glioblastoma. Molecules (Basel, Switzerland) *25*.
96. Pruitt, A.A., and Rosenfeld, M.R. (2005). 10 questions about temozolomide and the treatment of brain tumors. The neurologist *11*, 362-365.
97. Li, H., Nakashima, H., Decklever, T.D., Nace, R.A., and Russell, S.J. (2013). HSV-NIS, an oncolytic herpes simplex virus type 1 encoding human sodium iodide symporter for preclinical prostate cancer radiovirotherapy. Cancer gene therapy *20*, 478-485.

98. Spitzweg, C., Harrington, K.J., Pinke, L.A., Vile, R.G., and Morris, J.C. (2001). Clinical review 132: The sodium iodide symporter and its potential role in cancer therapy. The Journal of clinical endocrinology and metabolism *86*, 3327-3335.
99. Opyrchal, M., Allen, C., Iankov, I., Aderca, I., Schroeder, M., Sarkaria, J., and Galanis, E. (2012). Effective radiovirotherapy for malignant gliomas by using oncolytic measles virus strains encoding the sodium iodide symporter (MV-NIS). Human gene therapy *23*, 419-427.
100. Klutz, K., Willhauck, M.J., Wunderlich, N., Zach, C., Anton, M., Senekowitsch-Schmidtke, R., Göke, B., and Spitzweg, C. (2011). Sodium iodide symporter (NIS)-mediated radionuclide ((131)I, (188)Re) therapy of liver cancer after transcriptionally targeted intratumoral in vivo NIS gene delivery. Human gene therapy *22*, 1403-1412.
101. Willhauck, M.J., Sharif-Samani, B., Senekowitsch-Schmidtke, R., Wunderlich, N., Göke, B., Morris, J.C., and Spitzweg, C. (2008). Functional sodium iodide symporter expression in breast cancer xenografts in vivo after systemic treatment with retinoic acid and dexamethasone. Breast cancer research and treatment *109*, 263-272.
102. Frisch, A., Kälin, S., Monk, R., Radke, J., Heppner, F.L., and Kälin, R.E. (2020). Apelin Controls Angiogenesis-Dependent Glioblastoma Growth. International journal of molecular sciences *21*.
103. van den Bent, M.J., Gao, Y., Kerkhof, M., Kros, J.M., Gorlia, T., van Zwieten, K., Prince, J., van Duinen, S., Sillevis Smitt, P.A., Taphoorn, M., et al. (2015). Changes in the EGFR amplification and EGFRvIII expression between paired primary and recurrent glioblastomas. Neuro-oncology *17*, 935-941.
104. Plank, C., Zatloukal, K., Cotten, M., Mechtler, K., and Wagner, E. (1992). Gene transfer into hepatocytes using asialoglycoprotein receptor mediated endocytosis of DNA complexed with an artificial tetra-antennary galactose ligand. Bioconjugate chemistry *3*, 533-539.
105. Franklin, K.B., and Paxinos, G. (2019). Paxinos and Franklin's the Mouse Brain in Stereotaxic Coordinates, Compact: The Coronal Plates and Diagrams (London, United Kingdom: Academic press).
106. Kälin, R.E., Cai, L., Li, Y., Zhao, D., Zhang, H., Cheng, J., Zhang, W., Wu, Y., Eisenhut, K., Janssen, P., et al. (2021). TAMEP are brain tumor parenchymal cells controlling neoplastic angiogenesis and progression. Cell systems *12*, 248-262.e247.
107. Spitzweg, C., Baker, C.H., Bergert, E.R., O'Connor, M.K., and Morris, J.C. (2007). Image-guided radioiodide therapy of medullary thyroid cancer after carcinoembryonic antigen promoter-targeted sodium iodide symporter gene expression. Human gene therapy *18*, 916-924.
108. Spitzweg, C., and Morris, J.C. (2004). Gene therapy for thyroid cancer: current status and future prospects. Thyroid : official journal of the American Thyroid Association *14*, 424-434.
109. Grünwald, G.K., Klutz, K., Willhauck, M.J., Schwenk, N., Senekowitsch-Schmidtke, R., Schwaiger, M., Zach, C., Göke, B., Holm, P.S., and Spitzweg, C. (2013). Sodium iodide symporter (NIS)-mediated radiovirotherapy of hepatocellular cancer using a conditionally replicating adenovirus. Gene therapy *20*, 625-633.
110. Grünwald, G.K., Vetter, A., Klutz, K., Willhauck, M.J., Schwenk, N., Senekowitsch-Schmidtke, R., Schwaiger, M., Zach, C., Wagner, E., Göke, B., et al. (2013). EGFR-Targeted Adenovirus Dendrimer Coating for Improved Systemic Delivery of the Theranostic NIS Gene. Molecular therapy. Nucleic acids *2*, e131.
111. Grünwald, G.K., Vetter, A., Klutz, K., Willhauck, M.J., Schwenk, N., Senekowitsch-Schmidtke, R., Schwaiger, M., Zach, C., Wagner, E., Göke, B., et al. (2013). Systemic image-guided liver cancer radiovirotherapy using dendrimer-coated adenovirus encoding the sodium iodide symporter as theranostic gene. Journal of nuclear medicine : official publication, Society of Nuclear Medicine *54*, 1450-1457.
112. Weller, M., van den Bent, M., Tonn, J.C., Stupp, R., Preusser, M., Cohen-Jonathan-Moyal, E., Henriksson, R., Le Rhun, E., Balana, C., Chinot, O., et al. (2017). European

Association for Neuro-Oncology (EANO) guideline on the diagnosis and treatment of adult astrocytic and oligodendroglial gliomas. The Lancet. Oncology *18*, e315-e329.
113. Pearson, J.R.D., and Regad, T. (2017). Targeting cellular pathways in glioblastoma multiforme. Signal transduction and targeted therapy *2*, 17040.
114. Daneman, R., and Prat, A. (2015). The blood-brain barrier. Cold Spring Harbor perspectives in biology *7*, a020412.
115. Pardridge, W.M. (2005). The blood-brain barrier: bottleneck in brain drug development. NeuroRx : the journal of the American Society for Experimental NeuroTherapeutics *2*, 3-14.
116. Vetter, V.C., and Wagner, E. (2022). Targeting nucleic acid-based therapeutics to tumors: Challenges and strategies for polyplexes. Journal of controlled release : official journal of the Controlled Release Society *346*, 110-135.
117. Pardridge, W.M. (2012). Drug transport across the blood-brain barrier. Journal of cerebral blood flow and metabolism : official journal of the International Society of Cerebral Blood Flow and Metabolism *32*, 1959-1972.
118. Wiley, D.T., Webster, P., Gale, A., and Davis, M.E. (2013). Transcytosis and brain uptake of transferrin-containing nanoparticles by tuning avidity to transferrin receptor. Proceedings of the National Academy of Sciences of the United States of America *110*, 8662-8667.
119. Pardridge, W.M., Boado, R.J., Patrick, D.J., Ka-Wai Hui, E., and Lu, J.Z. (2018). Blood-Brain Barrier Transport, Plasma Pharmacokinetics, and Neuropathology Following Chronic Treatment of the Rhesus Monkey with a Brain Penetrating Humanized Monoclonal Antibody Against the Human Transferrin Receptor. Molecular pharmaceutics *15*, 5207-5216.
120. Prades, R., Oller-Salvia, B., Schwarzmaier, S.M., Selva, J., Moros, M., Balbi, M., Grazú, V., de La Fuente, J.M., Egea, G., Plesnila, N., et al. (2015). Applying the retro-enantio approach to obtain a peptide capable of overcoming the blood-brain barrier. Angewandte Chemie (International ed. in English) *54*, 3967-3972.
121. Spellerberg, R., Benli-Hoppe, T., Kitzberger, C., Berger, S., Schmohl, K.A., Schwenk, N., Yen, H.Y., Zach, C., Schilling, F., Weber, W.A., et al. (2021). Selective sodium iodide symporter (NIS) genetherapy of glioblastoma mediatedby EGFR-targeted lipopolyplexes. Molecular therapy oncolytics *23*, 432-446.
122. Benli-Hoppe, T., Göl Öztürk, Ş., Öztürk, Ö., Berger, S., Wagner, E., and Yazdi, M. (2021). Transferrin Receptor Targeted Polyplexes Completely Comprised of Sequence-Defined Components. Macromolecular rapid communications, e2100602.
123. Schlageter, K.E., Molnar, P., Lapin, G.D., and Groothuis, D.R. (1999). Microvessel organization and structure in experimental brain tumors: microvessel populations with distinctive structural and functional properties. Microvascular research *58*, 312-328.
124. Sarkaria, J.N., Hu, L.S., Parney, I.F., Pafundi, D.H., Brinkmann, D.H., Laack, N.N., Giannini, C., Burns, T.C., Kizilbash, S.H., Laramy, J.K., et al. (2018). Is the blood-brain barrier really disrupted in all glioblastomas? A critical assessment of existing clinical data. Neuro-oncology *20*, 184-191.
125. Lemée, J.M., Clavreul, A., and Menei, P. (2015). Intratumoral heterogeneity in glioblastoma: don't forget the peritumoral brain zone. Neuro-oncology *17*, 1322-1332.
126. Lemée, J.M., Clavreul, A., Aubry, M., Com, E., de Tayrac, M., Eliat, P.A., Henry, C., Rousseau, A., Mosser, J., and Menei, P. (2015). Characterizing the peritumoral brain zone in glioblastoma: a multidisciplinary analysis. Journal of neuro-oncology *122*, 53-61.
127. Wang, H.-X., Zuo, Z.-Q., Du, J.-Z., Wang, Y.-C., Sun, R., Cao, Z.-T., Ye, X.-D., Wang, J.-L., Leong, K.W., and Wang, J. (2016). Surface charge critically affects tumor penetration and therapeutic efficacy of cancer nanomedicines. Nano Today *11*, 133-144.
128. Luo, J., Schmaus, J., Cui, M., Hörterer, E., Wilk, U., Höhn, M., Däther, M., Berger, S., Benli-Hoppe, T., Peng, L., et al. (2021). Hyaluronate siRNA nanoparticles with positive charge display rapid attachment to tumor endothelium and penetration into tumors.

Journal of controlled release : official journal of the Controlled Release Society *329*, 919-933.

129. Soni, V., Kohli, D.V., and Jain, S.K. (2005). Transferrin coupled liposomes as drug delivery carriers for brain targeting of 5-florouracil. Journal of drug targeting *13*, 245-250.
130. Moody, P.R., Sayers, E.J., Magnusson, J.P., Alexander, C., Borri, P., Watson, P., and Jones, A.T. (2015). Receptor Crosslinking: A General Method to Trigger Internalization and Lysosomal Targeting of Therapeutic Receptor:Ligand Complexes. Molecular therapy : the journal of the American Society of Gene Therapy *23*, 1888-1898.
131. Brighi, C., Reid, L., Genovesi, L.A., Kojic, M., Millar, A., Bruce, Z., White, A.L., Day, B.W., Rose, S., Whittaker, A.K., et al. (2020). Comparative study of preclinical mouse models of high-grade glioma for nanomedicine research: the importance of reproducing blood-brain barrier heterogeneity. Theranostics *10*, 6361-6371.
132. Huszthy, P.C., Daphu, I., Niclou, S.P., Stieber, D., Nigro, J.M., Sakariassen, P., Miletic, H., Thorsen, F., and Bjerkvig, R. (2012). In vivo models of primary brain tumors: pitfalls and perspectives. Neuro-oncology *14*, 979-993.
133. Simeonova, I., and Huillard, E. (2014). In vivo models of brain tumors: roles of genetically engineered mouse models in understanding tumor biology and use in preclinical studies. Cellular and molecular life sciences : CMLS *71*, 4007-4026.
134. Khoshnevisan, A., Jauregui-Osoro, M., Shaw, K., Torres, J.B., Young, J.D., Ramakrishnan, N.K., Jackson, A., Smith, G.E., Gee, A.D., and Blower, P.J. (2016). [(18)F]tetrafluoroborate as a PET tracer for the sodium/iodide symporter: the importance of specific activity. EJNMMI research *6*, 34.

8. Acknowledgements

Many people contributed to this thesis and I would like to thank all of them for their great help and support, whether professionally or personally.

Foremost, I would like to thank Prof. Dr. Christine Spitzweg for giving me the possibility to work on this exciting project and be part of a great research group. I appreciated her professional guidance, continuous scientific support, and encouragement to manage our projects within self-responsibility and to grow with the challenges. Many thanks for the invitations to beergarden and Christmas dinner, for your chocolates and birthday flowers and for the one or other cheerful story in lab meetings and on the phone.

Furthermore, I would like to thank Prof. Dr. Ernst Wagner for accepting me as an external PhD student, for his scientific support, fruitful discussions after progress reports, always helpful advice, and quick Email responses. Additionally, thank you to his lab members for their support and advice, especially Teoman for meeting after our studies in Kiel in Munich again, sharing this exciting SFB824 project, and the continuous synthesis of oligomers and ligands.

I am very grateful to Prof. Dr. Peter Nelson for enthusiastic discussions, joyful lab meetings and for all his corrections on my manuscripts.

My warm appreciation goes to all current and former members of the NIS laboratory, who created a great working atmosphere, shared a lot of laughs at lunch breaks, and accepted me as a northern immigrant. Meanwhile, I agree that Munich might sometimes be windy as well. Thanks for your scientific support, for your help getting my project started and for an open ear to discuss various issues.
Thank you to Carolin for sharing the glioblastoma projects and being the rechts der Isar partner. Many thanks to Nathalie for keeping the lab running, lovely coffee breaks and all the short notice orders. Thank you, Yang, for disproving girls do the most shopping and of course, for the delicious Chinese peanuts. Thank you, Katy, for the weekly weather forecast of the alps, I experienced the mountains a lot with my Bollerbuchse and for unconsciously motivating me to do a half-marathon pace of less than 5.5. Mariella, thanks for being my pharmacist and ‘we do everything by bike’ partner and for many suggestions to do in and around Munich. Thank you to Christina and Viktoria for nice talks and keeping the joyful atmosphere.

Thank you to the people working at the Nuclear Medicine or pathology department at rechts der Isar for great and respectful collaborations, for the support to run my huge imaging series

and therapy studies and that really everyone was encouraged to help getting over drawbacks. Thank you to the impressive SFB network for continuous support and great collaboration and the joyful get-togethers.

Special appreciations go to the SFB824 for funding my work and to the Wilhelm-Sander-Stiftung and SPP1629 for generous financial support.

I owe special thanks to my parents, my brother and my friends, who always believed in me, cheered me up, supported me and listened to all the lab stories. Thank you to my Munich friends for exploring the surroundings and the alps by hiking, skiing, or biking and to my flatmates, especially Teresa, for being there after work and sharing stories over a beer or wine. Thank you to my friends at home for your longstanding friendship and always making me feel welcome and happy about coming home. Thank you, Lorena, for our great travels during holidays giving me new energy. I hope many other trips with great experiences will follow. Thank you to my friends from University and Canada for being at my side on the journey of becoming a pharmacist and scientist. Finally, I want to express my deepest gratitude to my parents. Thank you for your never-ending support and encouragement, for teaching me to take responsibility for myself and for accepting and supporting any of my plans, no matter where and how they take place. I always enjoy coming home to your warm-hearted place.